



National Library  
of Canada

Bibliothèque nationale  
du Canada

Acquisitions and  
Bibliographic Services Branch

Direction des acquisitions et  
des services bibliographiques

395 Wellington Street  
Ottawa, Ontario  
K1A 0N4

395, rue Wellington  
Ottawa (Ontario)  
K1A 0N4

*Your file* *voire référence*

*Our file* *Notre référence*

## NOTICE

## AVIS

The quality of this microform is heavily dependent upon the quality of the original thesis submitted for microfilming. Every effort has been made to ensure the highest quality of reproduction possible.

La qualité de cette microforme dépend grandement de la qualité de la thèse soumise au microfilmage. Nous avons tout fait pour assurer une qualité supérieure de reproduction.

If pages are missing, contact the university which granted the degree.

S'il manque des pages, veuillez communiquer avec l'université qui a conféré le grade.

Some pages may have indistinct print especially if the original pages were typed with a poor typewriter ribbon or if the university sent us an inferior photocopy.

La qualité d'impression de certaines pages peut laisser à désirer, surtout si les pages originales ont été dactylographiées à l'aide d'un ruban usé ou si l'université nous a fait parvenir une photocopie de qualité inférieure.

Reproduction in full or in part of this microform is governed by the Canadian Copyright Act, R.S.C. 1970, c. C-30, and subsequent amendments.

La reproduction, même partielle, de cette microforme est soumise à la Loi canadienne sur le droit d'auteur, SRC 1970, c. C-30, et ses amendements subséquents.

**THE UNIVERSITY OF ALBERTA**

**THE EFFECT OF THE DEGREE OF SHEAR STRESS REVERSAL ON THE  
LIQUEFACTION POTENTIAL OF SATURATED SANDS**

**BY**

**MIGUEL ANGEL PANDO**



**A THESIS**

**SUBMITTED TO THE FACULTY OF GRADUATE STUDIES AND RESEARCH IN  
PARTIAL FULFILLMENT OF THE REQUIREMENTS FOR THE DEGREE OF  
MASTER OF SCIENCE**

**DEPARTMENT OF CIVIL ENGINEERING**

**Edmonton, Alberta**

**Fall 1995**



National Library  
of Canada

Bibliothèque nationale  
du Canada

Acquisitions and  
Bibliographic Services Branch

Direction des acquisitions et  
des services bibliographiques

395 Wellington Street  
Ottawa, Ontario  
K1A 0N4

395, rue Wellington  
Ottawa (Ontario)  
K1A 0N4

*Your file* *Votre référence*

*Our file* *Notre référence*

THE AUTHOR HAS GRANTED AN IRREVOCABLE NON-EXCLUSIVE LICENCE ALLOWING THE NATIONAL LIBRARY OF CANADA TO REPRODUCE, LOAN, DISTRIBUTE OR SELL COPIES OF HIS/HER THESIS BY ANY MEANS AND IN ANY FORM OR FORMAT, MAKING THIS THESIS AVAILABLE TO INTERESTED PERSONS.

L'AUTEUR A ACCORDE UNE LICENCE IRREVOCABLE ET NON EXCLUSIVE PERMETTANT A LA BIBLIOTHEQUE NATIONALE DU CANADA DE REPRODUIRE, PRETER, DISTRIBUER OU VENDRE DES COPIES DE SA THESE DE QUELQUE MANIERE ET SOUS QUELQUE FORME QUE CE SOIT POUR METTRE DES EXEMPLAIRES DE CETTE THESE A LA DISPOSITION DES PERSONNE INTERESSEES.

THE AUTHOR RETAINS OWNERSHIP OF THE COPYRIGHT IN HIS/HER THESIS. NEITHER THE THESIS NOR SUBSTANTIAL EXTRACTS FROM IT MAY BE PRINTED OR OTHERWISE REPRODUCED WITHOUT HIS/HER PERMISSION.

L'AUTEUR CONSERVE LA PROPRIETE DU DROIT D'AUTEUR QUI PROTEGE SA THESE. NI LA THESE NI DES EXTRAITS SUBSTANTIELS DE CELLE-CI NE DOIVENT ETRE IMPRIMES OU AUTREMENT REPRODUITS SANS SON AUTORISATION.

ISBN 0-612-06516-2

Canada

UNIVERSITY OF ALBERTA

RELEASE FORM

NAME OF AUTHOR: Miguel-Angel Pando

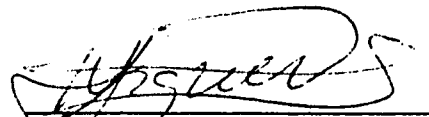
TITLE OF THESIS: The Effect of The Degree of Shear Stress Reversal on The  
Liquefaction Potential of Saturated Sands

DEGREE: Master of Science

YEAR OF DEGREE GRANTED: 1995

PERMISSION IS HEREBY GRANTED TO THE UNIVERSITY OF ALBERTA LIBRARY TO REPRODUCE SINGLE COPIES OF THIS THESIS AND TO LEND OR SELL SUCH COPIES FOR PRIVATE, SCHOLARLY OR SCIENTIFIC RESEARCH PURPOSES ONLY.

THE AUTHOR RESERVES ALL OTHER PUBLICATION AND OTHER RIGHTS IN ASSOCIATION WITH THE COPYRIGHT IN THE THESIS, AND EXCEPT AS HEREINBEFORE PROVIDED NEITHER THE THESIS NOR ANY SUBSTANTIAL PORTION THEREOF MAY BE PRINTED OR OTHERWISE REPRODUCED IN ANY MATERIAL FORM WHATEVER WITHOUT THE AUTHOR'S PRIOR WRITTEN PERMISSION.



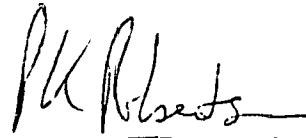
Miguel A. Pando  
610, 11135 - 83 Ave  
Edmonton, Alberta T6G 2C6  
Canada

Date: Oct. 6<sup>th</sup> 1995

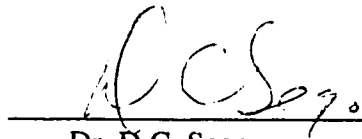
UNIVERSITY OF ALBERTA

FACULTY OF GRADUATE STUDIES AND RESEARCH

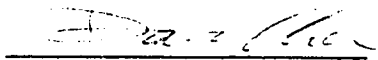
The undersigned certify that they have read, and recommend to the Faculty of Graduate Studies and Research for acceptance, a thesis entitled The Effect of The Degree of Shear Stress Reversal on The Liquefaction Potential of Saturated Sands submitted by Miguel-Angel Pando in partial fulfillment of the requirements for the degree of Master of Science



Dr. P.K. Robertson



Dr. D.C. Segó



Dr. D. Chan



Dr. A.W. Lipsett

Date: September 29<sup>th</sup>, 1995

**To my family**

## **ABSTRACT**

The response of cohesionless soils to cyclic loading is strongly influenced by whether or not shear stress reversal takes place. When shear stress reversal takes place during cyclic loading a condition of zero effective stress can occur resulting in an extreme loss of stiffness and large displacements. This condition is termed as cyclic liquefaction or cyclic softening. If no shear stress reversal takes place the condition of zero effective stress can not occur and there is generally no significant loss of stiffness and displacements are generally much smaller. This condition is termed as cyclic mobility. For level ground conditions shear stress reversal takes place on horizontal planes during earthquake loading and large ground oscillations can occur. However, for sloping ground the existing static shear stresses can exceed the cyclic shear stresses applied during an earthquake and shear stress reversal may not take place on horizontal planes. Hence, for regions of soil in a slope where no shear stress reversal takes place the response during earthquake loading can be very different. Therefore, it can be useful to identify regions in a soil slope where no shear stress reversal occurs. Two dimensional static and dynamic analyses have been carried out on slopes ranging from 5 m to 50 m in height and from 5 to 30 degrees in slope angle. Results are summarized to provide guidelines of zones where no shear stress reversal occurs.

## ACKNOWLEDGEMENTS

The author would like to thank Dr. P.K. Robertson for his interest, expertise and continual guidance throughout the thesis. His kindness and support will always be cherished.

The author also wishes to recognize the financial assistance that came from the Department of Civil Engineering of the University of Alberta and the Fundación para el Futuro de Colombia - COLFUTURO scholarship.

Special thanks to Carlos Emilio Ospina, Hector Gutierrez and Marcello Marelli for their unconditional friendship and tremendous help in order to meet the deadline.

I would also like to thank the camaraderie and support of my fellow peers in Geotechnical Engineering, specially Amin Touhidi, Peter Skopek and Mohammed Morsi.

The support and encouragement of my family is the main reason I was able to finish this important stage of my life. To all of you thank you.



# TABLE OF CONTENTS

	Page
Dedication .....	
Abstract.....	
Acknowledgments .....	
Table of contents .....	
List of figures .....	
List of tables.....	
List of nomenclature .....	
1. Introduction.....	1
1.1. Purpose of the Investigation.....	1
1.2. Organization of this thesis .....	3
2. Background Information .....	4
2.1. Introduction.....	4
2.2. Critical State Soil Mechanics Concepts .....	4
2.2.1. The ultimate Steady State of Sands.....	4
2.2.2. The State Boundary Surface .....	5
2.2.3. The State of a sand .....	6
2.3. Liquefaction Phenomena .....	7
2.3.1. Liquefaction terminology.....	9
2.4. Typical Liquefaction Analysis Procedure.....	10
2.5. Cyclic Behavior of Sands .....	13
3. Influence of Initial Static Shear Stress on Cyclic Liquefaction Resistance.....	28
3.1. Introduction.....	28
3.2. Summary of Previous Laboratory Investigations.....	29
3.2.1. Studies done in dense sand.....	29
3.2.1.1.Lee and Seed, 1967.....	30
3.2.1.2.Vaid and Finn, 1979 .....	30
3.2.1.3.Vaid and Chern, 1983 .....	31
3.2.1.4.Szerdy, 1985.....	31
3.2.1.5.Vaid and Chern, 1985 .....	32
3.2.1.6.Hyodo et al., 1991 .....	32

3.2.1.7.	Summary of all data .....	33
3.2.2.	Laboratory test in loose sands.....	33
3.2.2.1.	Yoshimi and Oh-Oka, 1975.....	33
3.2.2.2.	Castro et al., 1982.....	34
3.2.2.3.	Vaid and Chern, 1983 .....	34
3.2.2.4.	Szerdy, 1985.....	34
3.2.2.5.	Hyodo et al., 1994 .....	34
3.2.2.6.	Summary of results for loose sands .....	35
3.2.3.	General Remarks .....	35
3.3.	Seed's $K_{\alpha}$ correction factor.....	36
3.4.	Interpretation of Seed's $K_{\alpha}$ correction factor using steady state concepts	37
3.4.1.	Sacramento river sand (Szerdy, 1985).....	38
3.4.2.	Tailings sand (Vaid and Chern, 1985) .....	38
3.4.3.	Influence of the static shear stress using the state parameter.....	39
3.4.4.	Vaid and Chern (1983) data.....	40
3.4.5.	Hyodo et al. (1991 & 1994) data .....	40
3.4.6.	Dashihe Tailing Sand .....	41
3.4.7.	Summary .....	41
4.	Models used for the analyses .....	62
4.1.	Introduction.....	62
4.2.	Static analysis .....	62
4.3.	Dynamic analysis guidelines .....	63
4.3.1.	Definition of geometry.....	63
4.3.2.	Selection of earthquake induced motions .....	64
4.3.3.	Soil properties required for dynamic analysis.....	65
4.4.	Numerical modeling of earthquake related problems.....	66
4.4.1.	The equivalent linear method .....	66
4.4.2.	Shear modulus for sands.....	68
4.4.3.	Damping ratio for sands.....	69
4.5.	The dynamic model used in this research.....	70
4.5.1.	Program description.....	70
4.5.2.	Modeling and lessons learned.....	70

5.	Results.....	78
5.1.	Introduction.....	78
5.2.	Summary of input data.....	78
5.2.1.	The earthquake record.....	78
5.2.2.	Soil properties.....	79
5.2.2.1.	Properties used in the static analyses.....	79
5.2.2.2.	Properties used in the dynamic analyses.....	79
5.3.	Stress Reversal Evaluation for Infinite Slopes.....	80
5.3.1.	Static Shear stresses.....	80
5.3.2.	Dynamic Shear stresses.....	81
5.3.2.1.	Simplified approach.....	81
5.3.2.2.	Computer analyses using Quad4.....	83
5.4.	Stress Reversal Evaluation for Finite Slopes.....	85
5.4.1.	Introduction.....	85
5.4.2.	Static Analyses.....	85
5.4.3.	Dynamic Analyses.....	86
5.4.4.	Influence of the depth to Bedrock.....	86
5.4.5.	Definition of the zones of No Shear stress reversal.....	87
5.4.6.	Discussion of results.....	88
5.5.	Comparison of Results.....	89
5.5.1.	Introduction.....	89
5.5.2.	Duncan Dam study.....	90
6.	Conclusions.....	138
	<b>REFERENCES.....</b>	<b>140</b>
	Appendix A - Transformation of triaxial laboratory data.....	148
	Appendix B - Sensitivity analyses of the dynamic properties.....	151
	Appendix C - Infinite slope analyses results.....	154
	Appendix D - Description of the program QUAD4TB.....	175

## LIST OF FIGURES

Figure 2.1 Schematical representation of the ultimate steady state line.....	15
Figure 2.2 Three dimensional representation of the steady state boundaries for sands, after Sasitharan et al. (1994) .....	16
Figure 2.3 Normalized steady state boundary surface, after McRoberts and Sladen (1992).....	16
Figure 2.4 Definition of the state parameter, $\psi$ .....	17
Figure 2.5 Schematic behaviour of a cohesionless soil in monotonic undrained loading, after Robertson (1994).....	18
Figure 2.6 Schematic behaviour of elements of cohesionless soil under cyclic undrained loading in level or gently sloping ground, after Robertson (1994) .....	19
Figure 2.7 Schematic behaviour of elements of cohesionless soil in steeply sloping ground subject to monotonic or cyclic undrained loading, after Robertson (1994).....	20
Figure 2.8 Flow chart for evaluation of liquefaction, after Robertson (1994) .....	21
Figure 2.9 Typical Results of a Cyclic Shear Test with Shear Stress Reversal.....	22
Figure 2.10 Typical Results of a Cyclic Shear Test with No Shear Stress Reversal .....	23
Figure 2.11 Typical Results of a Cyclic Shear Test with Shear Stress Reversal.....	24
Figure 2.12 Correlation between the cyclic resistance ratio and SPT $(N_1)_{60}$ , after Seed et al. (1984).....	25
Figure 2.13 Typical hysteresis loop for a soil during cyclic loading.....	26
Figure 2.14 Variation of the shear modulus with strain amplitude, after Seed and Idriss (1970).....	27
Figure 3.1 Stresses for free field ground conditions.....	43
Figure 3.2 Static stresses in a typical element in a slope.....	43
Figure 3.3 Stress condition underneath a building.....	44
Figure 3.4 Typical test results with shear stress reversal and without, after Lee and Seed (1967).....	45
Figure 3.5 Result of cyclic triaxial tests on Sacramento river sands ( $Dr=40\%$ ), after Lee and Seed (1967).....	46

Figure 3.6 Summary of laboratory results for dense sands ( $D_r > 45\%$ ) .....	47
Figure 3.7 Summary of laboratory results for loose samples ( $D_r < 45\%$ ).....	48
Figure 3.8 Shear test results, after Seed (1983) .....	49
Figure 3.9 $K_\alpha$ versus $\alpha$ curve, after Seed (1983).....	50
Figure 3.10 $K_\alpha$ versus $\alpha$ curve, after Rollins (1985) .....	51
Figure 3.11 $K_\alpha$ versus $\alpha$ curve, after Seed and Harder (1991) .....	52
Figure 3.12 Relative density used as a parameter to define type of response .....	53
Figure 3.13 Correlation of $K_\alpha$ , $\alpha$ and the state parameter .....	54
Figure 3.14 Normalized state boundary surface ( after Pillai, 1991).....	55
Figure 3.15 $K_\alpha$ correction factor - Vaid and Chern (1983) data.....	56
Figure 3.16 $K_\alpha$ correction factor - Hyodo et al. (1991 and 1994) data.....	57
Figure 3.17 Steady state line for Dashihe fine sands (after Lee et al., 1992).....	58
Figure 3.18 Dashihe tailings sand cyclic triaxial results summary .....	59
Figure 3.19 Dashihe tailings sand $K_\alpha$ correction factor.....	60
Figure 3.20 $K_\alpha$ correction factor classified according to the state parameter.....	61
Figure 4.1 $K_2$ for different sands, after Seed and Idriss (1970).....	73
Figure 4.2 $G/G_{max}$ versus $\gamma$ curves for sands, after Seed and Idriss (1970) .....	74
Figure 4.3 Influence of confining pressure on the damping ratio, after Seed and Idriss (1970) .....	75
Figure 4.4 Damping ratio versus shear strain for sands .....	76
Figure 4.5 Typical finite element mesh used in the analyses .....	77
Figure 5.1 Typical Acceleration record used in the analyses .....	93
Figure 5.2 Dynamic properties used for the 30°, H= 20 m Finite Slope.....	94
Figure 5.3a Variation of the shear modulus with shear strain .....	95
Figure 5.3b Variation of the damping ratio with shear strain.....	95

Figure 5.4 Stresses in a submerged infinite slope .....	96
Figure 5.5 Shear stress in the horizontal plane for an infinite slope condition .....	97
Figure 5.6 Depth of zone of stress reversal - simplified approach (Ko=0.5) .....	98
Figure 5.7 Depth of zone of stress reversal - simplified approach (Ko=1.0) .....	99
Figure 5.8 Finite element mesh used for dynamic analyses in the infinite .....	100
Figure 5.9 Typical dynamic analysis results - variation of dynamic shear stresses with depth .....	101
Figure 5.10 Comparison of results between the simplified approach and Quad4 (Ko=0.5) .....	102
Figure 5.11 Comparison of results between the simplified approach and Quad4 (Ko=1.0) .....	103
Figure 5.12 Curves to obtain the depth of the zone of stress reversal ( Ko=0.5 ) (Based on Quad4 results).....	104
Figure 5.13 Curves to obtain the depth of the zone of stress reversal ( Ko=1.0 ) (Based on Quad4 results).....	105
Figure 5.14 Initial stresses for the 30°, H=20 m finite slope - $\sigma_x$ contours.....	106
Figure 5.15 Initial stresses for the 30°, H=20 m finite slope - $\sigma_y$ contours.....	107
Figure 5.16 Initial stresses for the 30°, H=20 m finite slope - $\tau_{xy}$ contours.....	108
Figure 5.17 Initial stresses for the 10°, H= 5 m finite slope - $\tau_{xy}$ contours.....	109
Figure 5.18 Initial stresses for the 10°, H=10 m finite slope - $\tau_{xy}$ contours.....	110
Figure 5.19 Initial stresses for the 10°, H=20 m finite slope - $\tau_{xy}$ contours.....	111
Figure 5.20 Initial stresses for the 10°, H=50 m finite slope - $\tau_{xy}$ contours.....	112
Figure 5.21 Initial stresses for the 20°, H= 5 m finite slope - $\tau_{xy}$ contours.....	113
Figure 5.22 Initial stresses for the 20°, H=10 m finite slope - $\tau_{xy}$ contours.....	114
Figure 5.23 Initial stresses for the 20°, H=20 m finite slope - $\tau_{xy}$ contours.....	115

Figure 5.24 Initial stresses for the 20°, H=50 m finite slope - $\tau_{xy}$ contours .....	116
Figure 5.25 Initial stresses for the 30°, H= 5 m finite slope - $\tau_{xy}$ contours .....	117
Figure 5.26 Initial stresses for the 30°, H=10 m finite slope - $\tau_{xy}$ contours .....	118
Figure 5.27 Initial stresses for the 30°, H=50 m finite slope - $\tau_{xy}$ contours .....	119
Figure 5.28 Influence of bedrock depth on the acceleration profile .....	120
Figure 5.29 Influence of the depth of bedrock in the surface acceleration profile .....	121
Figure 5.30 Influence of bedrock depth on the shear stresses profiles .....	122
Figure 5.31 Zones of no shear stress reversal, finite slope 10°, H = 5 m.....	123
Figure 5.32 Zones of no shear stress reversal, finite slope 10°, H = 10 m.....	124
Figure 5.33 Zones of no shear stress reversal, finite slope 10°, H = 20 m.....	125
Figure 5.34 Zones of no shear stress reversal, finite slope 10°, H = 50 m.....	126
Figure 5.35 Zones of no shear stress reversal, finite slope 20°, H = 5 m.....	127
Figure 5.36 Zones of no shear stress reversal, finite slope 20°, H = 10 m.....	127
Figure 5.37 Zones of no shear stress reversal, finite slope 20°, H = 20 m.....	128
Figure 5.38 Zones of no shear stress reversal, finite slope 20°, H = 50 m.....	128
Figure 5.39 Zones of no shear stress reversal, finite slope 30°, H = 5 m.....	129
Figure 5.40 Zones of no shear stress reversal, finite slope 30°, H = 10 m.....	130
Figure 5.41 Zones of no shear stress reversal, finite slope 30°, H = 20 m.....	131
Figure 5.42 Zones of no shear stress reversal, finite slope 30°, H = 50 m.....	132
Figure 5.43 Typical cross section and foundation of Duncan Dam.....	133
Figure 5.44 Zones of no shear stress reversal for maximum reservoir conditions.....	134
Figure 5.45 Zones of no shear stress reversal - simplified approach .....	135
Figure 5.46 Liquefaction extent - Lab method (after Pillai and Salgado, 1993) .....	136
Figure 5.47 Liquefaction extent - Seed's method (after Pillai and Salgado, 1993) ....	137

## **LIST OF TABLES**

Table 2.1 Test procedures for measuring moduli and damping characteristics.....	14
Table 3.1 Summary of laboratory tests on the influence of the initial static shear stress on the cyclic resistance of sands.....	42
Table 5.1 Soil properties infinite slope analysis .....	84



## LIST OF NOMENCLATURE

$a_{\max}$	maximum ground acceleration
CANLEX	Canadian Liquefaction Experiment
CRR	cyclic resistance ratio
CSR	cyclic stress ratio
CSSM	Critical State Soil Mechanics
D	duration
$D_r$	relative density
e	void ratio
g	gravity acceleration (9.8 m/s <sup>2</sup> )
G	shear modulus
$G_0$ or $G_{\max}$	Initial or small strain shear modulus
$G_s$	specific gravity of the solids
$K_\alpha$	Seed's initial shear stress correction factor
$K_2$	soil modulus coefficient
$K_c$	anisotropic stress ratio
$K_0$	coefficient of earth pressure at rest
LSS	limited strain softening
M	$q_{\text{uss}}/p'_{\text{uss}}$
N	SPT blow count per foot penetration
$p'$	mean normal effective stress
$p'_c$	mean normal effective consolidation stress

$p'_{uss}$	mean normal effective stress at USS
Pa	atmospheric pressure
q	deviator stress
$q_{uss}$	deviator stress at USS
$r_d$	stress reduction factor
SH	strain hardening
SPT	Standard Penetration Test
SS	strain softening
T	period
Uc	uniformity coefficient
USS	ultimate steady state
USSL	ultimate steady state line
$V_s$	shear wave velocity
z	depth
$\lambda$	Damping ratio or slope of steady state line in e-log $p'$ space
$\Gamma$	intercept of the steady state line in e-log $p'$ space at $p'=1$
$\nu$	poisson's ratio
$\alpha$	shear stress ratio ( $\tau_{hi}/\sigma'_o$ )
$\beta$	slope angle
$\Psi$	state parameter
$\gamma$	unit weight of soil
$\gamma'$	submerged unit weight of soil

$\sigma'_1$	mayor effective principal stress
$\sigma'_3$	minor effective principal stress
$\sigma'_c$	effective consolidation stress
$\sigma'_h$	effective stress in horizontal direction
$\sigma'_m$	effective mean confining pressure
$\sigma'_o$	initial effective stress
$\sigma'_v$	effective stress in vertical direction
$\varepsilon_a$	axial strain
$\tau_{cyc}$	cyclic shear stress
$\tau_{dyn}$	dynamic shear stress
$\tau_{hi}$	initial shear stress acting on the horizontal plane
$\tau_{sta}$	static shear stress
$\gamma_t$	total unit weight of soil
$\varepsilon_v$	volumetric strain

# Chapter 1

## General Introduction

### 1.1 Purpose of the Investigation

For the past 25 years the area of liquefaction of soils due to cyclic loading has been intensively studied. The problem of liquefaction of soils involves several aspects and considerations. A number of different approaches have been proposed to calculate the liquefaction potential of soil deposits, all of them attempting to represent in the most realistic way the true field conditions. Most liquefaction analysis procedures make the assumption that the sand deposit is under horizontal free-field ground conditions. Under such conditions a soil element would have no initial or static shear stress on the horizontal plane, and when subjected to earthquake loading the element will undergo through fully reversed cycles of shear stresses (Seed and Lee, 1966; Finn et al., 1971). However, there are many practical situations in which initial static shear stresses act on the horizontal plane of the soil element (e.g. dams, slopes, near buildings, etc.). For these elements it is possible that no shear stress reversal occurs, depending mainly on the relative magnitude between the dynamic shear stresses induced and the initial static shear stress. Shear stress reversal will only occur if the dynamic shear stress is greater than the initial static shear stress. The response of cohesionless soils to cyclic loading is strongly influenced by whether or not shear stress reversal takes place (Yoshimi and Oh-oka, 1975; Vaid and Chern, 1983; Vaid and Finn, 1979). Seed and his co-workers suggested the use of a correction factor ( $K_\alpha$ ), based on cyclic laboratory tests, to include the influence of the initial static shear stress into their design procedure (Seed, 1983 and Seed et al., 1984). Cyclic laboratory tests carried out to evaluate  $K_\alpha$  have usually been cyclic triaxial tests on anisotropically consolidated samples (e.g. Lee and Seed, 1967; Castro et al., 1982; Vaid and Chern, 1985) or cyclic simple shear tests with an initial static shear stress (e.g. Vaid and Finn, 1979). Most laboratory results, considered the relative density as an initial state parameter to define its undrained response. Under this assumption results indicate that for dense samples the cyclic liquefaction resistance increases with increasing initial static shear stress. The opposite trend appears to be true for loose samples. However, laboratory

results have shown a considerable scatter when their initial states (after consolidation) are classified according to their relative density, and not all the laboratory results tend to follow the general trends established for the two major groups (loose and dense samples). Relative density can be regarded as a state parameter for certain sands under relatively low confining pressures, but for higher confining pressures and shear stresses, and particularly for angular sands, it fails to be an independent state parameter (Vaid and Chern, 1985). Analyzing the phenomena under the framework of Critical State Soil Mechanics (CSSM) suggests that the initial state of the soil in terms of stress and void ratio, with respect to the ultimate steady state (USS) governs the type of response (contractive or dilative) under loading. Pillai (1991) suggested the use of the initial state parameter,  $\psi$ , defined by Been and Jeffries, (1985) as a fundamental governing parameter, and proposed that laboratory results should be classified according to this parameter and not just based on the relative density. One of the goals of this research is to review the available laboratory data and evaluate them under a CSSM framework in an effort to better characterize the cyclic behavior of sands when subjected to initial static shear stress.

The seismic liquefaction problem can be divided into two types; cyclic liquefaction (or cyclic softening) and cyclic mobility (Robertson, 1994). For each type of seismic liquefaction the soil response is essentially different, and the design approach should be modified accordingly. The fundamental difference between cyclic liquefaction and cyclic mobility is the occurrence of shear stress reversal or not. For the case of cyclic liquefaction, shear stress reversal occurs and the effective confining pressure can drop to zero (if sufficient loading is applied) and large deformations can develop. On the other hand for cyclic mobility no shear stress reversal occurs, therefore the condition of zero effective stress never develops, and smaller deformations are experienced. Since each phenomena is completely different, the design process should aim to differentiate clearly what type of liquefaction is occurring. Unfortunately, for the practitioner there are no clear guidelines regarding the extent of the zones where shear stress reversal occurs in typical sloping ground situations. The main goal of this research is to provide useful guidelines, for the practitioner, of the extent of the zones of no shear stress reversal, for

different types of slope geometries, when subjected to different magnitudes of earthquakes. Hence, different design considerations can be used in the different zones of the slope, to represent in a more realistic way the true field conditions.

## **1.2. Organization of Thesis**

In chapter 2 a review of the most relevant concepts of CSSM applied to cohesionless soils is presented. The liquefaction phenomena is described and its terminology defined. The typical liquefaction analysis procedure used in practice is discussed. Chapter 2 also includes a review of the cyclic behavior of sands and the dynamic properties required for dynamic numerical analysis.

Chapter 3 reviews the existing cyclic laboratory test data with initial static shear stresses. The first part of the chapter presents the data using relative density as the parameter to define state. The final portion of the chapter focuses on Pillai's hypothesis of using the state parameter as a governing fundamental parameter, the available laboratory data is presented using this hypothesis.

The methodology used in the numerical analyses required to obtain the zones of no shear stress reversal is presented in chapter 4. Both the static and dynamic models used are described. A review of numerical modeling considerations for earthquake related problems is given.

Chapter 5 presents a summary of the results of the investigation. The results were classified according to the two types of slope geometries analyzed, the infinite slope and the finite slope. In chapter 6 the overall conclusions are presented and recommendations for further study are given.

## **Chapter 2**

### **Background Information**

#### **2.1 Introduction**

The main goal for this research has been to study the effects that the initial static shear stress has on the resistance to cyclic liquefaction of sands. In order to study the liquefaction of sands it is appropriate to analyze the phenomena under a Critical State Soil Mechanics (CSSM) framework. Using this framework all the soil states will be contained inside a 3 dimensional state boundary surface in a deviator stress  $q = \sigma_1 - \sigma_3$ , effective mean normal stress  $p' = (\sigma'_1 + \sigma'_2 + \sigma'_3)/3$  and void ratio  $e$ , space. In this chapter a brief review of the most relevant concepts regarding CSSM will be presented. The liquefaction phenomena will be defined for cohesionless soils under various types of loading conditions. A section of this chapter deals with the liquefaction terminology used throughout this thesis. The general methodology of a typical liquefaction analysis procedure will be described and how the effects of the initial static shear stress is incorporated into the analysis. The final section of this chapter will review the cyclic behavior of sands, since the dynamic properties are required for subsequent dynamic analysis.

#### **2.2 Critical State Soil Mechanics Concepts**

##### **2.2.1. The Ultimate Steady State of Sands**

The concept of critical or steady state of sands can be of great importance in the design of sand fills and natural sand deposits. The critical state has been defined as the state at which the soil continues to deform at constant stress and constant void ratio (Roscoe et al., 1958) while the steady state of a sand is defined as the state at which any mass of particles will continuously deform at constant volume, constant normal effective stress (constant pore pressure), constant shear stress, and constant velocity. During the process of developing the steady state of deformation the structure is reworked into a flow

structure (Poulos, 1981). It is generally agreed that critical state is the same as steady state. Some controversy exists regarding the uniqueness of the critical/steady state for sands. Poorooshasb (1989) and Been et al. (1991) suggest that the steady state is independent of the stress path followed, and point out that for sands there appears to be little difference between the steady and critical states. The difference appear to lie mainly with the method of measurement. The critical state has usually been measured using drained, strain-rate-controlled tests on dilatant samples, while the steady state typically has used undrained tests on contractive samples. They suggest that for practical purposes the steady/critical state can be considered as the same, although further research is required. In order to unify terminology, the term ultimate steady state (USS) will be used through out this thesis, which will be considered as the same for steady/critical state. The ultimate steady state shall be considered to be reached after a triaxial sample has been strained to large deformations (typically 20% axial strain).

The ultimate steady state line (USSL) is defined as the locus of the ultimate steady state points in the void ratio/stress space. To define the stress state it is convenient to use the stress invariants  $p' = (\sigma'_1 + \sigma'_2 + \sigma'_3)/3$  and  $q = \sigma_1 - \sigma_3$ . Figure 2.1 shows schematically how the USSL varies with void ratio. From this figure we can see how this line projects in the  $p'$ - $q$  plane as a straight line, usually expressed mathematically as  $q = Mp'$ , whereas the projection onto  $p'$ - $e$  plane is a curve. If we plot the USSL as void ratio against the logarithm of effective normal stress ( $p'$ ) or minor effective principal stress ( $\sigma'_3$ ) it results in an approximate straight line, for a given stress range.

### 2.2.2. The State Boundary Surface

It is widely recognized that soil behavior is dependent on the initial state of the soil in  $e$ - $p'$ - $q$  space and the stress path during loading. In this space there are boundary surfaces that define the limits beyond which the stress paths can not go, i.e. all possible states of the soil are within these state boundaries. Figure 2.2 shows a 3-D representation of the state boundaries for a sand, according to CSSM framework. In this figure, three state boundary surfaces are shown. The Roscoe surface and the Hvorslev surface, typically



used also for clays, are described in detail elsewhere (Schofield and Wroth, 1968, Atkinson and Bransby, 1978). Siaden et al. (1985) showed that there is a surface that defines the trigger of collapse and strain softening of loose sands leading to steady state under undrained loading. Further studies were made on the collapse surface by Alarcon-Guzman et al., (1988) and Ishihara et al., (1991), amongst others, confirming the existence of a collapse surface, but all these studies were based on undrained tests. Sasitharan et al., (1993 and 1994) carried out a detailed study of the collapse behavior of loose sands under a variety of loading conditions, using both drained and undrained tests, and suggested the use of the collapse surface as a state boundary surface. This three-dimensional state boundary can be conveniently reduced to a two dimensional plot by normalizing the stresses with the corresponding stresses at the USSL for the same void ratio. Figure 2.3 shows schematically a normalized state boundary and typical undrained stress paths.

The state boundary surface is divided by the USSL into two domains, the contractive and the dilative domains. The dilative domain is bounded by the Hvorslev surface, while the contractive domain is bounded by the Roscoe surface and the collapse surface. All soils regardless of their initial state, upon prolonged loading in shear will ultimately move towards the USSL. The soil depending whether it is in the dilative or contractive domain will exhibit completely different strength - deformation characteristics during shearing. Contractive cohesionless soils are generally of more concern in geotechnical design, since large deformations can result.

To define if a soil is contractive or dilative, depends whether the state of the sand is located to the right or the left of the USSL, in the  $e - \log p'$  space. The degree of contractiveness or dilativeness of a soil depends on the relative location of the state with respect to the USSL. The next section will discuss this in more detail.

### 2.2.3. The state of a sand

In the previous section it was shown that the behavior of soil under any loading is governed by its initial state relative to the USSL. This initial state is usually presented

using a plot of the USSL represented as void ratio against the logarithm of effective normal stress ( $p'$ ), as shown in figure 2.4. From this figure it can be seen that there are two possible approaches to define the initial state of the soil. One would be to use the difference between the insitu void ratio and the corresponding void ratio at the USSL for the same confining pressure. The second would be to use the ratio between the insitu mean effective stress ( $p'$ ) and the mean effective stress at the USSL for the insitu void ratio ( $p'_{cs}$ ). These two approaches are related to each other by the slope of the USSL ( $\lambda$ ). The first approach was proposed by Been and Jeffries (1985) and it was termed the state parameter ( $\psi$ ). Figure 2.4 shows how this parameter is defined. A positive state parameter ( $\psi > 0$ ) would mean that the initial state of the sand is above of the USSL, i.e. in the contractive domain, on the other hand a negative state parameter would imply a dilative behavior of the sample when sheared.

The use of the state parameter method is a very attractive approach, since it combines both the effect of the initial void ratio (or relative density) and the stress level into a single parameter. This approach will be used later in chapter 3, to correlate the cyclic liquefaction resistance of sands with the initial static shear stress level.

### **2.3. Liquefaction phenomena**

The main goal of this research was to study the influence that the initial shear stress has on the liquefaction resistance of sands. A great number of studies have been carried out on the liquefaction of sands. Much controversy and confusion exist in the literature regarding the definition and the consequences of soil liquefaction (Robertson, 1994). Two main methodologies have been used in practice, the cyclic liquefaction methodology (proposed by Seed and his co-workers) and the steady-state approach (e.g. Castro 1969, 1975; Castro and Poulos 1977 and Castro et al., 1982). A brief discussion is presented below, describing both approaches and a set of definitions are presented to clarify what is meant by liquefaction in this research.

Castro et al. (1982) defined liquefaction as: a phenomenon wherein a mass of soil loses a large percentage of its shear resistance, when subjected to undrained monotonic, cyclic or shock loading, and flows in a manner resembling a liquid until the shear stresses acting on the mass are as low as the reduced shear resistance. Liquefaction as defined by Castro implies that the soil will undergo large shear deformations tending towards the ultimate state. Seed et al. (1983), based on extensive cyclic laboratory testing, defined liquefaction as the condition of zero effective confining stress due to cyclic loading. Under this condition the soil becomes very soft and develops large deformations under cyclic loading.

In the previous section the importance of the initial state of the soil on the strength - deformation characteristics was discussed. The response characteristics will vary according to the relative location of the initial state of the soil with respect to the USSL. Figure 2.5, after Robertson, (1994), divides the possible undrained responses into three types, strain softening response (SS), limited strain softening (LSS) and strain hardening (SH), depending on their relative location with respect to the USSL. This figure shows that if the initial state is higher than the ultimate steady state (typically loose to very loose sands), the soil will quickly reach a peak strength followed by strain softening, triggered by what is termed the collapse surface, approaching rapidly the ultimate steady state. However, if the initial state is below the USSL the soil will show a strain hardening behavior at large strains. For soil states above the USSL, but close to the steady state the soil may show initially a limited strain softening behavior, but ultimately will strain harden to steady state.

### 2.3.1. Liquefaction Terminology

The set of definitions presented below were proposed by Robertson (1994) for liquefaction phenomena. The author divided the liquefaction problem into two main types, one is Flow liquefaction and the second is Cyclic softening. These definitions are as follows:

- **Flow liquefaction**: This requires a strain softening response under undrained loading resulting in ultimate steady state. It requires that the insitu shear stress is greater than the undrained residual or steady state strength. It can be triggered by either monotonic or cyclic loading. A sufficient volume of material with strain softening characteristics must exist in the soil structure in order for failure to occur. If the volume of strain softening material is limited then the deformations are usually contained. The resulting deformations in both cases can continue after the trigger event.
- **Cyclic Softening**:
  - **Cyclic Liquefaction**: This occurs under cyclic undrained loading, where the insitu static shear stress is low compared to the cyclic shear stress, i.e. shear stress reversal occurs. It also requires sufficient cyclic loading to allow the effective confining pressure to essentially reach zero. At this point if any shear stress is applied large deformations are developed. These deformations stop when the cyclic loading ends. It can occur in almost all sands, but for very dense sands the duration and magnitude of the cyclic loading should be enough to achieve the condition of zero effective confining stress.
  - **Cyclic Mobility**: Requires undrained cyclic loading, but in this case no shear stress reversal occurs (shear stresses are always greater than zero). In the case of cyclic mobility the condition of zero effective confining pressure does not develop. The deformations experienced are not large and only occur during cyclic loading.

In this research we are mainly interested in cyclic softening. From the above definitions, it can be concluded that the existence of shear stress reversal or not is very important in defining the type of response the soil will have under cyclic loading. For level

or gently sloping ground, shear stress reversal can be expected to occur. Figure 2.6 illustrates the schematic behavior under these conditions. When a soil element reaches the condition of zero effective stress, the stiffness is very low and large deformations occur during the cyclic loading. On the other hand for a soil deposit with steeply sloping ground no shear stress reversal will occur, unless the cyclic loading is very high, and therefore only limited deformations will occur, as shown schematically in figure 2.7.

Based on the above definitions, Robertson (1994) proposed a flow chart to guide the design process in the liquefaction evaluation of a cohesionless deposit. This flow chart is presented in Figure 2.8.

Figures 2.9 and 2.10 further illustrate the important influence that the occurrence of shear stress reversal has on the type of response of a sand under cyclic loading. Figure 2.9 shows typical results of a cyclic simple shear test where shear stress reversal occurs. The sample quickly develops, in a few cycles, large strains and high pore pressures tending towards a state of zero effective stress. On the other hand figure 2.10 shows the results corresponding to a sample where no shear stress reversal occurs. In this case the rate of development of shear strains and pore pressures is much slower and large deformations do not develop. Figure 2.11 compares both types of behaviours. The upper half shows a test with no shear stress reversal, while the lower set of charts shows the results with shear stress reversal. Figure 2.11 clearly illustrates the difference in behaviour depending on the occurrence of shear stress reversal or not.

#### **2.4. Typical Liquefaction Analysis Procedure**

Typically a liquefaction analysis for seismic loading involves three main steps. First, the resistance of the soil to cyclic liquefaction is estimated. Second, the stresses induced by the earthquake are calculated, and third, the induced stresses are compared with the resistance of the soil to cause cyclic liquefaction, to determine if liquefaction would be expected.

To evaluate the cyclic resistance of sands one approach would be to use high quality undisturbed samples, and then by using laboratory testing obtain its resistance to cyclic liquefaction. This approach although probably the most reliable and accurate is expensive and therefore not feasible for all projects. Therefore, a commonly used procedure in practice is to use empirical correlations between penetration tests (e.g. Standard Penetration Test, SPT and Cone Penetration Test, CPT) and the cyclic strength of sands. The SPT- based liquefaction analysis procedures are the most popular among engineers, due to its simplicity. Figure 2.12 shows a typical correlation of the cyclic resistance with SPT blow count (after Seed et al., 1984 and 1985). In this plot the cyclic resistance is represented by the cyclic resistance ratio ( $CRR = \tau_{av} / \sigma'_o$ ) required to cause cyclic liquefaction (i.e. pore pressure ratio,  $r_u = 100\%$ ).  $\tau_{av}$  represents the equivalent uniform cyclic shear stress induced by an earthquake of magnitude 7.5 that could be resisted, and  $\sigma'_o$  is the vertical effective stress. For the abscissas the corrected SPT blow count  $(N_1)_{60}$  is used. This plot is based on a series of case histories of various earthquake affected sites with approximately level ground conditions. The above chart is restricted to clean sands (fines < 5%), an effective confining pressure not greater than 100 kPa (1 tsf) and level ground conditions. For these conditions the initial static shear stress, on the horizontal plane, is zero. Therefore, modifications were introduced to allow liquefaction analysis for soil elements at large depths, i.e. high confining pressures, or in slopes, dams, or near buildings with initial static shear stresses on the horizontal plane. Seed et al.(1984) proposed the following expression, to obtain the cyclic resistance of sands, for a more general situation:

$$C.R.R._{\alpha=\alpha} = C.R.R._{\alpha=0} \times K_{\alpha} \times K_{\sigma}$$

where  $\alpha$  is defined as the ratio of the static driving shear stress on a horizontal plane to the initial effective overburden stress (i.e.  $\alpha = \tau_{hi} / \sigma'_o$ ),  $C.R.R._{\alpha=\alpha}$  is the cyclic resistance ratio for the soil elements where there is some initial static shear stress,  $C.R.R._{\alpha=0}$  is the cyclic

resistance ratio for free-field level ground conditions,  $K_\alpha$  and  $K_\sigma$  are correction factors to take into account the effects of the initial static shear stress and the change in confining pressure. In this study the primary interest is in studying the influence of the initial static shear stress. Therefore, major emphasis has been placed on the  $K_\alpha$  correction factor. Studies on  $K_\sigma$  can be found elsewhere (e.g. Seed and Harder, 1990; Pillai and Byrne, 1993). The next chapter will review the  $K_\alpha$  correction factor.

Once the cyclic resistance has been estimated, the next step is to determine the cyclic stress ratio (CSR) induced in the soil deposit by the earthquake loading. This can be done by applying the acceleration record for the design earthquake at the base of a finite element model and compute the induced cyclic shear stresses. Usually the cyclic shear stresses are expressed as a cyclic stress ratio,  $CSR = \tau_{cyc}/\sigma'_o$ . More details on the dynamic analysis will be given in chapter 4.

The final step consists simply of comparing the cyclic resistance ratio, CRR with the cyclic stress ratio, CSR. Ishihara, (1993) suggested to express the liquefaction potential of a sand in terms of a safety factor against liquefaction:

$$F_l = \frac{\frac{\tau_{avrg}}{\sigma'_o}}{\frac{\tau_{cyc}}{\sigma'_o}} = \frac{C.R.R.}{C.S.R.}$$

This safety factor is defined in terms of cyclic liquefaction, since the C.R.R. is based on the resistance that a sand has to achieve the state of zero effective confining stress. It was clear from the previous section that a necessary condition to achieve this state is to have shear stress reversal during cyclic loading. Therefore, it is important to have an understanding of the zones where shear stress reversal is possible within a soil deposit, since, for the zones where no shear stress reversal occurs the above procedure is not valid and the problem should be treated as one of cyclic mobility. A goal of this research was to give some guidelines, on the extent of the zones where no shear stress

reversal would occur within typical slopes, for different magnitudes of earthquakes. These results will be presented and discussed in chapter 5.

## 2.5. Cyclic behavior of sands

A soil under cyclic loading has a non-linear stress-strain relationship, exhibiting hysteresis loops even at small strains (Saada, 1985). Figure 2.13 shows a typical nonlinear hysteretic behavior of soil. To represent this stress-strain relationship, an equivalent elastic solution can be used which requires at least two soil properties, the secant shear modulus and the damping factor. The secant shear modulus,  $G$ , can be defined as the slope of the line determined by connecting the two ends of the cycle (slope line AD), while the damping factor,  $\lambda$ , is defined by the ratio of the area of the hysteresis loop (dissipated energy) to the area of the triangle ODE (elastic energy):

$$\lambda = \frac{A_L}{4\pi A_T}$$

where  $A_L$  is the area of the hysteresis loop and  $A_T$  is the area of the triangle. Also, as the number of cycles of load increases the modulus decreases. This is usually referred as modulus degradation due to cyclic loading. Therefore, we need to include some kind of relationship that allows the shear modulus to decrease with strain amplitude. Figure 2.14 shows schematically the nature of the variation of the shear modulus with strain. It is clear from this figure that shear modulus decreases as the shear strain increases. Tests have also shown that the damping factor is also strain dependent. In order to adjust these properties to the strain levels it is necessary to obtain the variation of these properties with strain. For shear modulus these curves are usually presented in normalized form with respect to the initial or small strain shear modulus ( $G_{max}$ ). The damping factor also varies with shear strain. These relationships are required as input data in the computer analysis when using the equivalent linear analysis approach, and they can be derived from laboratory tests. In chapter 4 we will present a summary of the most commonly used relationships and curves to estimate the dynamic properties of sands. For large projects it is recommended to carry out laboratory tests on representative samples, to measure the dynamic soil properties.

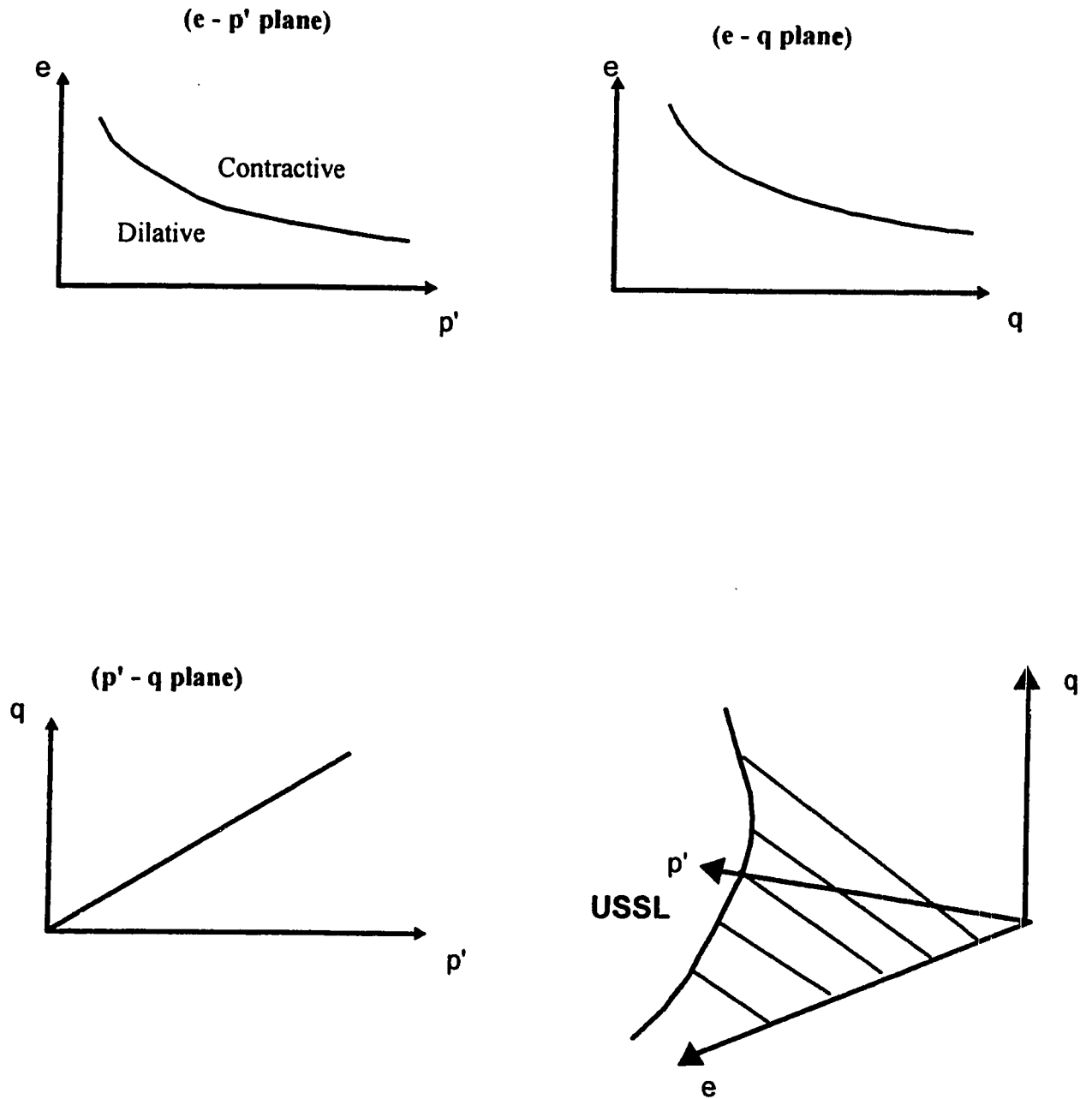


Table 2.1 summarizes the different techniques commonly used in these kind of measurements.

**Table 2.1 Test Procedures for Measuring Moduli and Damping Characteristics<sup>1</sup>**

<b>General Procedure</b>	<b>Test Condition</b>	<b>Approximate Strain Range</b>	<b>Properties Determined</b>
Determination of hysteretic stress-strain relationships	Triaxial compression	$10^{-2}$ to 5%	Modulus; damping
	Simple shear	$10^{-2}$ to 5%	Modulus; damping
	Torsional shear	$10^{-2}$ to 5%	Modulus; damping
Forced vibration	Longitudinal vibration	$10^{-4}$ to $10^{-2}\%$	Modulus; damping
	Torsional vibration	$10^{-4}$ to $10^{-2}\%$	Modulus; damping
	Shear vibration-Lab	$10^{-4}$ to $10^{-2}\%$	Modulus; damping
	Shear vibration-field		Modulus
Free vibration tests	Longitudinal vibration	$10^{-3}$ to 1%	Modulus; damping
	Torsional vibration	$10^{-3}$ to 1%	Modulus; damping
	Shear vibration-Lab	$10^{-3}$ to 1%	Modulus; damping
	Shear vibration-field	$10^{-3}$ to 1%	Modulus
Field wave velocity measurements	Compression waves	$\approx 5 \times 10^{-4} \%$	Modulus
	Shear waves	$\approx 5 \times 10^{-4} \%$	Modulus
	Rayleigh waves	$\approx 5 \times 10^{-4} \%$	Modulus
Field seismic response	Measurements of motions at different levels in deposit		Modulus; damping

<sup>1</sup>After Seed and Idriss, 1970 (Table 1).



**Figure 2.1 Schematical Representation of the Ultimate Steady State Line**

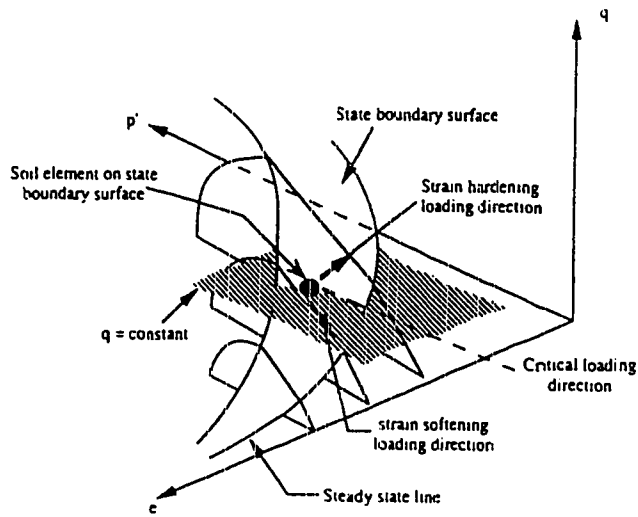


**Figure 2.2 Three Dimensional Representation of the Steady State Boundaries for Sands, after Sasitharan et al. (1994)**

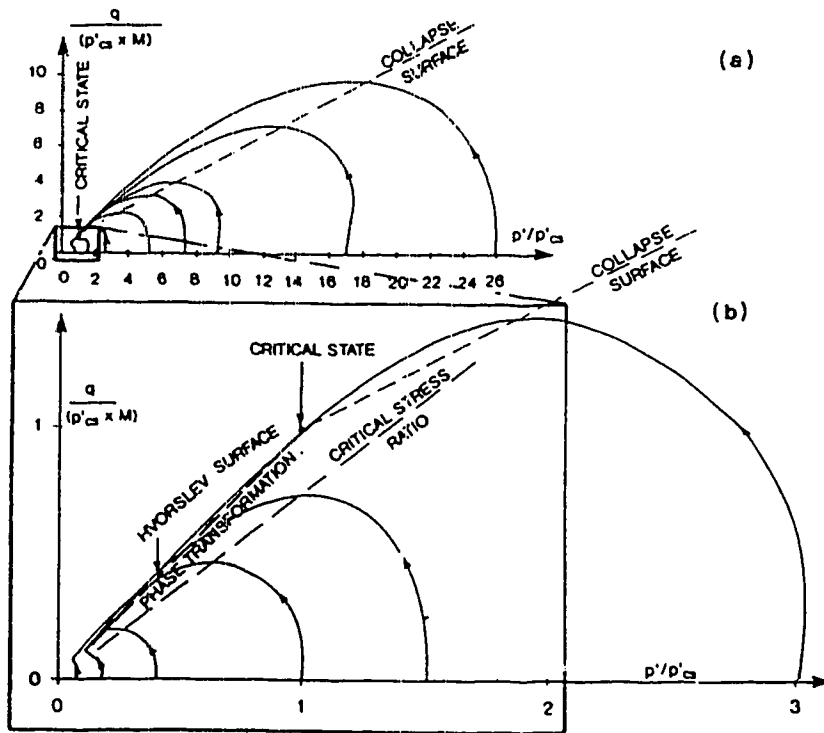


**Figure 2.3 Normalized Steady State Boundary Surface, after McRoberts and Sladen (1992)**

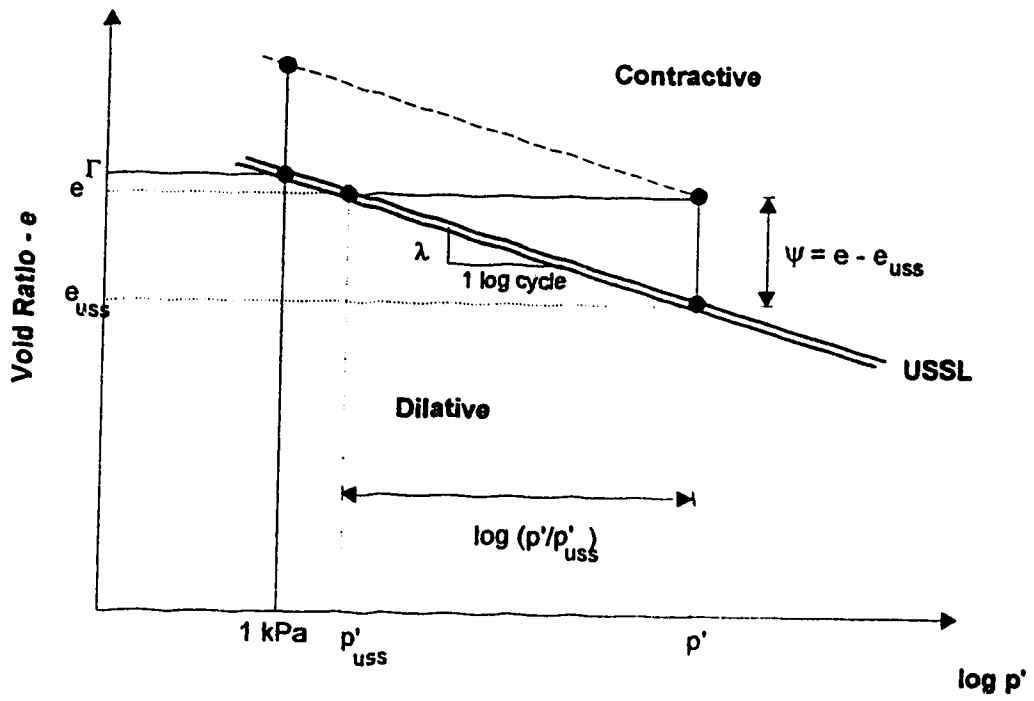
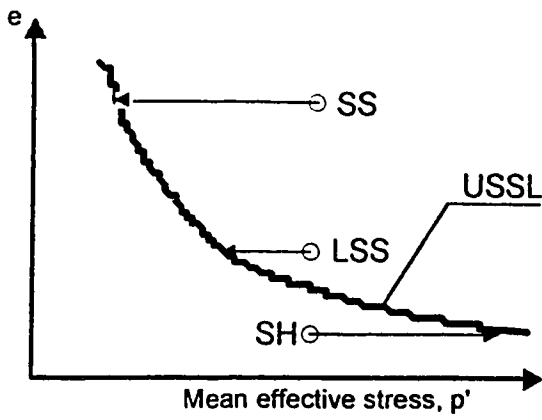


**Figure 2.4 Definition of the State Parameter,  $\psi$**



**Notation:**

- SS: Strain softening response
- SH: Strain hardening response
- LSS: Limited strain softening response
- q<sub>st</sub> : Static gravitational shear stress
- S<sub>u</sub> : Ultimate undrained steady state shear strength
- USS: Ultimate Steady state

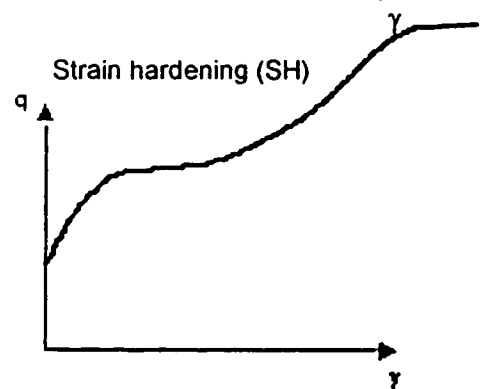
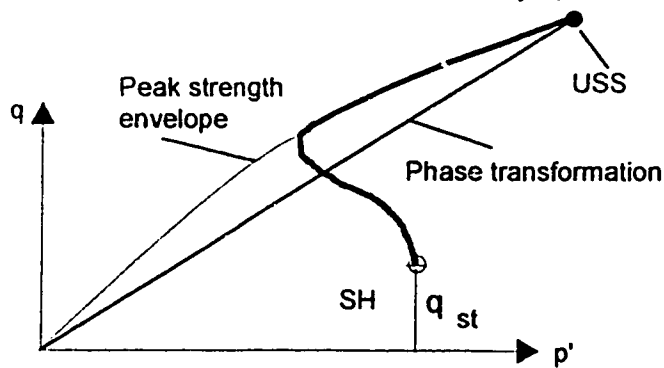
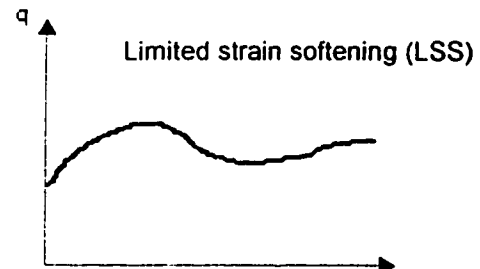
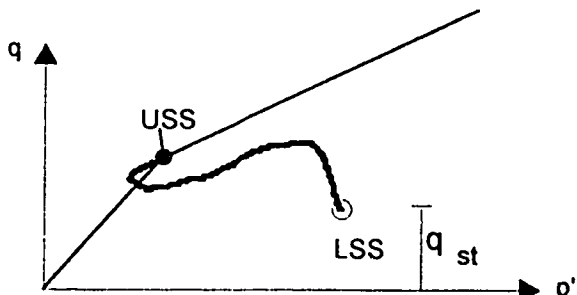
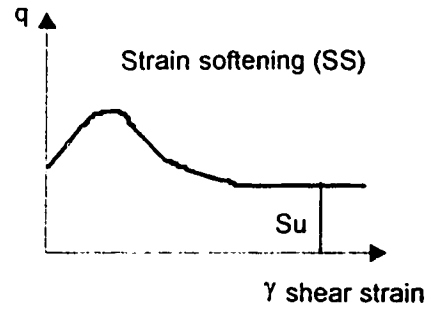
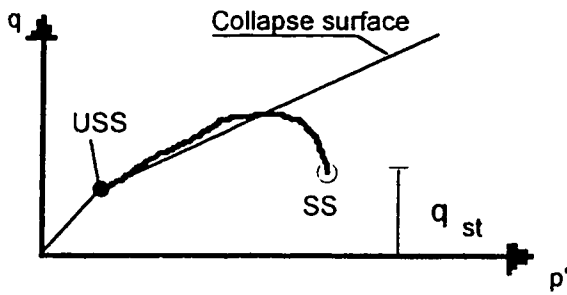


**Figure 2.5 Schematic behaviour of a cohesionless soil in monotonic undrained loading (after Robertson, 1994)**

## LEVEL OR GENTLY SLOPING GROUND

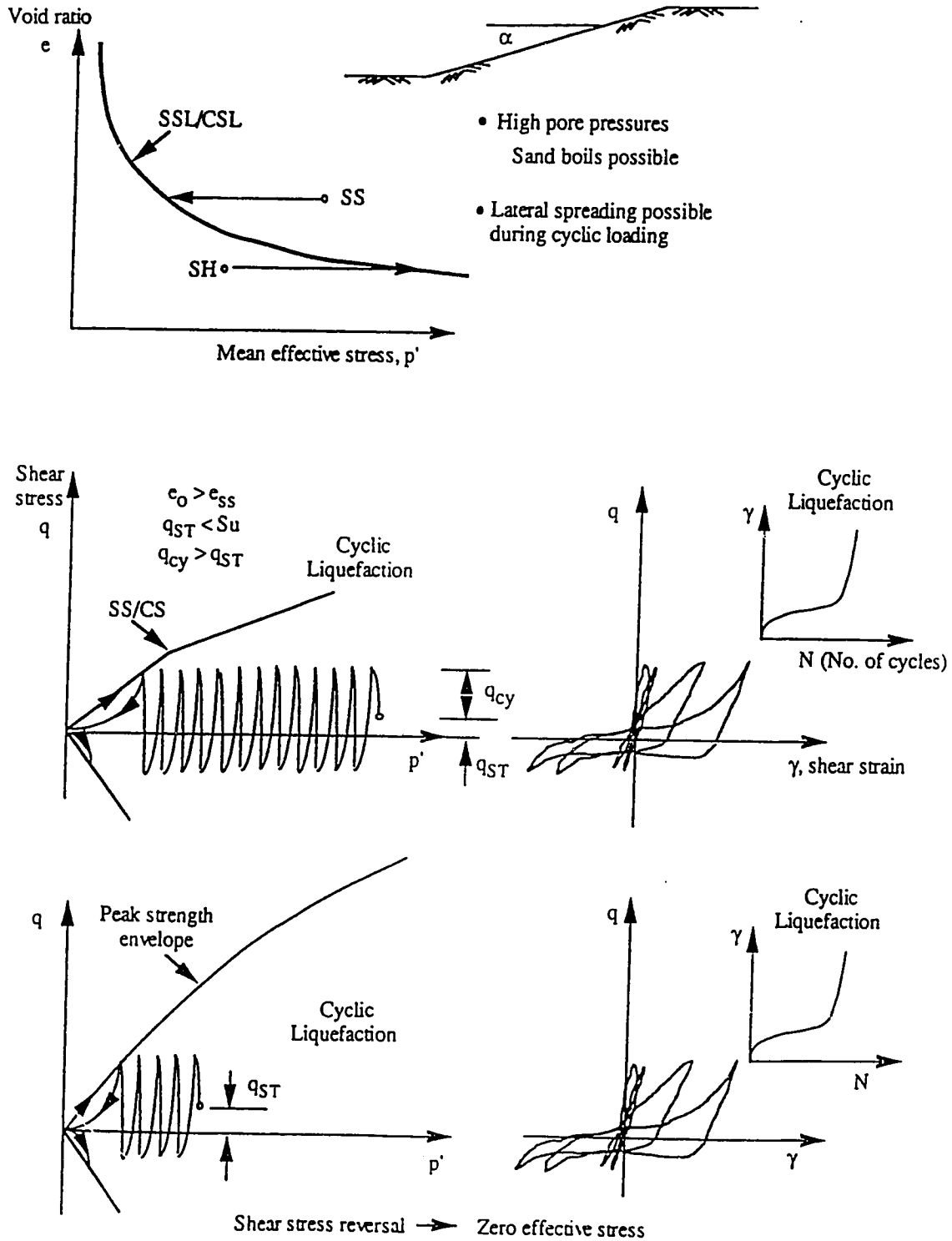


**Figure 2.6 Schematic behaviour of elements of cohesionless soil under cyclic undrained loading in level or gently sloping ground, after Robertson (1994)**

STEELY SLOPING GROUND  
( NO STRAIN SOFTENING SOIL)

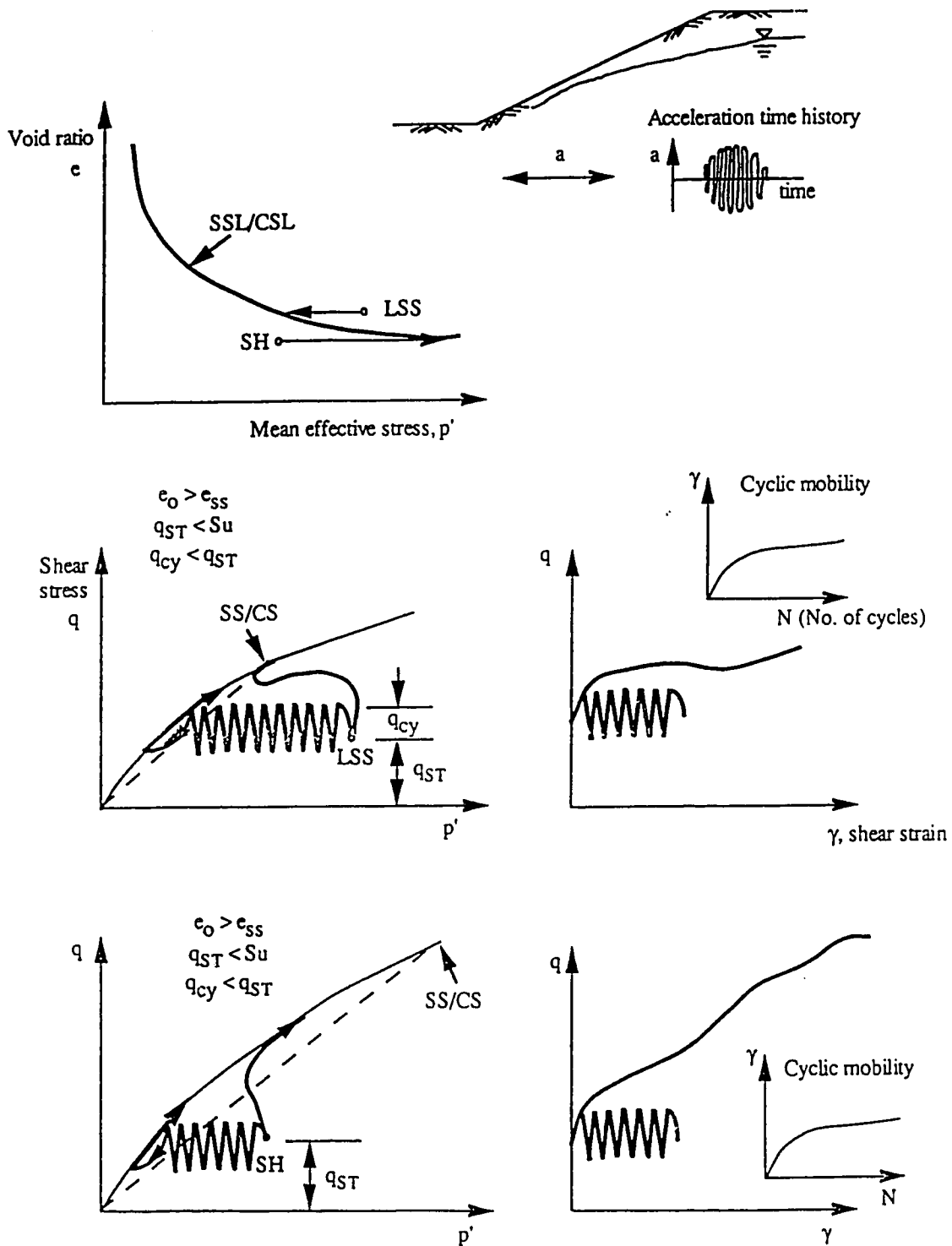


Figure 2.7 Schematic behaviour of elements of cohesionless soil in steeply sloping ground subject to monotonic or cyclic undrained loading, after Robertson (1994)

# FLOW CHART FOR LIQUEFACTION

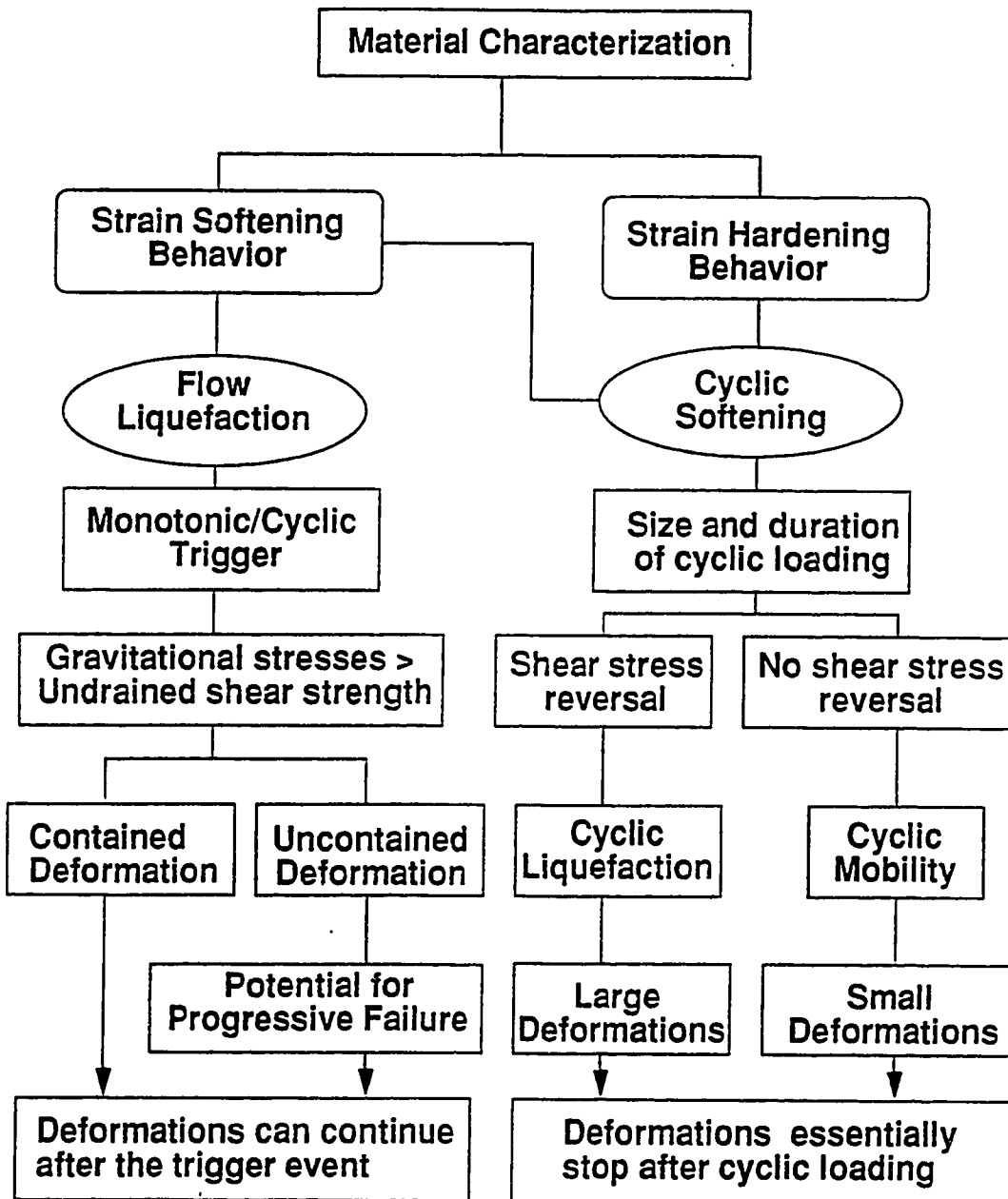


Figure 2.8 Flow chart for evaluation of liquefaction, after Robertson (1994)



CYCLIC SIMPLE SHEAR TEST RESULTS: DD3-S1

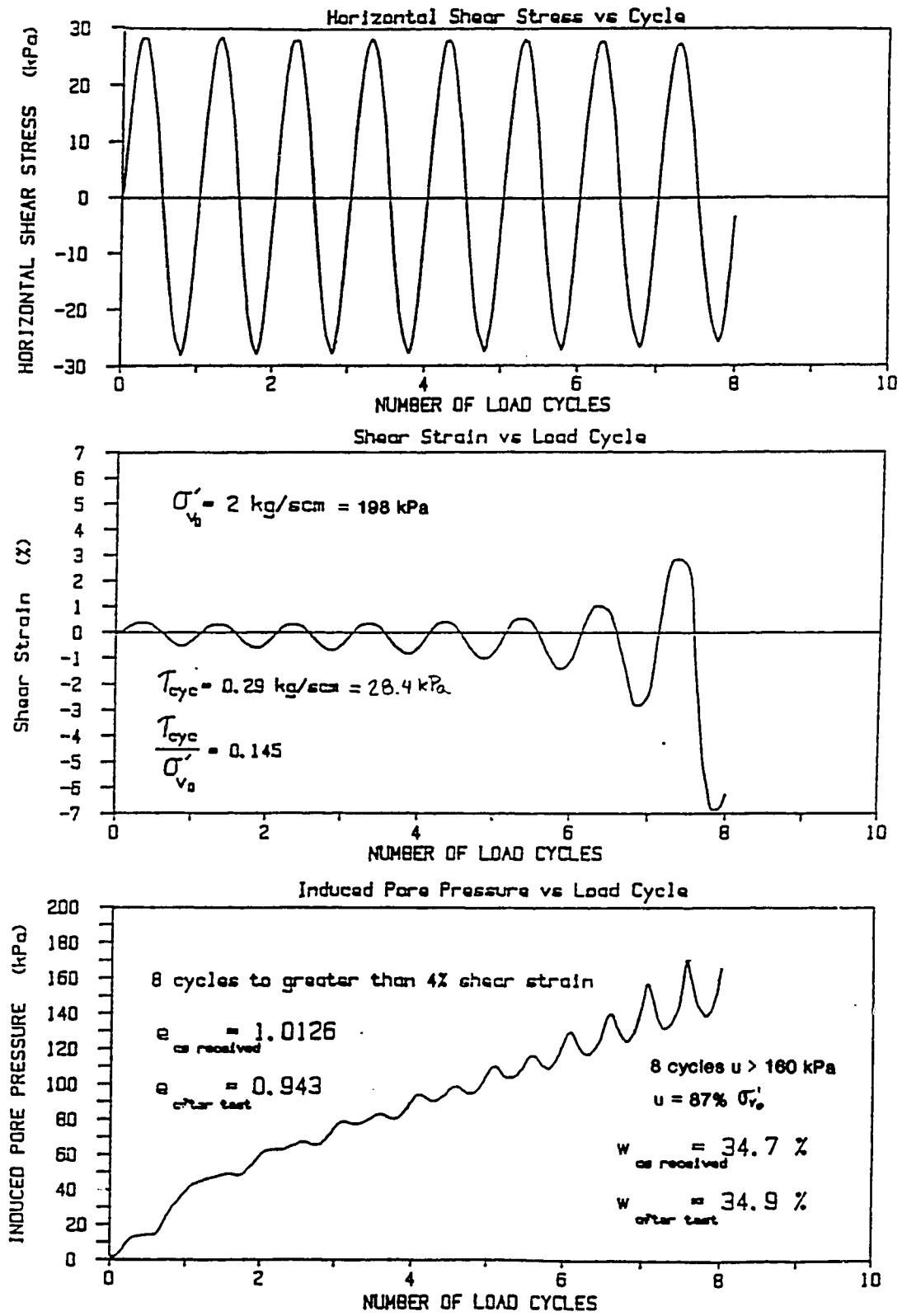


Figure 2.9 Typical Results of a Cyclic Shear Test with Shear Stress Reversal  
 adapted from Lee et al. (1993)

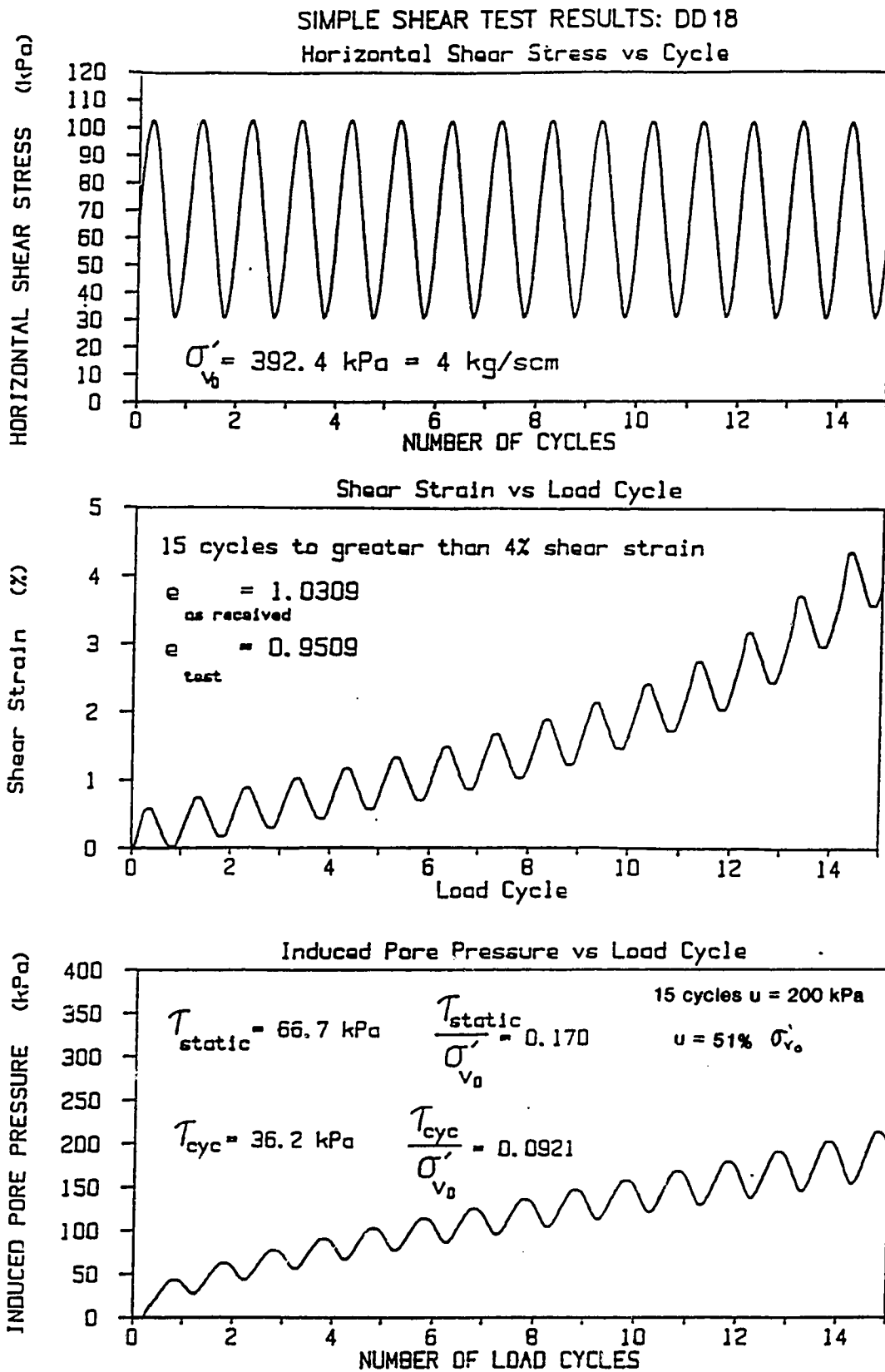
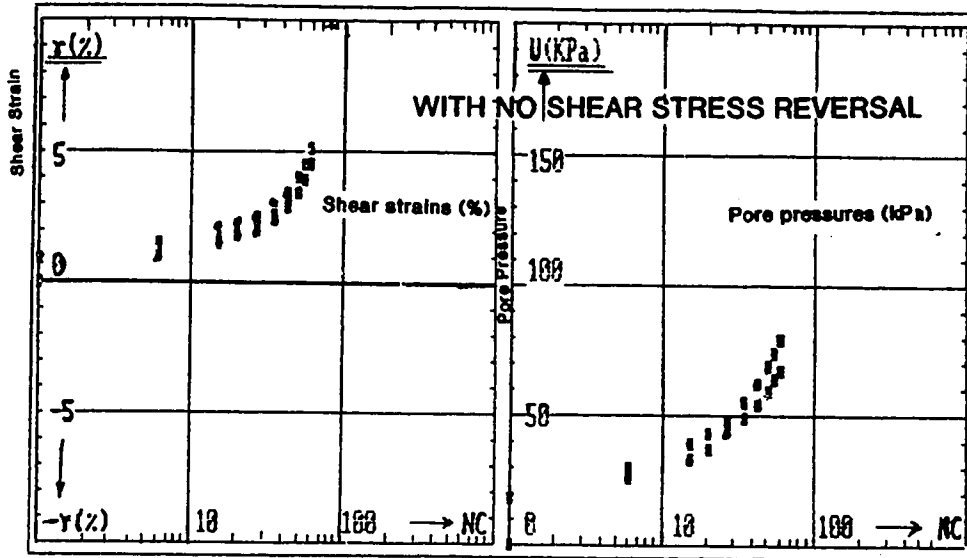


Figure 2.10 Typical Results of a Cyclic Shear Test with No Shear Stress Reversal  
adapted from Lee et al. (1993)

Fine sand  
TEST NO.: A9H4

$\sigma_v = 117.0$  KPa  
 $\rho_d = 1.58$  g/cc

$\tau_{AD} = 14.2$  KPa  
 $N(5\%) = 60$



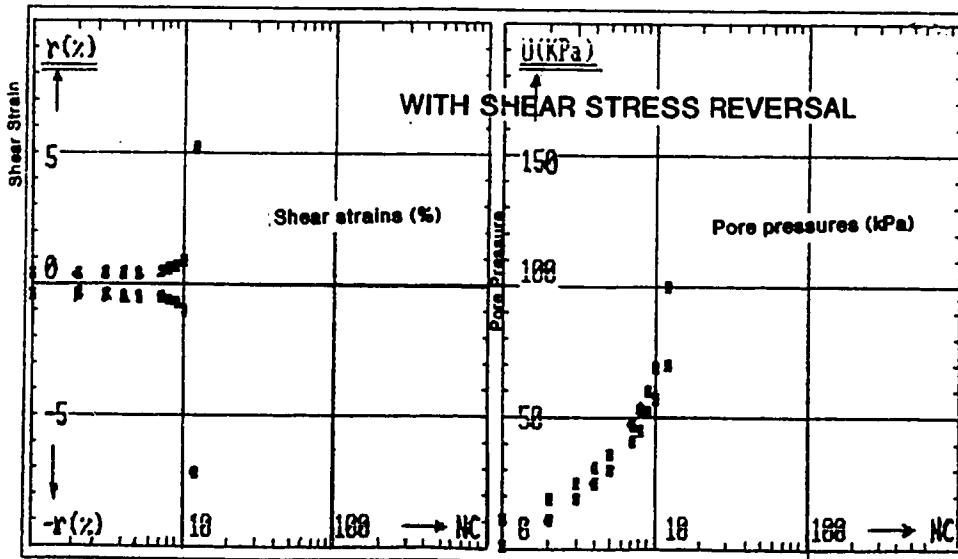
NORMAL CONFINING STRESS= 117.0 KPa  
STATIC SHEAR STRESS= 21.0 KPa

STATIC SHEAR STRAIN(%)= 0.54  
DATAFILE NAME: sf1.103

Fine sand  
TEST NO.: A9S5

$\sigma_v = 100.0$  KPa  
 $\rho_d = 1.59$  g/cc

$\tau_{AD} = 19.9$  KPa  
 $N(5\%) = 12$



NORMAL CONFINING STRESS= 100.0 KPa  
STATIC SHEAR STRESS= 0.0 KPa

STATIC SHEAR STRAIN(%)= 0.00  
DATAFILE NAME: sf1.104

Figure 2.11 Typical Comparison of Results of Cyclic Shear Tests  
adapted from Lee et al. (1993)

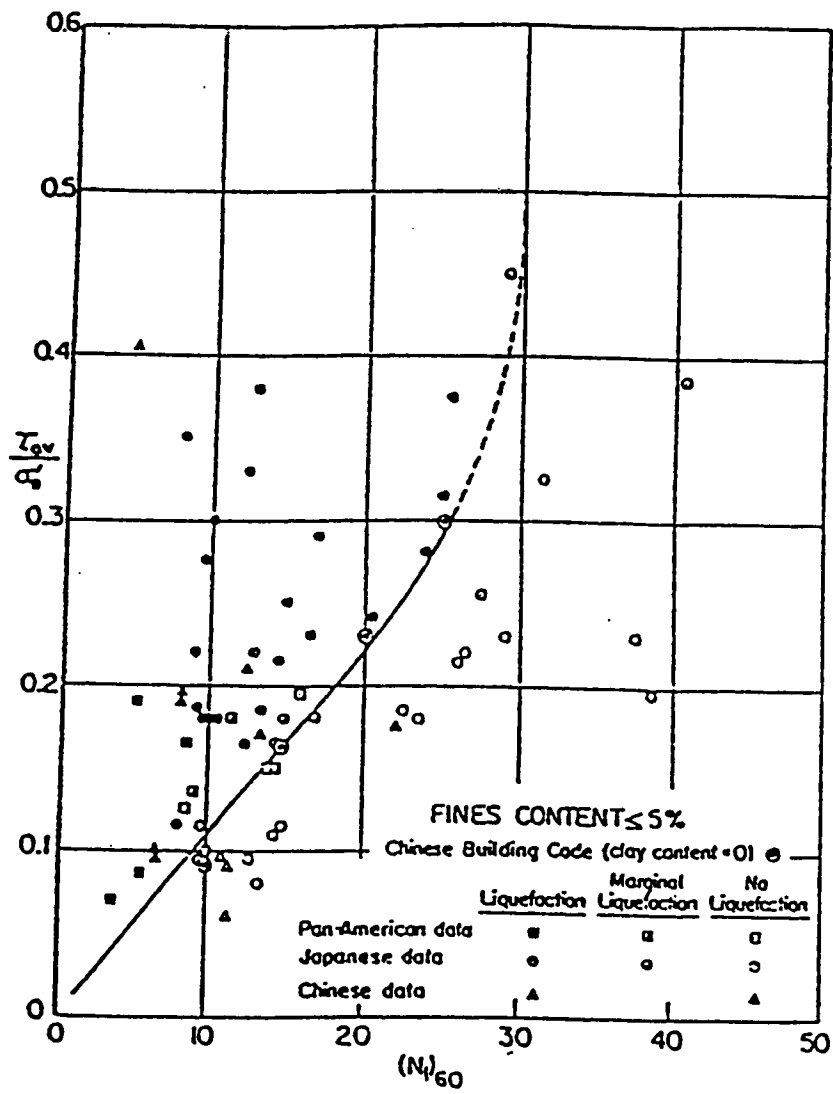
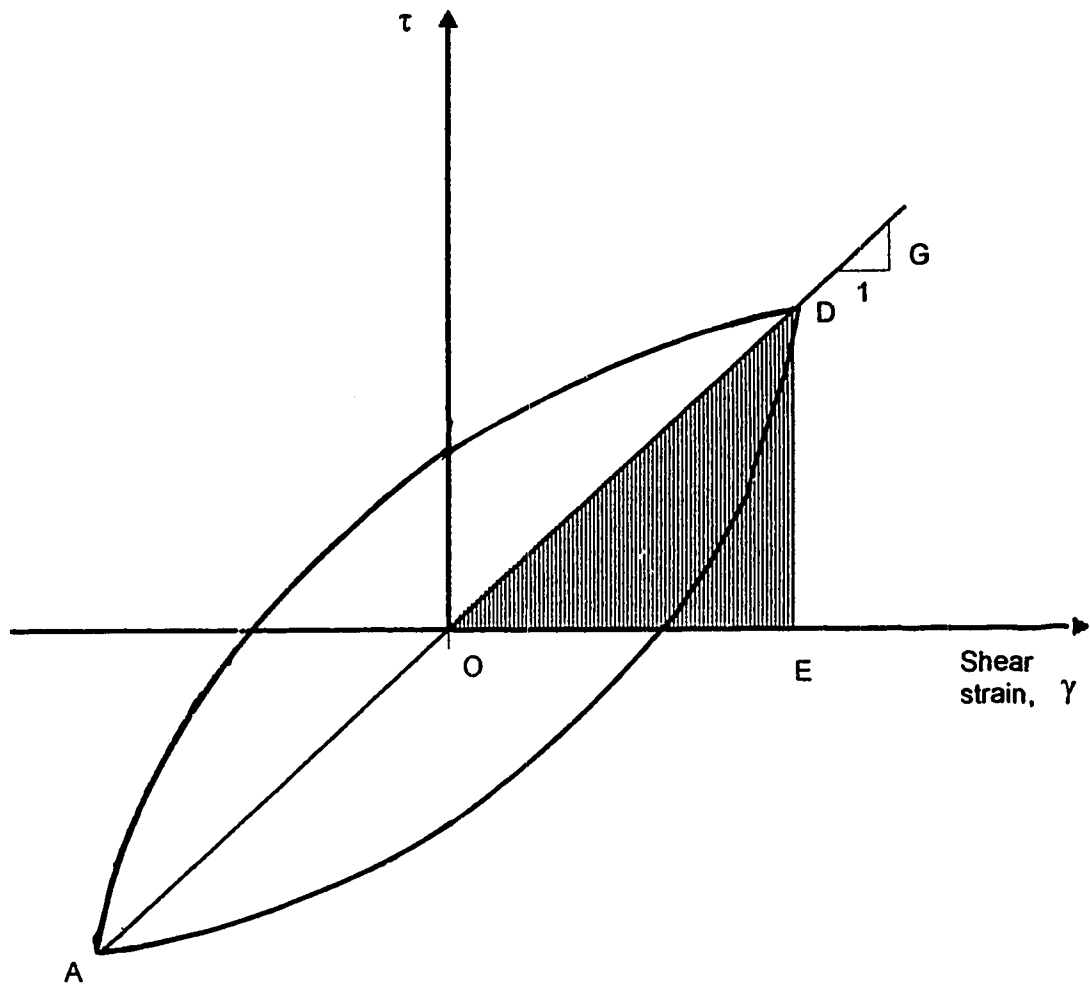
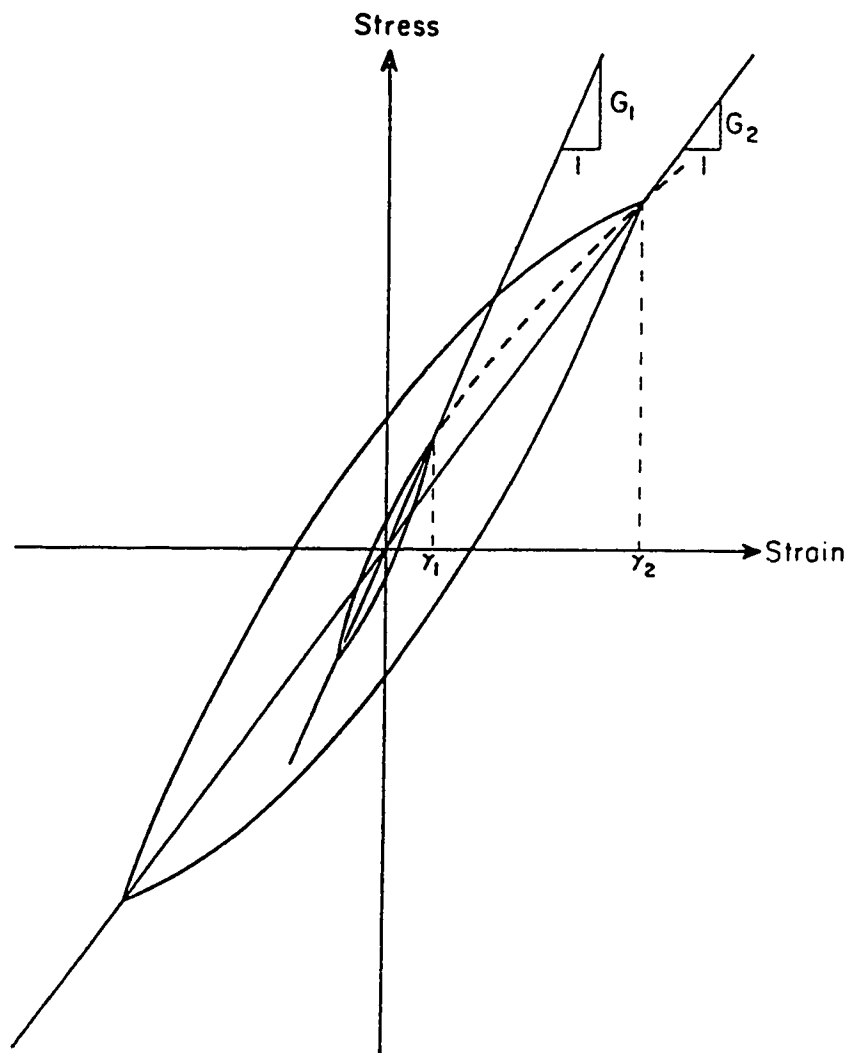


Figure 2.12 Correlation between the Cyclic Resistance Ratio and SPT  $(N_1)_{60}$   
 (After Seed et al. 1984)



**Figure 2.13 Typical hysteresis loop for a soil during cyclic loading**



**Figure 2.14 Variation of the Shear Modulus with strain amplitude, after Seed and Idriss (1970)**

## Chapter 3

### Influence of Initial Static Shear Stress on Cyclic Liquefaction Resistance

#### 3.1 Introduction

Generally liquefaction analyses are made for free field level ground conditions. For this type of situation a soil element would have an insitu state of stress as shown in figure 3.1a. When the soil deposit is affected by earthquake loading the soil element will be subjected to cyclic shear stresses, generated by the vertically propagating shear waves propagating upwards. Figure 3.1b shows the soil element under the dynamic shear stresses  $\tau_d$ . It is clear from these two figures that the soil element goes through complete shear stress reversal, on the horizontal plane, during the earthquake. However, this condition of full shear stress reversal would only be applicable to soil elements in the free field level ground condition (i.e. far away from the influence of nearby buildings) or underneath the axis of symmetry of the building. For situations different from the above, such as in dams, slopes, embankments or near buildings, it is clear that there is an initial static shear stress on horizontal planes of soil elements. Figures 3.2 and 3.3 show typical soil elements for the case of a slope and adjacent to a building, respectively. For these types of elements the initial static shear stress is superimposed on the dynamic shear stresses and depending on the relative magnitude reversal or non-reversal of cyclic shear stresses can occur.

The influence of the initial static shear stress on the cyclic liquefaction resistance is clear from field evidence. Probably the best example is the 1964 Niigata earthquake, in Niigata, Japan, where several hundred structures were damaged due to cyclic liquefaction of the saturated sandy soils in the area (Watanabe, 1966). This dramatic experience clearly illustrated the influence of initial static shear stresses (buildings) on the liquefaction process. Other cases were noted during the 1960 Chilean earthquake, where large settlements and lateral displacements of foundations occurred (Duke and Leeds, 1963). Studies on the slide in the Lower San Fernando Dam (Seed et al., 1973) and the Sheffield Dam (Seed, 1968) also provided evidence of the influence of the initial static shear stress.

### **3.2 Summary of previous laboratory investigations**

Many laboratory studies have been performed to study cyclic liquefaction for level ground conditions (e.g. Seed and Lee, 1966, Seed et al., 1971, etc). The main factors, found by these studies, to influence the cyclic behavior of sands are:

- Relative density,  $D_r$
- Confining stress
- Consolidation stress (stress history)
- Cyclic shear stresses
- Grain characteristics
- Period under sustained loading
- Prior strain history
- Soil structure
- Lateral earth pressure coefficient

A good review of these laboratory investigations can be found in Finn, (1981). The first laboratory investigation done to study the influence of the initial static shear stress was performed by Lee and Seed, (1967). Similar studies have followed. In the following sections a summary of some of the most relevant studies will be presented. The studies are divided into two groups, those that tested Dense or Dilative sands (i.e.  $D_r \geq 45\%$ ) and those studies that tested Loose or Contractive sands (i.e.  $D_r < 45\%$ ).

#### **3.2.1 Studies done in Dense Sands**

Several studies have been carried out on dense sands. Most of the results tend to indicate that the cyclic liquefaction resistance, i.e. the cyclic resistance ratio, tends to increase with increasing initial stress ratio. A summary of the most representative results are presented in the following sections.



### 3.2.1.1. Lee and Seed, 1967:

Lee and Seed (1967) studied Sacramento River sand samples at relative densities between 40 to 80%. Undrained cyclic triaxial tests on anisotropically consolidated saturated samples were performed (ACU-C tests). They concluded that the effective stress in the sample did not drop to zero unless the peak cyclic stress was greater than the initial deviator stress, i.e. shear stress reversal occurs. If there was no reversal, the sample would continue to strain with every cycle of load, but there was no rapid strain accumulation or dramatic increase in pore pressure. Figure 3.4 shows two typical test results with reversal and no reversal of shear stresses. The failure criterion adopted was 20% axial strain. Based on this criteria they concluded that the cyclic resistance increases with increasing density, increasing confining pressure and increasing static shear stress, defined in terms of  $K_c = \frac{\sigma'_{1c}}{\sigma'_{3c}}$ . The ratio  $K_c$  is indirectly a measure of the initial static shear stress (see appendix A). Figure 3.5 shows the results of the loosest samples of their study ( $D_r=40\%$ ). These results show how the cyclic resistance to straining (failure criterion 20% axial strain) increased with initial shear stress on the failure plane ( $45^\circ+\phi/2$ ). These results were verified by many subsequent studies (Seed et al., 1973, Vaid and Finn, 1979, Finn and Byrne, 1976, Vaid and Chern, 1983, etc.).

### 3.2.1.2. Vaid and Finn, 1979:

Vaid and Finn (1979) tested Ottawa sand samples in a constant volume simple shear device. Two relative densities were tested; 50% and 68%. The resistance to liquefaction or straining was defined as 5% shear strain in 10 cycles of stress. This definition was selected since, in the presence of initial static shear stress, where no reversal or partial reversal occurred, it was not possible to reach a state of zero effective stress. The confining pressure used in most tests was 200 kPa (2 kg/cm<sup>2</sup>). However for a particular series of tests, corresponding to an initial stress ratio,  $\alpha = 0.093$  and a relative density,  $D_r=50\%$ , the influence of the initial confining pressure was analyzed. The values

of confining pressure used were 200 kPa (2 kg/cm<sup>2</sup>), 300 kPa (3 kg/cm<sup>2</sup>) and 400 kPa (4 kg/cm<sup>2</sup>). It was found that for this range of confining pressures investigated, as long as the initial stress ratio is kept constant, the same cyclic stress ratio will be needed to obtain a fixed amount of strain in a given number of cycles.

#### 3.2.1.3. Vaid and Chern, 1983:

Cyclic undrained triaxial tests were carried out on reconstituted samples of Ottawa Sand. All samples were initially consolidated isotropically to 200 kPa, then by applying a static deviator stress they were anisotropically consolidated under drained conditions until the required anisotropic stress ratios,  $K_c$  were obtained. Two values of  $K_c$  were studied, 1.19 and 1.48. The range of relative densities studied were from 33% to 76%.

For the medium to dense samples it was found that cyclic resistance increased with initial stress ratio. The resistance to liquefaction or straining was defined as a specified amount of axial strain in a given number of cycles. Three levels of single amplitude axial strain were presented in their paper, 1%, 2.5% and 5%.

#### 3.2.1.4. Szerdy, 1985:

Tests were performed on clean, fine uniform sands from the Sacramento River. The minimum and maximum void ratios for this sand were 0.567 and 0.972, respectively. Anisotropically consolidated undrained cyclic triaxial tests were used to characterize their dynamic behavior. The dense samples had relative densities ranging from 45% to 55%. The confining pressures were 50 kPa (0.5 kg/cm<sup>2</sup>), 100 kPa (1 kg/cm<sup>2</sup>) and 200 kPa (2 kg/cm<sup>2</sup>). Failure was defined as 5% single amplitude axial strain in 10 cycles.

### 3.2.1.5. Vaid and Chern, 1985

Both monotonic and cyclic triaxial tests were carried out on angular tailings sands. The samples were reconstituted by water pluviation. The sand had a uniformity coefficient of 1.6,  $e_{max}=1.06$  and  $e_{min}=0.688$ . Two levels of confining stress were used, 1570 kPa (16 kg/cm<sup>2</sup>) and 196 kPa (2 kg/cm<sup>2</sup>).

Failure was defined when cyclic liquefaction occurred and the sample developed 2.5% axial strain in 10 cycles (only tests where shear stress reversal occurred) or when strain softening response was observed (termed limited liquefaction by the authors). The strain softening response was only observed in some contractive samples with low initial confining pressure and high initial static shear stresses.

### 3.2.1.6. Hyodo et al., 1991:

Cyclic triaxial tests on anisotropically consolidated samples were performed. The soil tested was Toyoura Sand, with the following index properties,  $G_s=2.64$ ,  $D_{50}=0.18$  mm,  $U_c=1.2$ ,  $e_{max}=0.973$ ,  $e_{min}=0.635$ . The samples were prepared by air pluviation. All tests were performed at a constant mean principal stress of 100 kPa.

Two relative densities were studied,  $Dr=70\%$  (dense sands) and  $Dr=50\%$  (medium dense sand). A later paper, Hyodo et al., 1994, presents results from the same sand, but in a loose state,  $Dr=35\%$ , these results will be discussed in the section corresponding to loose sands.

The results obtained by the above researchers greatly depend on the degree of shear stress reversal. To facilitate interpretation, the results are classified in three categories, Reversal, No reversal and Intermediate reversal tests. This last category included tests where  $q_{cyc}/q_s$  ranged from 0.9 to 1.1. For tests from the reversal category, large amplitude cyclic axial strains were observed. For the other two categories residual

strains were the dominant factor for failure, sometimes without cyclic liquefaction occurring. The failure criterion chosen to determine the cyclic shear strength, depended on the type of failure, 5% double amplitude cyclic axial strain in ten cycles was the criterion for the tests that reversal occurred. For tests with no reversal, since accumulation of residual strain is the main problem, 5% residual axial strain was chosen as criterion for defining the shear strength.

#### 3.2.1.7. Summary of all data

Figure 3.6 summarizes all the above data presented for dense sands. It can be seen from this figure, that most of the data follows a similar trend of increasing C.R.R. with increasing  $\alpha$ . The tests by Vaid and Chern, (1985), which were carried on dense tailings sands ( $D_r=70\%$ ) at high confining pressure, did not follow the general trend for dense sands. This behavior will be explained in a later section of this chapter.

#### 3.2.2. Laboratory test in Loose Sands

The general trend in loose sands is that the resistance decreases with increasing initial stress ratio. The most relevant data in loose sands will be discussed in the following sections.

##### 3.2.2.1. Yoshimi and Oh-Oka, 1975:

Fine sand from Bandaijima, Niigata was tested at a relative density of 40%. The samples were initially consolidated at an effective vertical stress,  $\sigma'_{z0} = 97$  kPa (0.97 kg/cm<sup>2</sup>). The sands were tested with a ring torsion device. Liquefaction was defined as the instant when a discontinuity was observed in the porewater pressure record. Their conclusion was that the resistance decreased with increasing initial stress ratio,  $\alpha$ .

#### 3.2.2.2. Castro et al., 1982:

Castro et al. tested very loose Banding (Ottawa Silica Co.) sand with a relative density of around 23%. The sand was a subrounded sand,  $e_{\max}=0.82$ ,  $e_{\min}=0.52$ ,  $C_u=1.70$  and  $D_{50}=0.157\text{mm}$ . Cyclic triaxial tests were performed at a confining pressure  $\sigma_{3c}=400$  kPa ( $4\text{ kg/cm}^2$ ).

#### 3.2.2.3. Vaid and Chern, 1983:

The test material and equipment was described in section 3.2.1.3 corresponding to dense samples. The average relative density was 35%. The results for loose samples indicated that the resistance to liquefaction can be lower or higher depending on the level of initial shear stress.

#### 3.2.2.4. Szerdy, 1985:

The samples tested by Szerdy, 1985, also included loose samples with relative densities of 35%. Description of the sand tested and failure criteria used was presented in section 3.2.1.4.

#### 3.2.2.5. Hyodo et al. 1994:

In this paper the authors continue their cyclic characterization of Toyoura sand, presented in Hyodo et al., 1991. In the previous paper, as described in section 3.2.1.5, they studied two relative densities,  $Dr=50\%$  and  $Dr=70\%$ . In this study the same type of tests were performed on loose samples of Toyoura sand, with relative densities ranging from 30 to 40%, mostly 35%. In these tests the samples were consolidated to the same mean principal stress of 100 kPa.

The cyclic shear strength was defined by Hyodo et al.,(1991), as the cyclic deviator stress ratio  $q_{cyc} / p_c'$  required to develop a specified amount of cyclic or residual strain (5%) in a given number of cycles (10). The cyclic shear strength based on this definition tended to decrease with increasing initial static deviator stress, when the initial static deviator stress ratio was above 0.5. Below this value the strength increased with increasing shear stress. This point will be discussed in a later section of this chapter.

#### 3.2.2.6. Summary of results for Loose sands

Most of the tests results on loose sands, show a clear tendency of a reduction of cyclic stress ratio with increasing initial static shear stress ratio. Some tests results show initially a tendency to increase but at higher values of  $\alpha$  they start decreasing. Figure 3.7 shows a summary of all these results.

#### 3.2.3. General remarks

In the above discussion, all the tests results have been classified according to their relative density. In general, we have seen that two trends are expected, one is that  $K_\alpha$  tends to increase with  $\alpha$  for dense sands and the other one is that  $K_\alpha$  tends to decrease with  $\alpha$  for loose sands. Some tests departed from these general trends and in some cases the scatter was quite appreciable. Another very important factor is the fact that different failure criteria were used in the different studies. Table 3.1. summarizes all the tests presented in the previous sections. The different failure criteria obviously complicates the interpretation and comparison of the different results. In a later section of this chapter this same data will be interpreted using a different approach to classify the behavior. It should be kept in mind that it is important to characterize a sand according to its contractive or dilative behavior, i.e. its initial state (defined mainly by the relative density and the confining pressure) with respect to the steady state line.

### 3.3. Seed's $K_\alpha$ correction factor

This section will review the development of the  $K_\alpha$  correction factor proposed by Seed. In 1983 based on the results from simple shear tests (figure 3.8) Seed (1983) suggested that the resistance to cyclic loading increased with increasing static shear (i.e.  $\alpha = \tau_{hi} / \sigma'_o$ ). From these results and other tests done on several sands with relative densities greater than 50%, a graph of  $K_\alpha$  versus initial shear stress ratio was obtained, as shown in figure 3.9.

In 1987, Rollins (1987) summarized laboratory data, and grouped the results in two categories, dense and loose sand samples. This updated version of the  $K_\alpha$  curve is shown in figure 3.10. From this last figure we can see that there is a clear difference from the original  $K_\alpha$  curve, since now there is no positive influence of  $\alpha$  in the C.R.R. for relative densities lower than 45%. Furthermore for relative densities of approximately 45% the liquefaction resistance of a sand, according to Rollins, is unaffected by static shear stresses.

Seed and Harder (1990) suggested a modified relationship as shown in figure 3.11. The authors caution the use of this curve for situations where the effective overburden pressure is larger than 300 kPa (3 kg/cm<sup>2</sup>). For higher pressures the soils will be less dilatant or more contractive, and  $K_\alpha$  will decrease (Seed and Harder, 1990). Hence, the data from Vaid and Chern (1985) corresponding to tailings sand at  $\sigma'_{3c} = 1600$  kPa (16 kg/cm<sup>2</sup>), would not be applicable. In the next section a new correlation proposed by Pillai (1991) will be discussed, in an effort to explain some of the apparent contradictions of the laboratory data.

### 3.4. Interpretation of Seed's $K_\alpha$ correction factor using steady state concepts

As discussed in the previous sections, existing relationships for  $K_\alpha$  have been based on relative density. According to Pillai (1991), basing  $K_\alpha$  on relative density fails to identify the phenomenon correctly. Pillai (1991) suggested using the state parameter ( $\psi$ ) as the controlling parameter. Figure 3.12 shows schematically how a constant relative density ( $D_r$ ) is not sufficient to define the response of the soil, since at low confining pressures soil can be dilative, but at high confining pressure the soil can be contractive.

The review of the available laboratory results presented in section 3.2., showed that a certain scatter in the data exists. For example for the case of dense sands ( $D_r > 45\%$ ), the dominant trend is that the cyclic resistance ratio increases with increasing initial static stress ratio. From table 3.1 we can see that most of the tests were performed at confining pressures in the range of 200 kPa (2 kg/cm<sup>2</sup>), but for higher confining pressures ( $\sigma'_{3c} = 1600$  kPa) we observe that the C.R.R. actually decreases with  $\alpha$  (data from Vaid and Chern, 1985). For the case of loose sands there is also evidence that at low confining pressures the C.R.R. may increase with  $\alpha$  (Lee and Seed, 1967 results).

Recognizing that soil behavior is dependent on its initial state in terms of stress and void ratio, Pillai (1991), proposed the use of the state parameter,  $\psi$  (Been and Jefferies, 1985). Pillai's hypothesis can be expressed in a functional way as follows:

$$K_\alpha = f(\psi_i, \alpha)$$

Pillai's hypothesis consisted mainly in assuming that all soils denser than critical (i.e.  $\psi_i < 0$ ) would be dilative and therefore  $K_\alpha$  would increase with  $\alpha$ . For all contractive soils, i.e. states looser than critical ( $\psi_i > 0$ ),  $K_\alpha$  would decrease with  $\alpha$ . And for all soils at critical state ( $\psi_i = 0$ ), the cyclic resistance would not be affected by the initial static shear stress. If the above is true, there should be a unique function of  $K_\alpha$  and  $\alpha$  for any given  $\psi_i$  (Pillai, 1991). Figure 3.13 shows schematically Pillai's hypothesis.



In order to support his hypothesis, Pillai (1991), used the laboratory results from two type of sands, Sacramento river sand (Szerdy, 1985) and Tailings sands (Vaid and Chern, 1985).

#### 3.4.1. Sacramento river sand (Szerdy, 1985)

Section 3.2.1.4 describes the type of tests and sand used in Szerdy's study. All tests were done at an initial confining pressure of  $\sigma_{3c} = 200$  kPa ( $2 \text{ kg/cm}^2$ ). Szerdy's results confirm that for dilative soils ( $\psi_i < 0$ ),  $K_\alpha$  has a tendency to increase with  $\alpha$ . For the contractive soil ( $\psi_i > 0$ ),  $K_\alpha$  decreases with increasing  $\alpha$ , although for small values of  $\alpha$  ( $\alpha < 0.1$ ),  $K_\alpha$  increases slightly with  $\alpha$ .

#### 3.4.2. Tailings Sand (Vaid and Chern, 1985)

Vaid and Chern performed tests on very dense sands ( $D_r = 70\%$ ). Their experimental data, when plotted in the traditional way, i.e. using relative density as the fundamental governing parameter, did not agree with the general trend of the other data of sands with the same density. Specifically for the case of high confining pressure  $K_\alpha$  decreased with increasing  $\alpha$ . For the series of tests done at a confining pressure of  $\sigma_{3c} = 200$  kPa ( $2 \text{ kg/cm}^2$ ) the state parameter is  $\psi_1 = -0.091$ , on the other hand the tests done at  $\sigma_{3c} = 1600$  kPa ( $16 \text{ kg/cm}^2$ ) the state parameter is found to be  $\psi_1 = +0.175$ . Therefore, although the two sets of tests were done at the same relative density, the test at low confining pressure was dilative ( $\psi_1 < 0$ ) and at large confining pressure the same sand was contractant ( $\psi_1 = +0.175 > 0$ ).

### 3.4.3. Influence of the static shear stress using the state parameter.

To explain the influence of the initial static shear stress on the liquefaction resistance of sand under a critical state soil mechanics framework, Pillai (1991) suggested the use of a normalized plot of the state boundary surface, i.e. a  $q'/p':\psi$  space plot as shown in figure 3.14. In this plot the corresponding shear stress in the  $q' - p'$  space is reduced to a single ordinate. The  $q'/p'$  ratio represents the stress ratio during loading, at any stress level (e.g. initial ( $\alpha$ ), peak or residual). In this same plot the abscissa,  $\psi$  represents the changing states along the effective stress path (Pillai, 1991).

In figure 3.14 it is important to distinguish some key points. The steady state is defined by a single point labeled "S" ( $\psi = 0$ ). Point "C" ( $\psi = \psi_c$ ) represents in this normalized plot the intersection of the state boundary surface with the collapse surface. Point C represents the divide between loose samples that can experience strain softening or "flow liquefaction" (samples very loose of critical,  $\psi > \psi_c$ ), and dense samples where only limited strain softening or "limited liquefaction" may occur ( $0 < \psi < \psi_c$ ). Pillai (1991) suggests that  $\psi_c$  can be represented by what Castro (1969) called the "L line". On the other hand for dilative states ( $\psi < 0$ ) only cyclic mobility is possible.

Figure 3.14 shows how the initial static shear stress ratio affects the response of a sand. For dilative sands the stress paths show increasing peaks (i.e. resistance) with increasing levels of static shear stress. The fact that the resistance increases with increasing  $\alpha$  and/or decreasing  $\psi$  is due to the rising nature of the normalized state boundary surface (Hvorslev surface for  $\psi < 0$ ). For the case of initial state  $\psi = 0$ , all the peaks of the stress paths will be at point "S" (critical state), therefore the C.R.R. remains constant regardless of initial shear stress,  $\alpha$  (Pillai, 1991). However for contractive sands the peaks are limited by the collapse point "C", any increase in initial shear stress,  $\alpha$  would reduce the C.R.R., particularly for initial states  $\psi > \psi_c$ . Unfortunately, most laboratory data available for loose sands falls into the region  $0 > \psi > \psi_c$ , where only limited liquefaction is possible,

this could explain why some curves of  $K_\alpha$  versus  $\alpha$  show an initial flat or slightly raising portion at low values of  $\alpha$  (Pillai, 1991).

In the following sections, other available more recent experimental data will be presented, under this framework, and the method evaluated.

#### 3.4.4. Vaid and Chern (1983) data

The data from Vaid and Chern (1983) was presented in sections 3.2.1.3 and 3.2.2.3 on the base of relative density. In order to use Pillai's framework we must first estimate the initial state parameter for each relative density tested. The steady state line was estimated using average parameters proposed by Cunning (1994), as follows;

$$\Gamma=0.926 \quad \lambda_{in}=0.034 \quad \text{SSL: } e = 0.926 - 0.034 \ln(p')$$

The  $K_\alpha$  versus  $\alpha$  curves for these three states are presented in figure 3.15. It can be seen from this figure that the trend is reasonable compared to the previous data presented. Although figure 3.15 helps to explain why for apparently low relative densities ( $D_r=45\%$ ), there is an increase in  $K_\alpha$  for increasing  $\alpha$ , however,  $K_\alpha$  starts to drop after a certain point opposed to what we would expect.

#### 3.4.5. Hyodo et al. (1991 & 1994) data

This data has been presented in sections 3.2.1.6 and 3.2.2.5. Following a similar procedure the steady state line was estimated using average parameters suggested by Sasitharan et al. (1993) for Toyoura sand:

$$\Gamma=0.938 \quad \lambda_{in}=0.0043 \quad \text{SSL: } e = 0.938 - 0.0043 \ln(p')$$

The three tests fall in the dilative domain ( $\psi < 0$ ), therefore we would expect that the  $K_\alpha$  versus  $\alpha$  curves will show an increasing  $K_\alpha$  with  $\alpha$  tendency. The curves are shown in figure 3.16. For the tests with higher degrees of dilativeness the curves show a behavior as expected. However, for the loosest samples, with an initial state quite close to critical

( $\psi = -0.06 \approx 0$ ), the trend is different and  $K_\alpha$  actually decreases with  $\alpha$  despite the negative initial state parameter.

#### 3.4.6. Dashihe Tailing Sand

A series of laboratory tests were carried out on Dashihe tailings sands (Lee et al., 1992). This sand has a  $D_{50} = 0.19$  mm,  $C_u = 2.95$ ,  $e_{max} = 1.1$  and  $e_{min} = 0.42$ . The corresponding steady state line is shown in figure 3.17. The cyclic triaxial tests were done on sands at an average relative density of 43%. Three sets of test data are presented, each set using a different initial consolidating effective stress,  $\sigma'_{3c} = 50$  kPa, 100 kPa and 200 kPa. Figure 3.18 shows how the cyclic resistance ratio varied with the initial static shear stress ratio, and figure 3.19 shows the  $K_\alpha$  versus  $\alpha$  curves. From figure 3.19 it can be seen that for low state parameters (approaching zero) the curve shows a behavior opposite to what we expected.

#### 3.4.7. Summary

Figure 3.20 summarizes all the data presented in the previous sections using the state parameter as the governing parameter. Unfortunately the scatter is large and the data is limited such that it is not possible to develop average relationships. Although the scatter in results shown in figure 3.20 is large, the trends do appear to fit the hypothesis by Pillai (1991). A major problem with the existing data relates to the uncertainty in the steady state line for of the sand and hence the ability to define the state parameter ( $\psi$ ) correctly. Also, as discussed before, for each of the laboratory studies there have been different criteria to define liquefaction. Many of the studies defined liquefaction as a certain level of deformation after a given number of cycles. Clearly, further research is required to better evaluate the influence of  $\alpha$  on the CRR.

**Table 3. 1 Summary of Laboratory tests on the influence of the initial static shear stress on the cyclic resistance of sands**

Researcher	Sand Type	Grain Description	Test	Relative Density	Confining Pressure	Failure Criteria
Lee and Seed (1967)	Fine Sacramento River Sand	Subrounded to Subangular	ACU-C triaxial	D <sub>r</sub> =38%	$\sigma_{3c} = 5 \text{ kg/cm}^2$ $\sigma_{3c} = 15 \text{ kg/cm}^2$	20 % axial strain in 100 cycles
Yoshimi and Oh-oka (1975)	Bandajjama, Nijigata	----	Ring torsion	D <sub>r</sub> =40%	$\sigma'_{z0} = 2 \text{ kg/cm}^2$	Discontinuity on porewater pressure record
Vaid and Finn (1979)	Ottawa sand	Rounded	Simple Shear	D <sub>r</sub> =50% D <sub>r</sub> =68%	$\sigma'_{v0} = 2 \text{ kg/cm}^2$	5% shear strain in 10 cycles
Castro et al. (1982)	Banding sand	subrounded	ACU-C triaxial	D <sub>r</sub> =20%	$\sigma_{3c} = 4 \text{ kg/cm}^2$	Steady state achieved or until 5% axial strain
Vaid and Chern (1983)	Ottawa sand	Rounded	ACU-C triaxial	D <sub>r</sub> =45% D <sub>r</sub> =55% D <sub>r</sub> =65%	$\sigma_{3c} = 2 \text{ kg/cm}^2$	5% single amplitude axial strain in 10 cycles
Vaid and Chern (1985)	Tailings sand	Angular	ACU-C triaxial	D <sub>r</sub> =70%	$\sigma_{3c} = 2 \text{ kg/cm}^2$ $\sigma_{3c} = 16 \text{ kg/cm}^2$	2.5% axial strain in 10 cycles
Szerdy (1985)	Fine Sacramento River Sand	Subrounded to Subangular	ACU-C triaxial	D <sub>r</sub> =35% D <sub>r</sub> =45% D <sub>r</sub> =55%	$\sigma_{3c} = 2 \text{ kg/cm}^2$	5% single amplitude axial strain in 10 cycles
Hyodo et al. (1991)	Toyoura sand	Subangular	ACU-C triaxial	D <sub>r</sub> =50% D <sub>r</sub> =70%	$p'_c = 200 \text{ kPa}$	5% double amplitude axial strain or 5% residual axial strain
Hyodo et al. (1994)	Toyoura sand	Subangular	ACU-C triaxial	D <sub>r</sub> =35%	$p'_c = 200 \text{ kPa}$	5% double amplitude axial strain or 5% residual axial strain

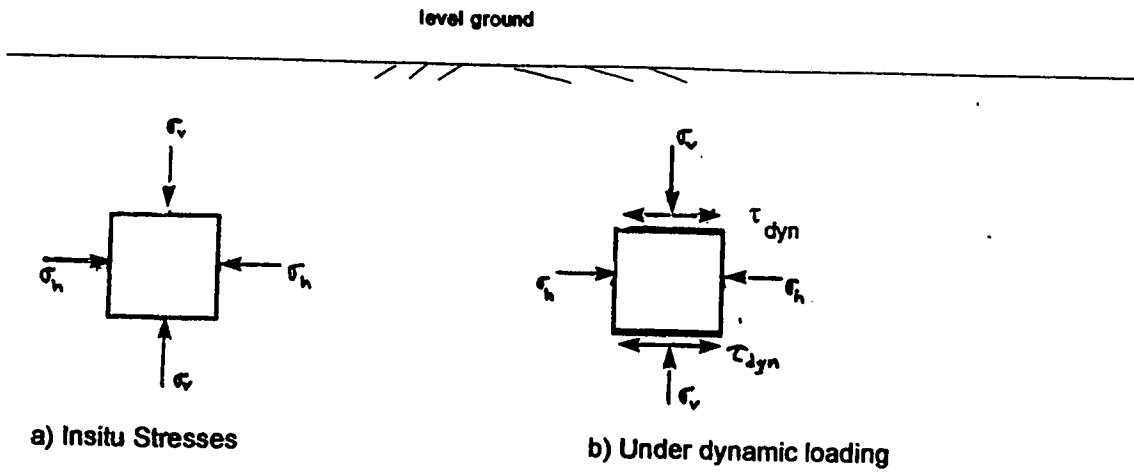


**Figure 3.1 Stresses for Free Field ground Conditions**

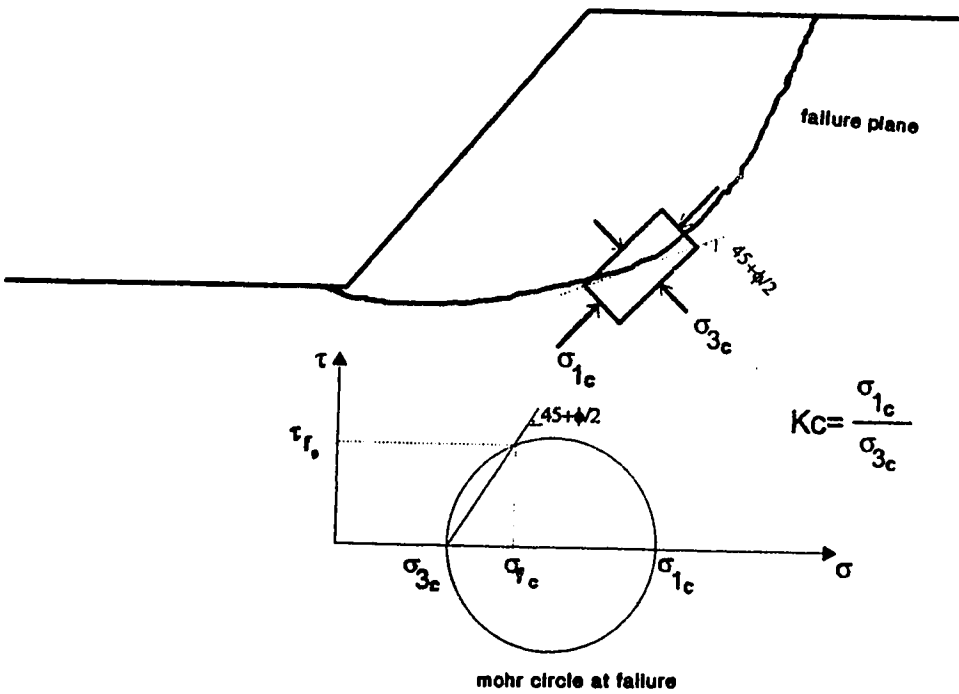
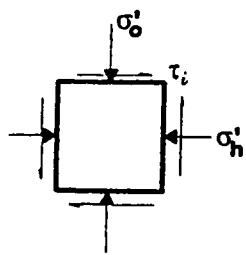
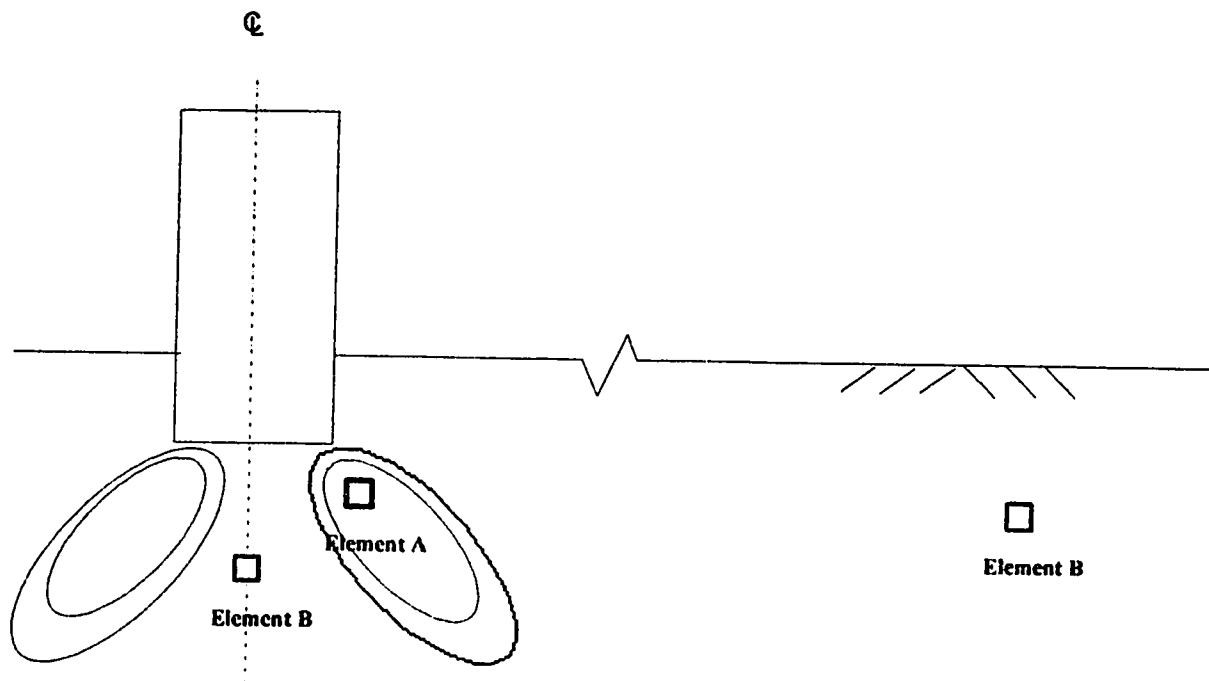
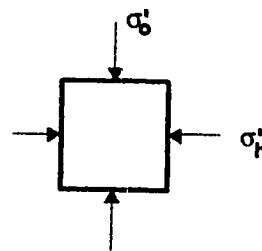


**Figure 3.2 Static Stresses in a Typical element in a Slope**



Element A

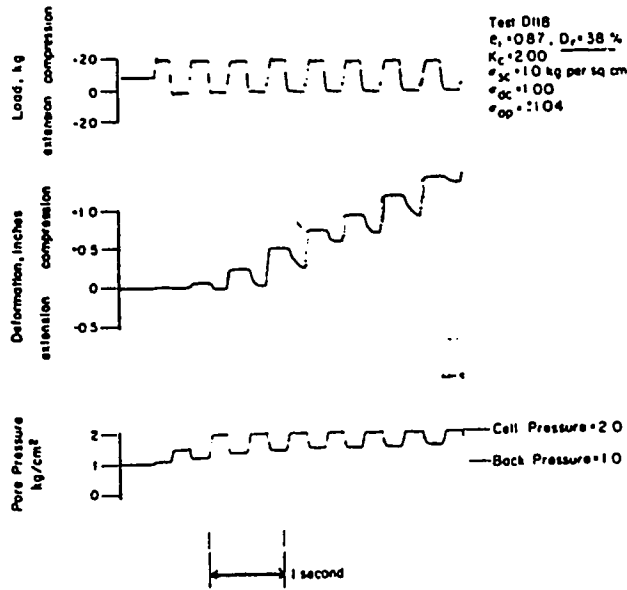
$$\alpha = \left| \tau_i / \sigma'_v \right| > 0$$



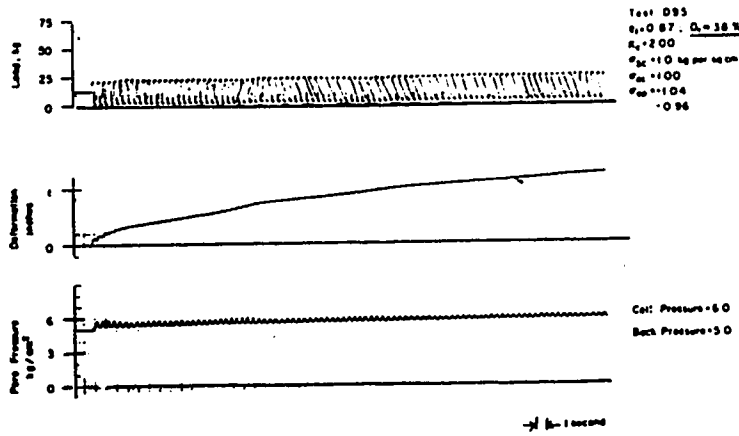
Element B

$$\alpha = \left| \tau_i / \sigma'_v \right| = 0$$

**Figure 3.3 Initial Stress Conditions underneath a Building**



RECORD OF TYPICAL REVERSING STRESS



RECORD OF TYPICAL NONREVERSING STRESS TEST

Figure 3.4 Typical test results with shear stress reversal and without, after Lee and Seed (1967)



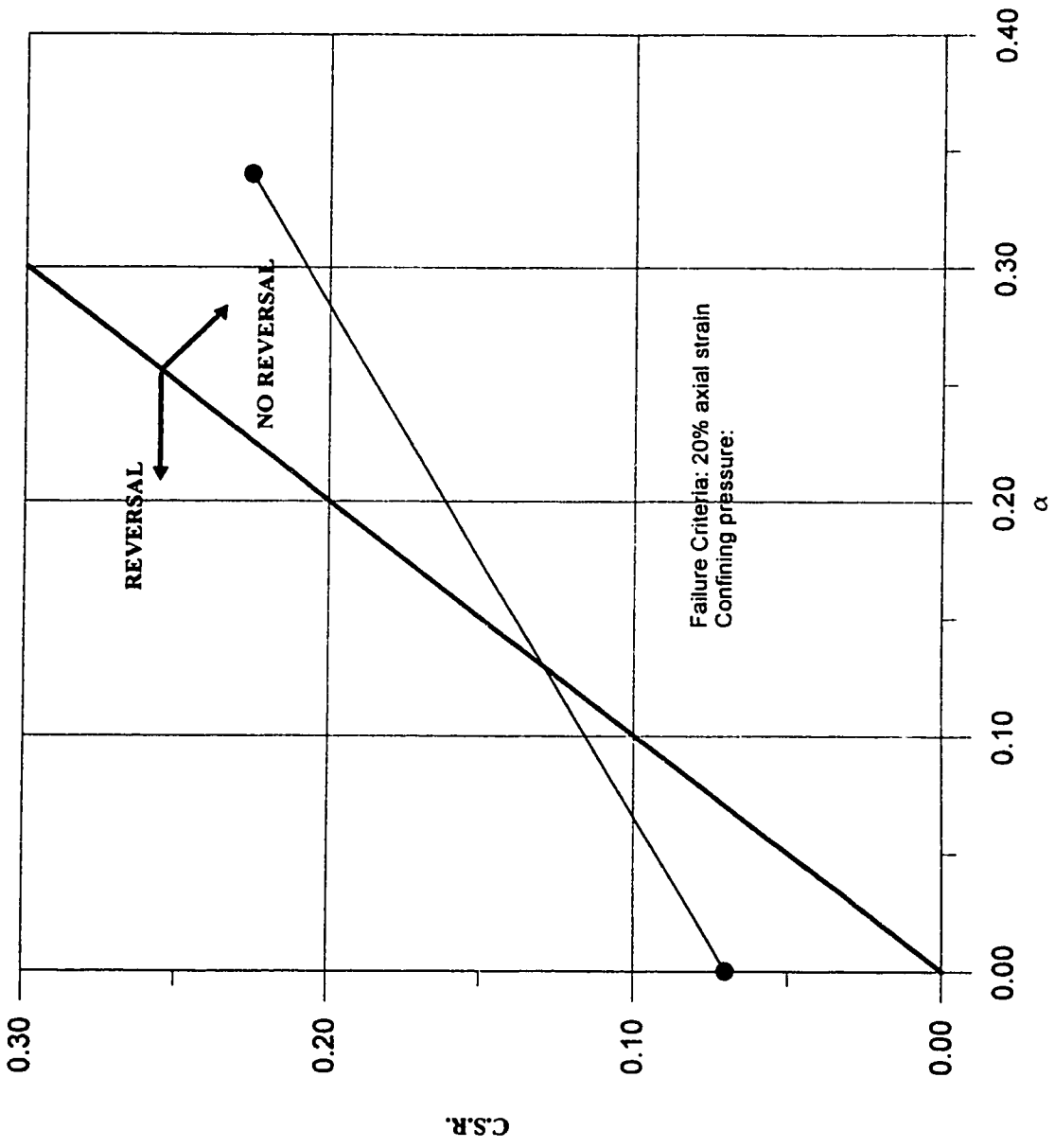


Figure 3.5 Result of Cyclic triaxial tests on Sacramento River Sands ( $D_r=40\%$ ), after Lee and Seed (1967)

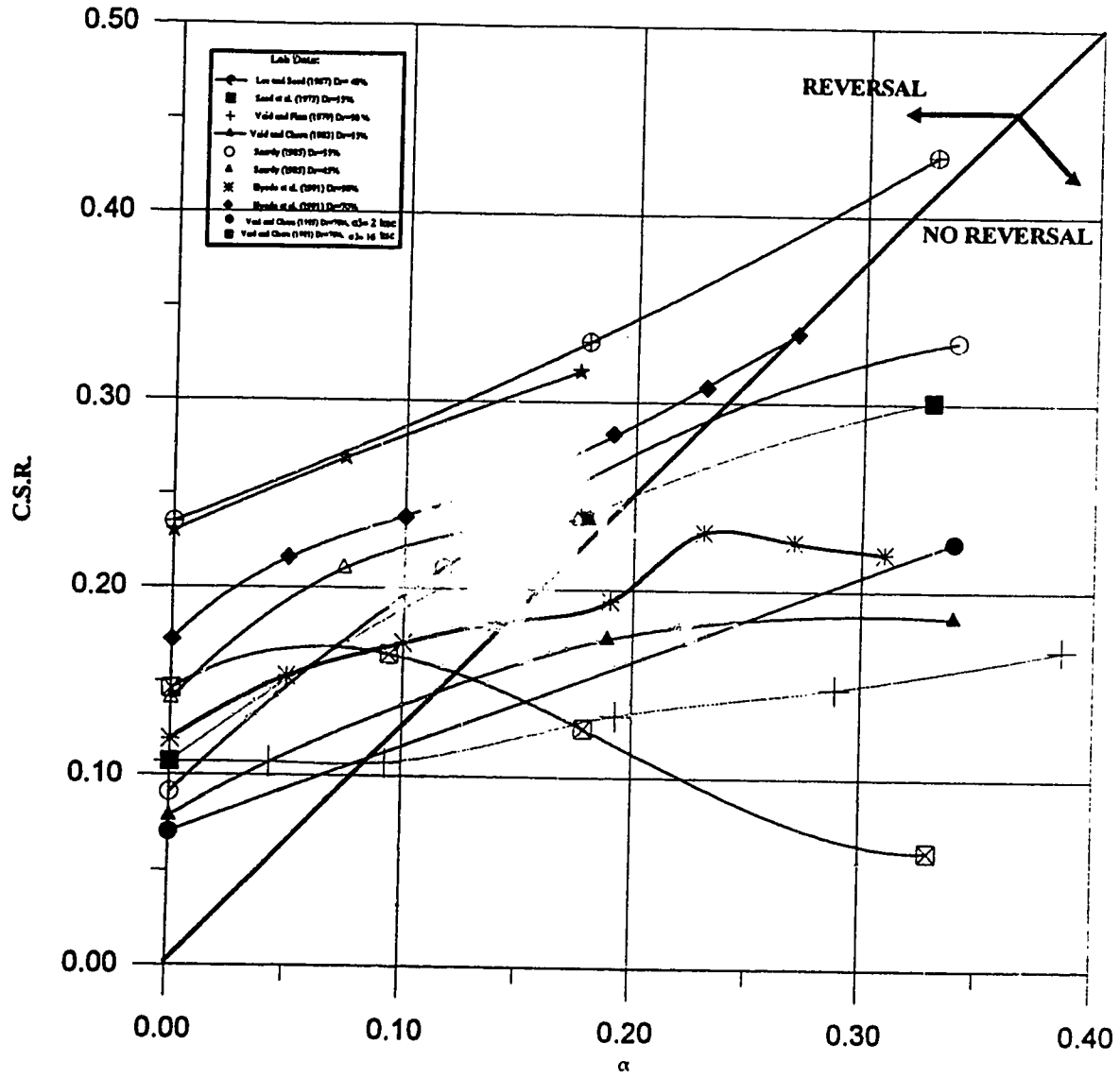


Figure 3.6 Summary of Laboratory Results for Dense Sands ( $D_r > 45\%$ )

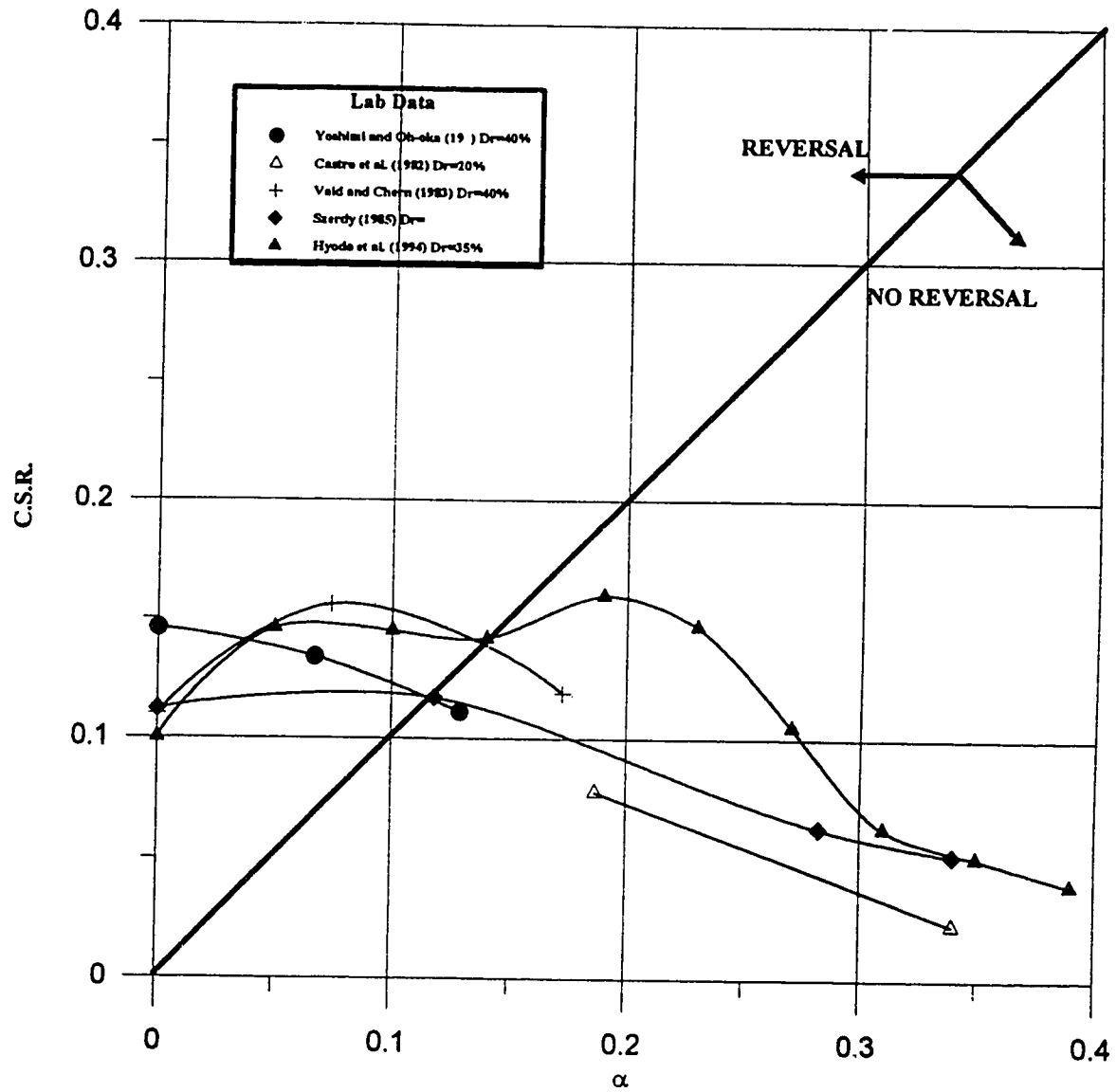
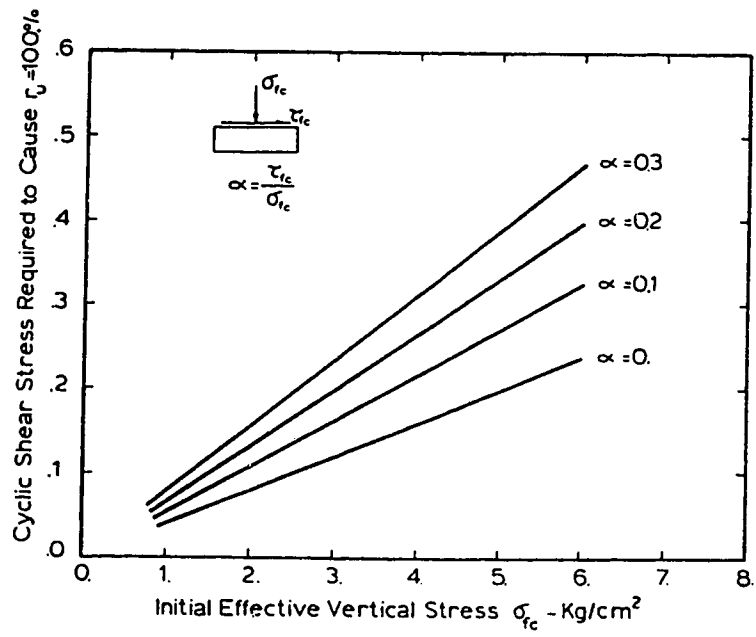
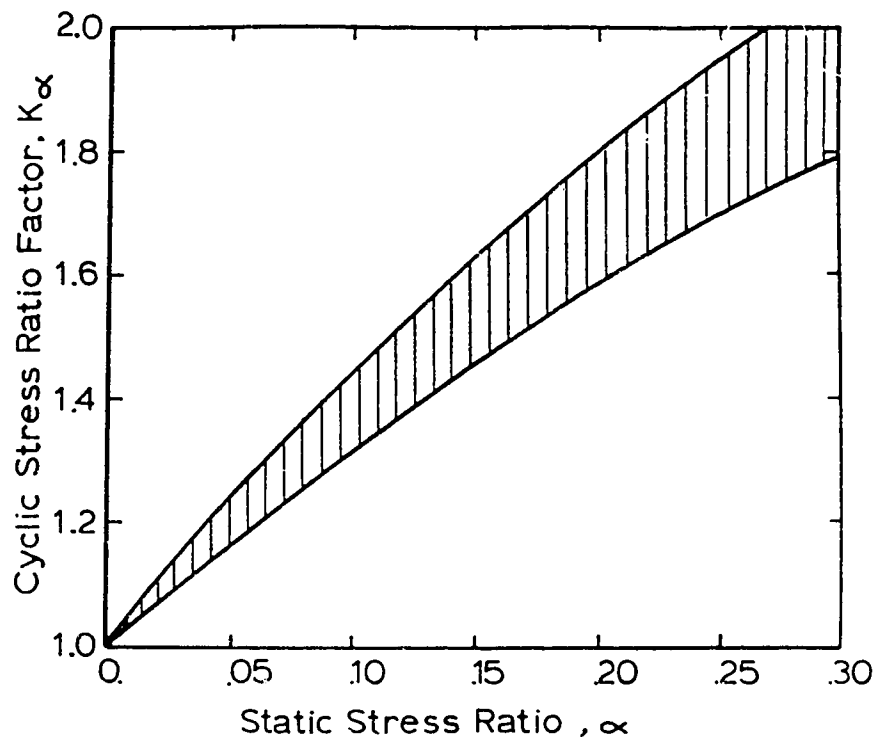


Figure 3.7 Summary of Laboratory Results for Loose Samples ( $D_r < 45\%$ )



**Figure 3.8 Shear test results, after Seed (1983)**



Static Stress Ratio,  $\alpha = \frac{\tau_h}{\sigma_v}$

$\left(\frac{\tau_c}{\sigma_v}\right)_L$  for  $\alpha = \alpha \approx \left(\frac{\tau_c}{\sigma_v}\right)_L$  for  $\alpha = 0 \times K_\alpha$

Figure 3.9  $K_\alpha$  versus  $\alpha$  curve, after Seed (1983)

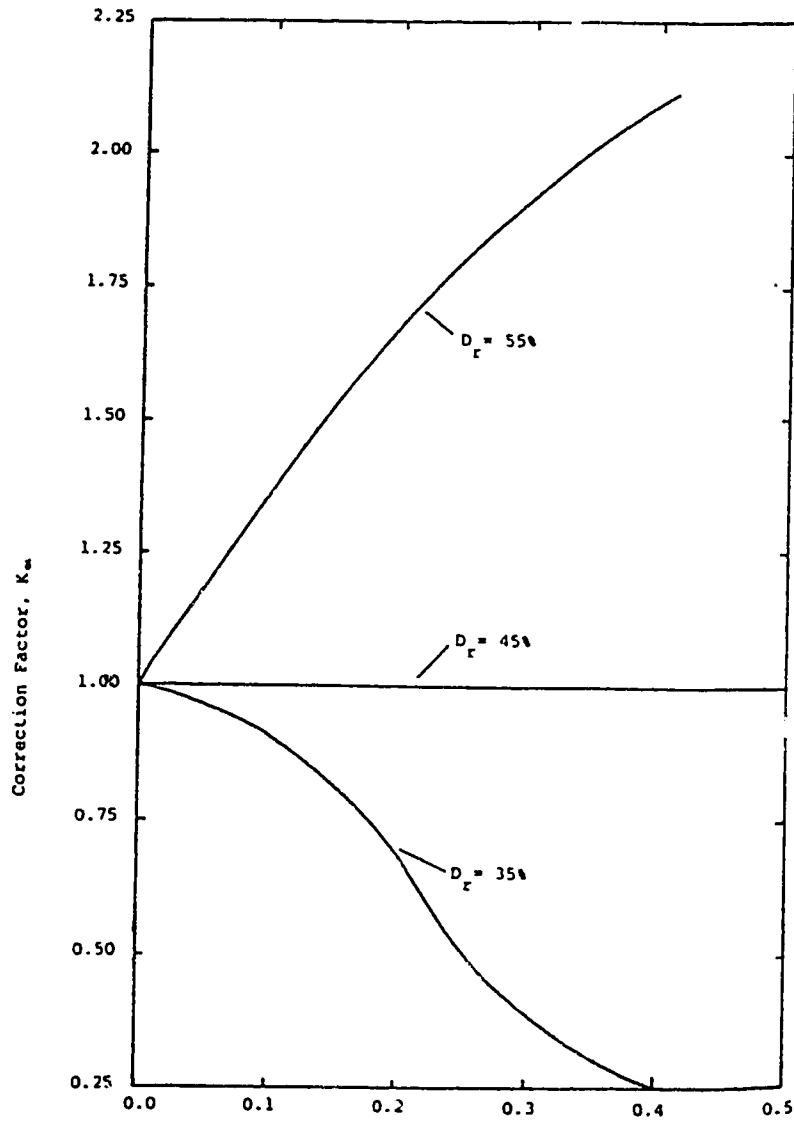


Figure 3.10  $K_{\alpha}$  versus  $\alpha$  curve, after Rollins (1985)

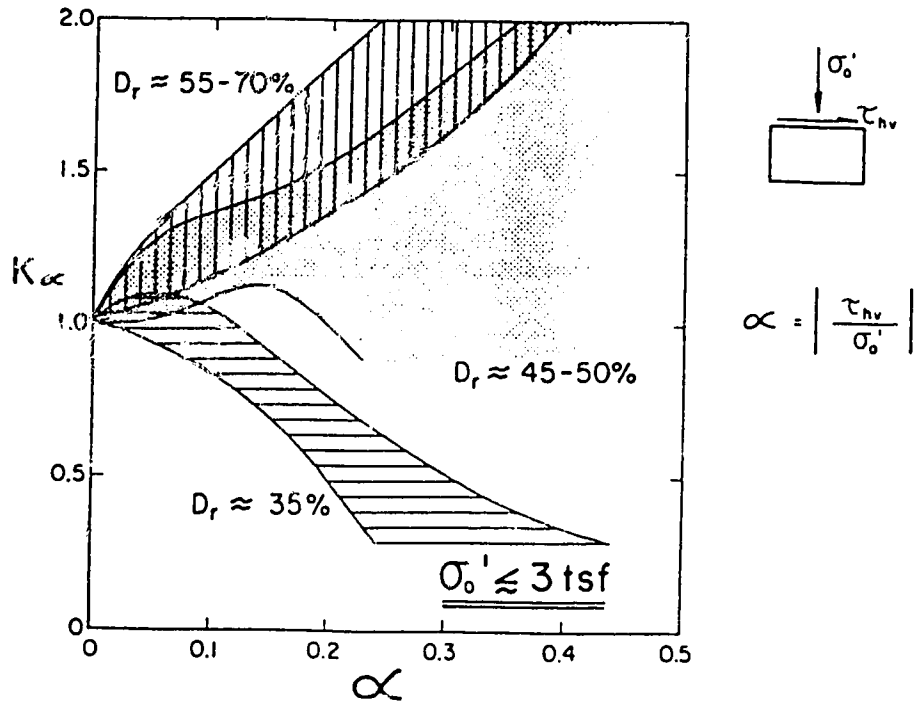
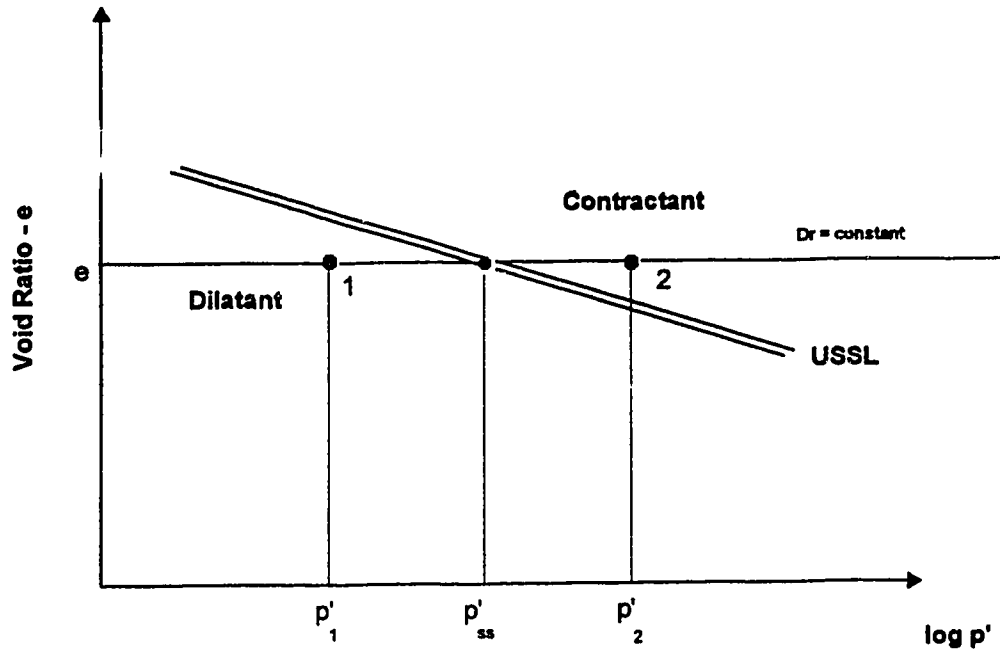
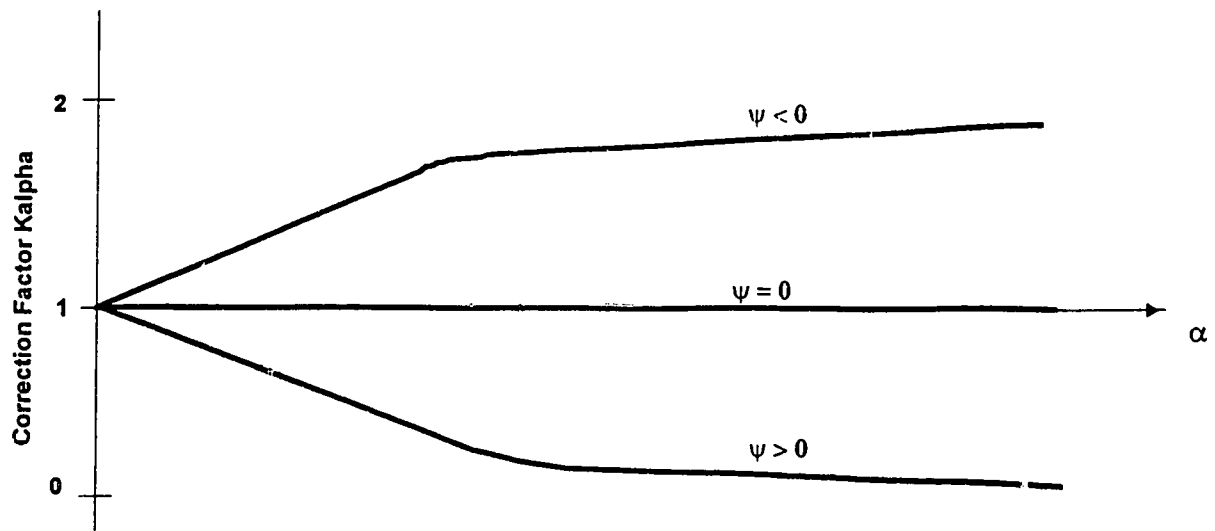


Figure 3.11  $K_\alpha$  versus  $\alpha$  curve, after Seed and Harder (1991)



**Figure 3.12 Relative Density used to Define Type of Response**





**Figure 3.13 Correlation of Kalpha, Alpha and the State Parameter**

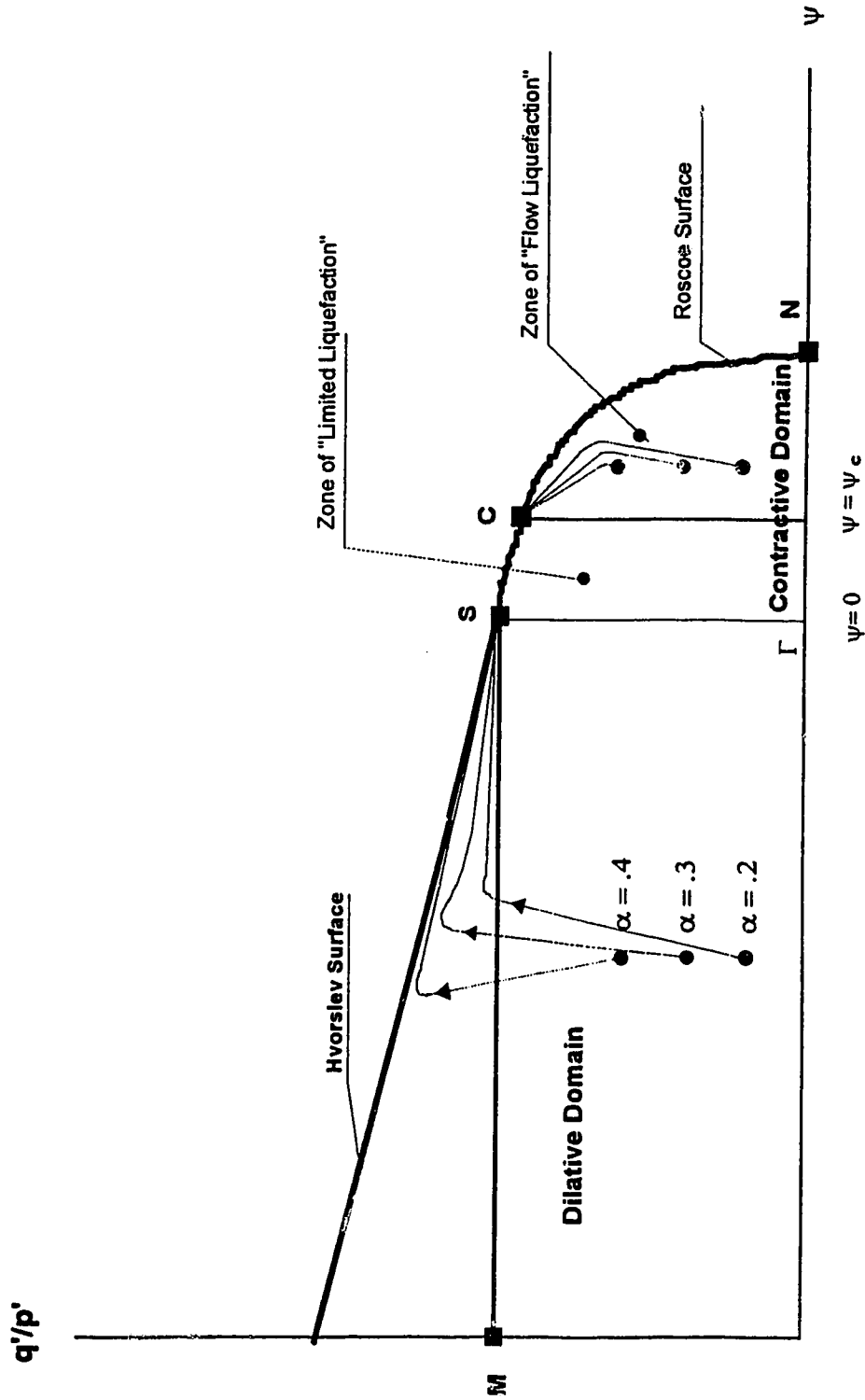


**Figure 3.14 Normalized State Boundary Surface (After Pillai, 1991)**

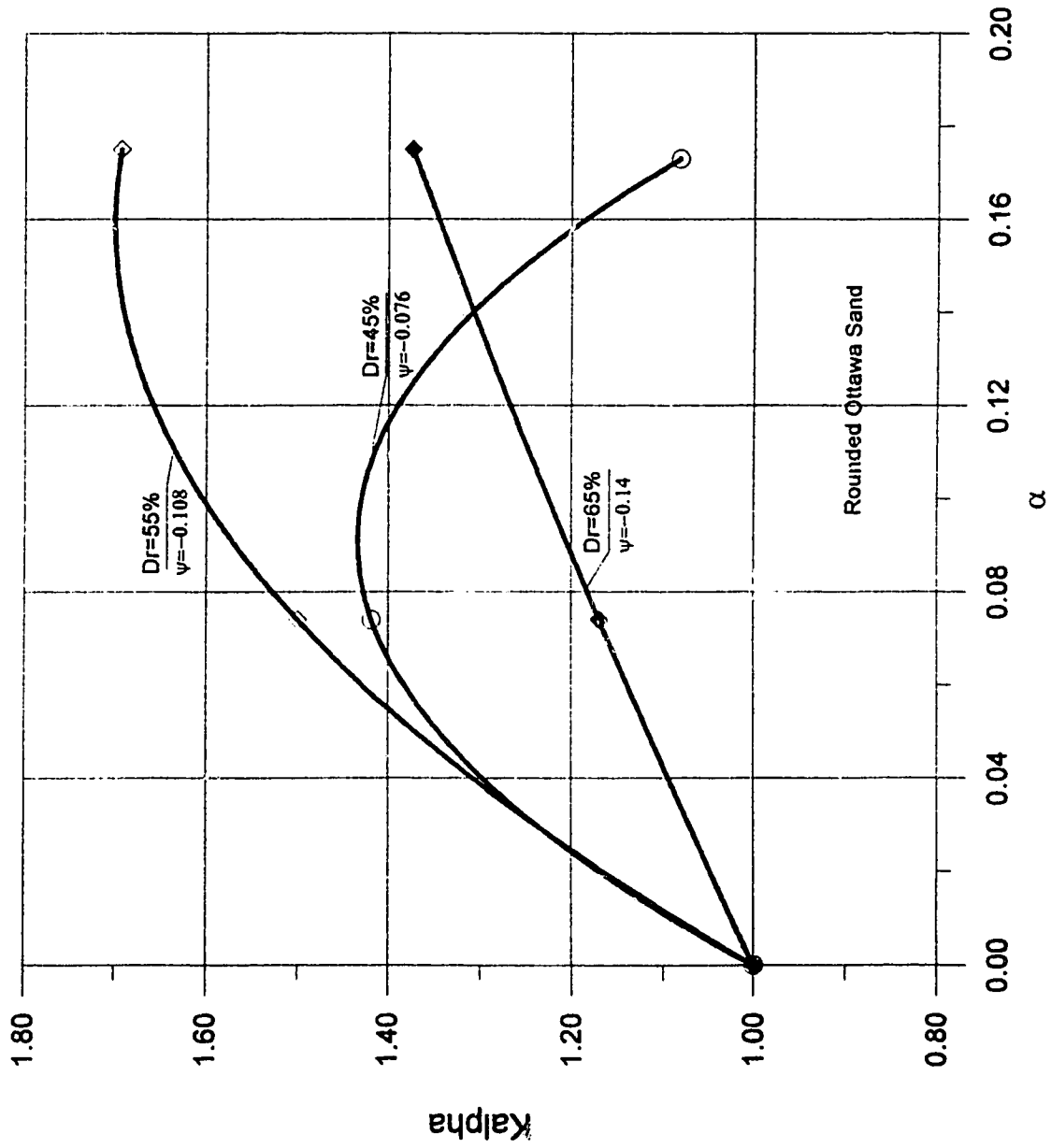


Figure 3.15 Kalpha correction factor - Vaid and Chern (1983) data

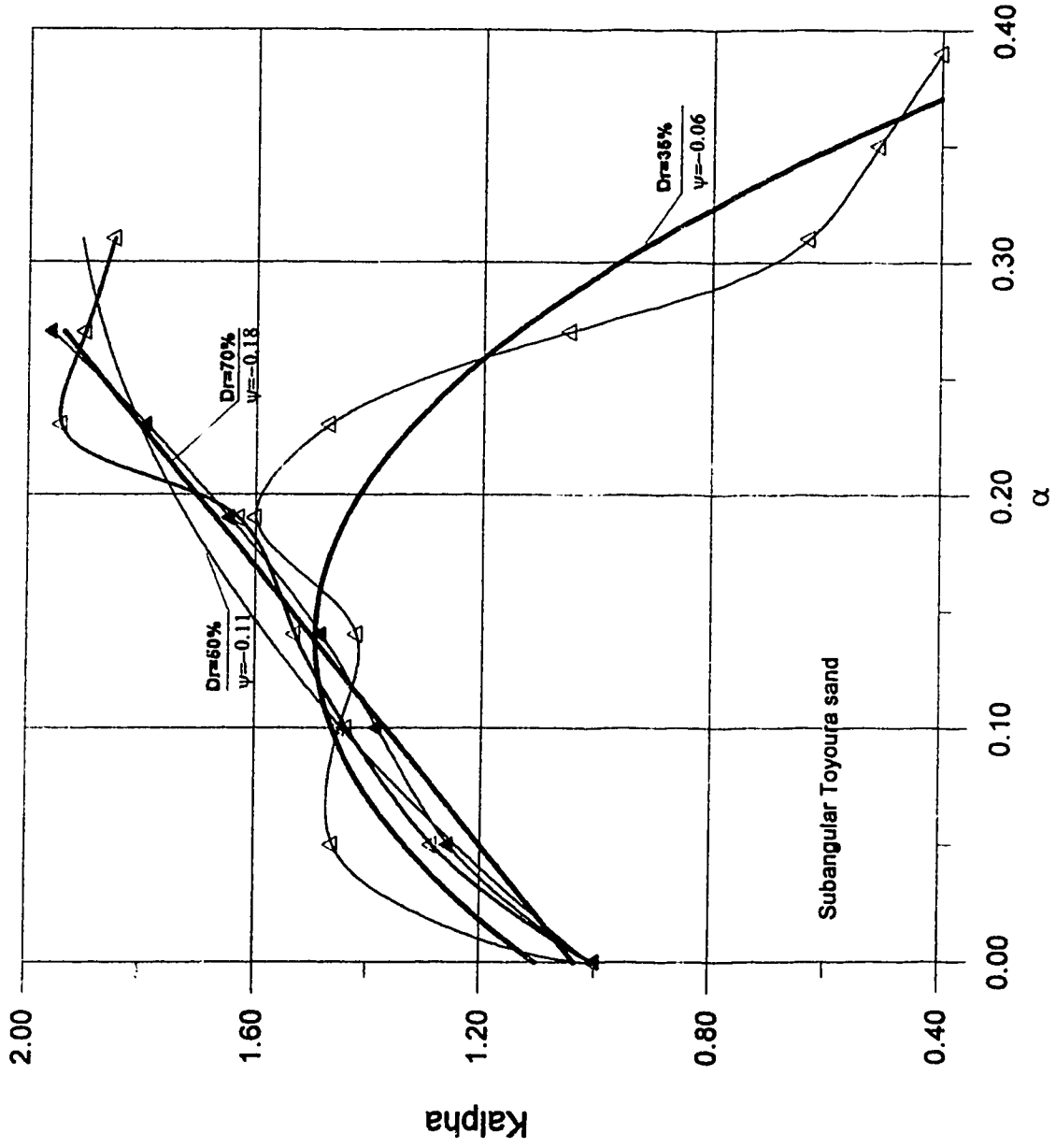


Figure 3.16 Kalpha correction factor - Hyodo et al. (1991 and 1994) data

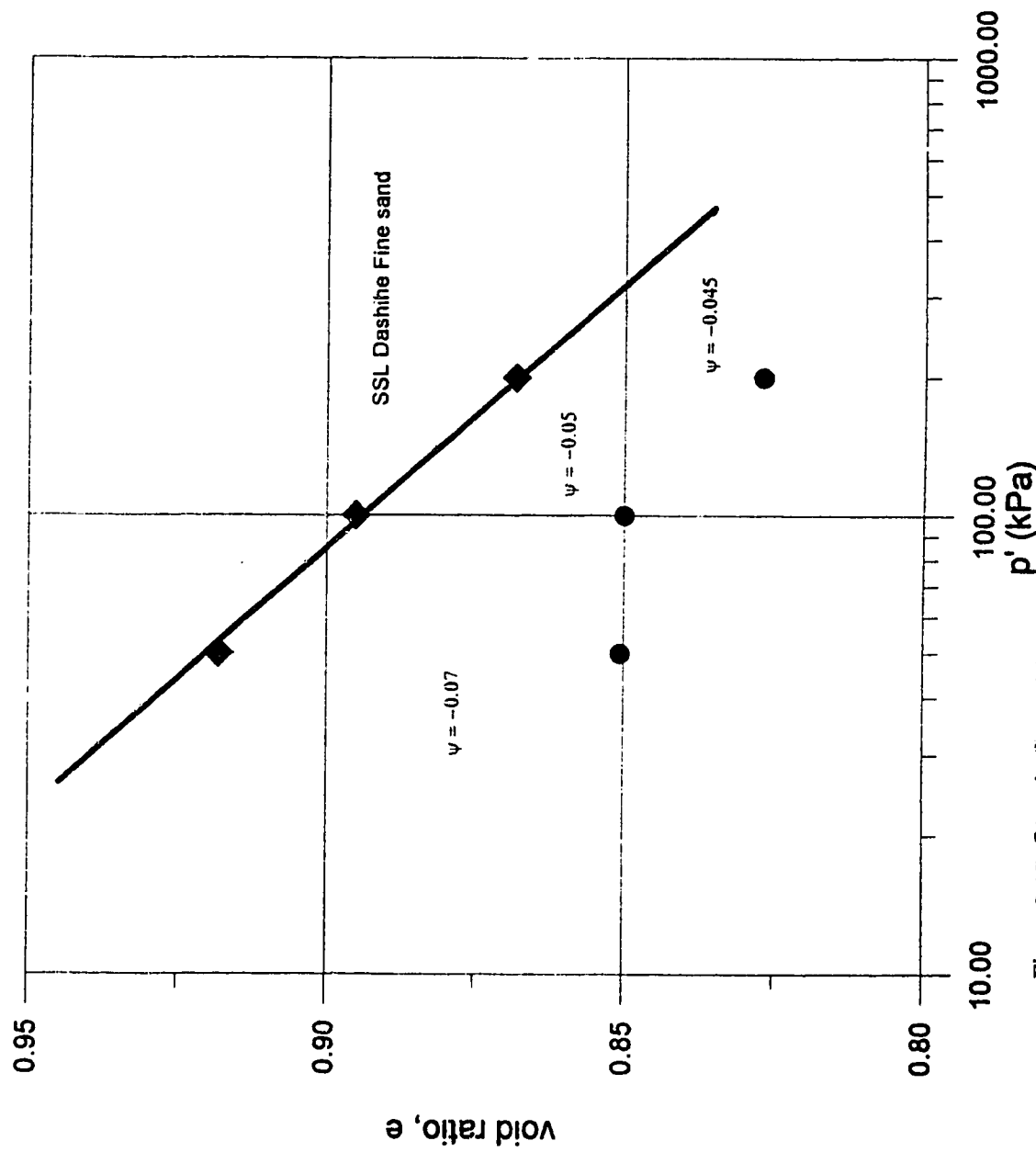


Figure 3.17 Steady State Line for Dashihine Fine Sands (After Lee et al, 1992)

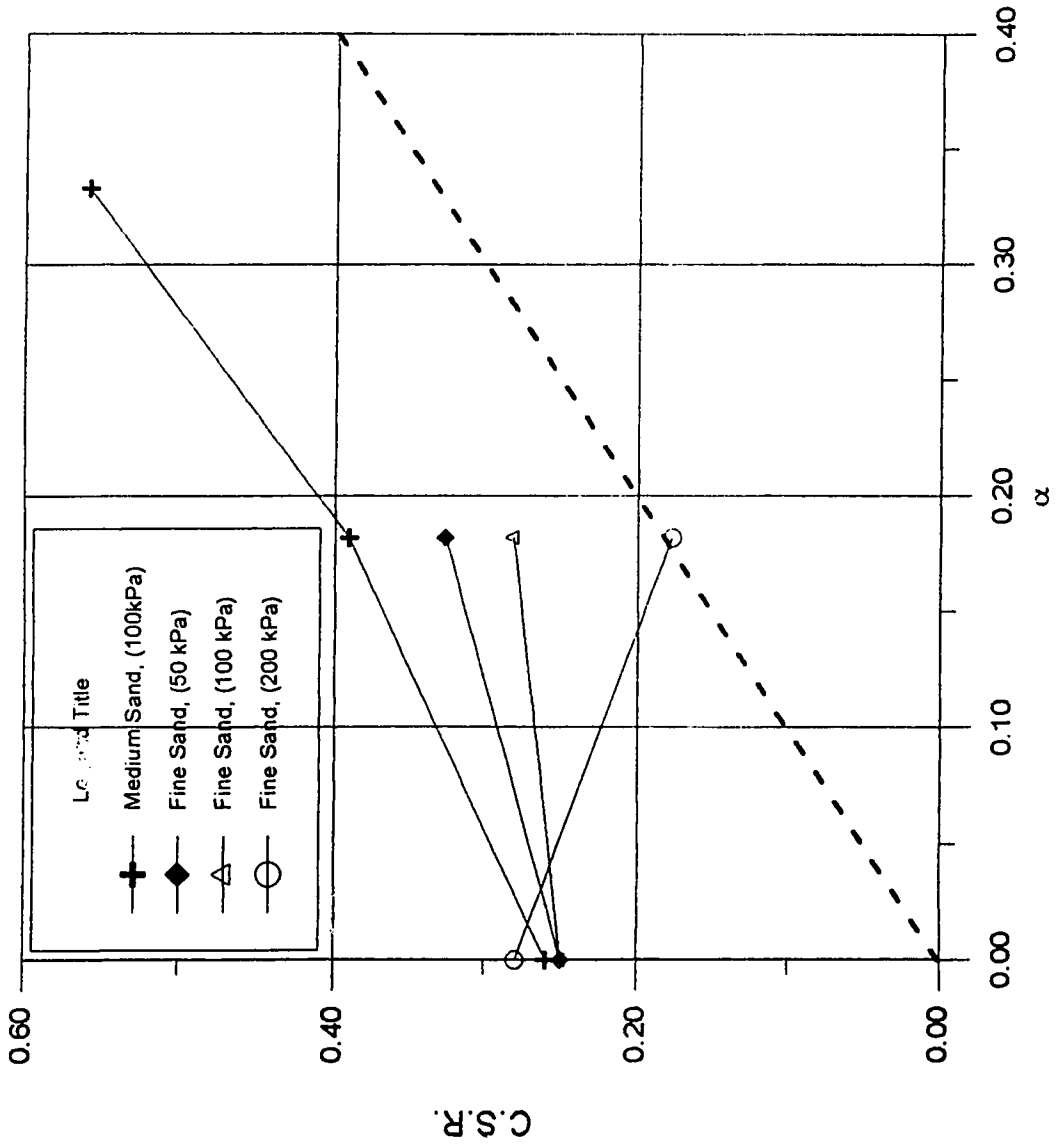


Figure 3.18 Dashuie Tailings Sand Cyclic triaxial results summary

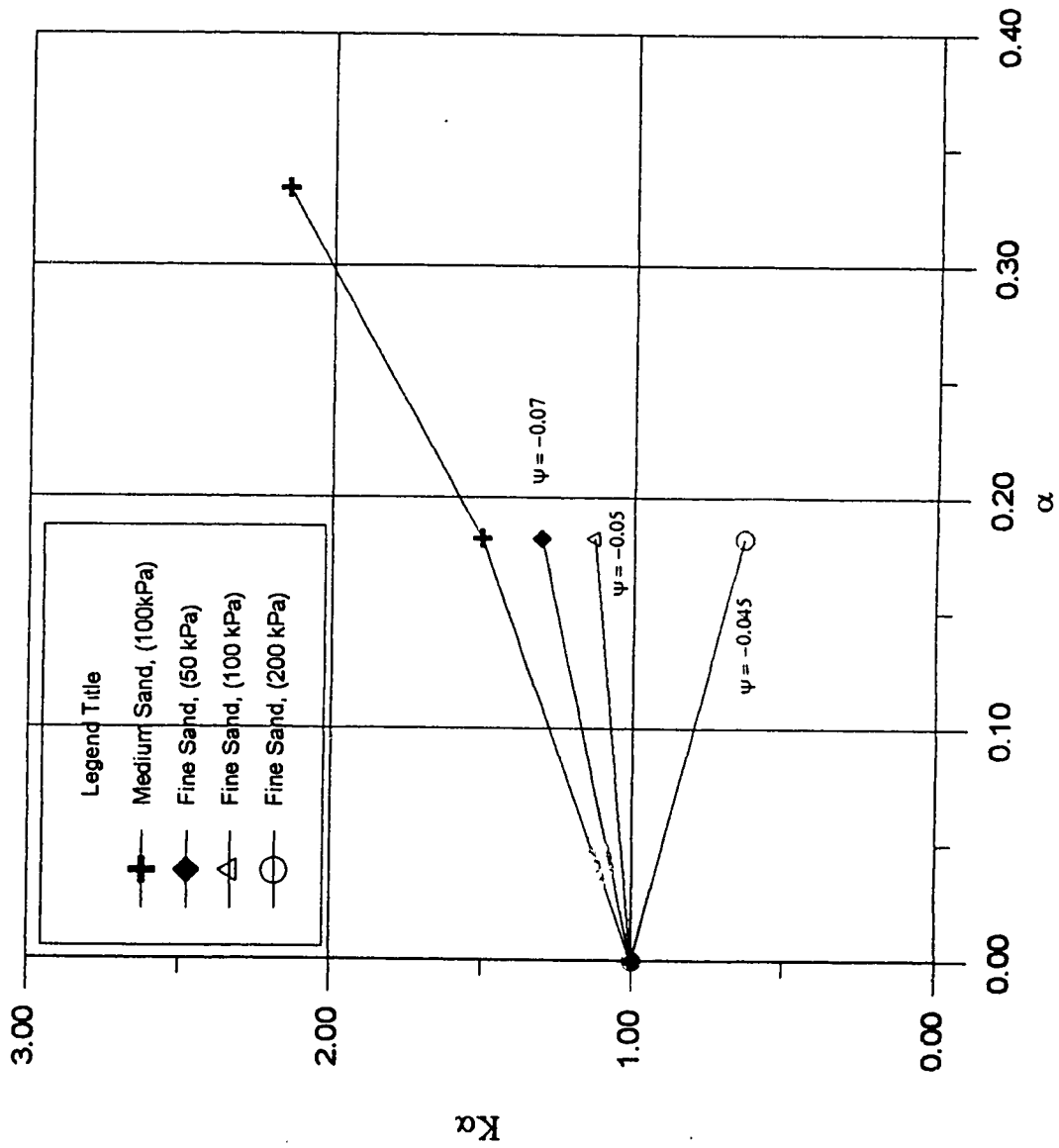


Figure 3.19 Dashihe Tailings Sand K alpha correction factor

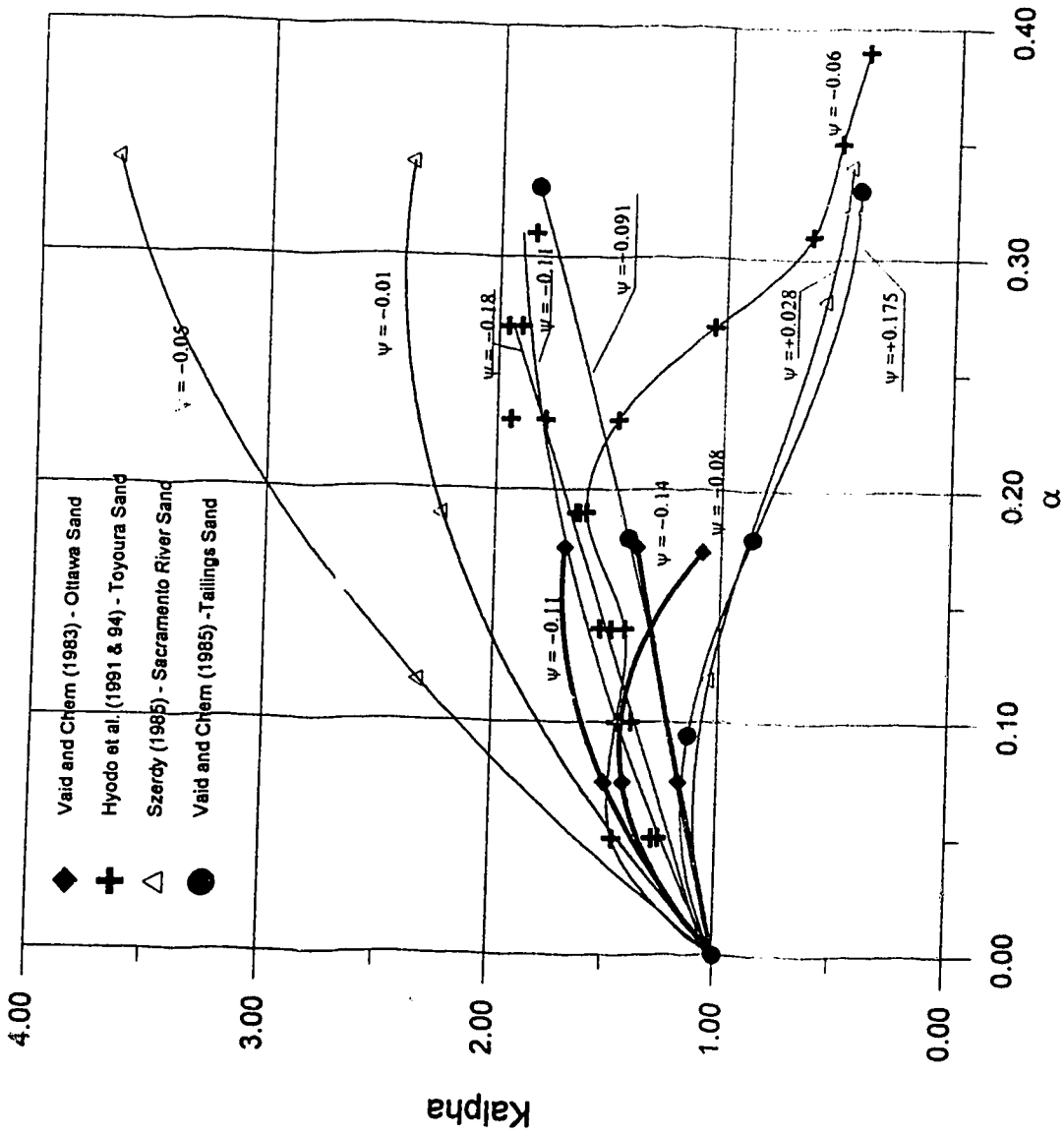


Figure 3.20 Kalpha correction factor classified according to the State Parameter



## Chapter 4

### Models used for the Analyses

#### 4.1 Introduction

In order to define zones where shear stress reversal occurs on horizontal planes of soil elements within a soil structure, it is necessary to calculate two stresses. First, by means of a conventional static finite element analysis, the static shear stresses on horizontal planes,  $\tau_{xy}$  can be determined. Secondly, the cyclic shear stresses, induced by the earthquake, must be determined using a dynamic analysis. Since the static analysis is relatively straight forward and is extensively used in geotechnical engineering, it will be briefly described. On the other hand the dynamic analysis involves several considerations and aspects to be taken into account. Therefore, a summary of the general guidelines to estimate the seismic response of a soil deposit will be presented, followed by a description of the program and model used in this study.

#### 4.2 Static Analysis

The objective of the static analysis is to obtain the initial horizontal static shear stresses within the soil deposit. Since deformations of the deposit are not required, it was considered sufficient to estimate the initial stresses using the “Switch on Gravity” approach. This method, as its name suggests, consists in applying, without increments, the weight of the deposit as an external load. The deformations obtained are not representative of the field conditions, nevertheless this method is considered to give a good approximation of the insitu stresses of the soil deposit.

The computer program used to carryout the static analysis was Sigma/W<sup>®</sup> v.2 (GeoSlope International Ltd., 1992). The assumed stress-strain relationship for the soil was linear elastic, therefore the only input properties were the elastic modulus, Poisson’s ratio and the unit weight of the soil. It is important to point out here that the same finite element mesh was used for the dynamic analysis, therefore special care was given when

defining the mesh, so that the geometry effects on the dynamic analysis could be properly taken into account. Results of the static analyses are summarized in chapter 5.

### **4.3 Dynamic Analysis Guidelines**

In order to evaluate the seismic response of soil structures several steps should be followed:

1. Definition of Geometry:
  - Surface topography
  - Underlying rock configuration
  - Irregularities in boundaries between soil layers
  
2. Motions in underlying rock:
  - Peak acceleration,  $a_{max}$
  - Period, T
  - Duration, D
  
3. Geotechnical characterization:
  - Types of soils
  - Dynamic characteristics and properties

#### **4.3.1 Definition of Geometry**

The definition of geometry is a very important part of the dynamic analysis. Idriss, Seed and Dezfulian (1969) carried out a study that showed how important the geometry can be in assessing the seismic response of a soil deposit. They studied the influence of the geometry on mainly the maximum accelerations and the dynamic stresses. They concluded that the response of soil deposits is highly dependent on the distribution of material properties and the geometric configuration, but that the geometry affects the response mainly in the vicinity of geometrical changes, while material property distribution has a more marked influence. Several other studies (Silva, 1989 and 1990) have shown how the two-dimensional effects can greatly influence the amplification effects of the seismic

waves. In the case of dams 2-D plain strain analysis are only valid if the dams are long relative to their width. However many dams are built in narrow valleys. For these cases 3-D analysis may be more correct.

#### 4.3.2. Selection of the earthquake induced motions:

When studying the seismic behavior of a soil deposit it is common practice to evaluate their response to the motions developed in the underlying rock formation or rocklike formation (shear wave velocity  $V_s \cong 700$  m/s). This approach has been successfully used in the evaluation of ground surface motions, liquefaction potential studies, etc. (Seed et al., 1969). Therefore for analysis purposes, it is necessary to determine the time history of motions at the base of the soil deposit. The acceleration record is chosen according to seismic ground motion studies, which can be deterministic or probabilistic and they obviously depend on the seismic setting of the site. ICOLD (International Committee on Large Dams) suggests procedures to select design earthquakes for dams (ICOLD, 1989). In Canada seismogenic models are available to perform ground motion estimates (Heidebrecht et al., 1983; Basham et al., 1985). Usually three parameters are required for the dynamic analysis of soil deposits, these are:

- Peak acceleration,  $a_{max}$
- Period, T
- Duration, D

From the seismic studies mentioned before the most probable set of values for these three parameters can be obtained. Seed et al., (1969) provides a detailed description of how to determine these rock motion characteristics for a specific site. With these parameters defined it is possible to either use a generated synthetic earthquake record (Housner, G.W. and Jennings, P.C., 1964) or scale an existing earthquake record to fit our requirements.

For this study the number of variables involved in the exciting motion needed to be restricted. It was decided that a synthetic accelerogram would be used, having a duration,  $D = 40$  seconds and a period,  $T = 0.4$  seconds, which are values within the normal range of typical earthquake records. The only remaining variable is the rock peak acceleration,  $a_{max}$ . For each geometry analyzed in this study several dynamic response calculations were done by varying the peak acceleration of the motion applied at the base. It is important to point out here that the synthetic accelerogram used was a uniform record. Therefore, it was not possible to account for any possible shear stress reversal occurring during the high peak accelerations commonly seen in real earthquake records. There are procedures to convert irregular earthquake records to equivalent uniform cycles (Seed et al. 1975a and Lee and Chan, 1972). The accelerogram used in this research will be discussed in Chapter 5.

#### 4.3.3. Soil properties required for dynamic analysis

For each type of soil present in the soil deposit a series of properties should be determined. These properties are:

1. Total unit weight,  $\gamma_t$
2. Maximum shear modulus,  $G_{max}$
3. Variation of  $G_{max}$  with depth
4. Variation of shear modulus,  $G$ , with shear strain
5. Variation of damping ratio,  $\lambda$ , with shear strain
6. Poisson's ratio

For low amplitude strain vibrations, such as vibrating machine foundations, linear elastic models can be applied using a single value of shear modulus. In earthquake problems, the shear strains imposed can be high, having an important effect on both the shear modulus and the damping of the soils. Details on the dynamic behavior of sands and their properties have been presented in chapter 2.

#### 4.4. Numerical Modeling of Earthquake related Problems

In order to carry out a dynamic analysis several simplifying assumptions are required. One of the common assumptions made is to consider that the soil elements are subjected only to vertically propagating shear waves. The shear stresses induced have associated shear strains,  $\gamma$ . In earthquake related problems the strains can be high making the soil behavior clearly nonlinear (see chapter 2). For analysis purposes there are two approaches. One is to model the true nonlinear hysteretic behavior, trying to use a stress-strain relationship that represents the actual cyclic loop in the analysis. To do so it is possible to use a Ramberg-Osgood type of model (backbone curve) along with the Masing criterion. A complete description of how to model sands with a nonlinear hysteresis behavior can be found elsewhere (e.g. Matasovic and Vucetic, 1993, Faccioli and Resendiz, 1976 and Saada, 1985 amongst others). Few two-dimensional programs are available using this approach (Finn, 1981). The other possible approach for modeling is to use the equivalent linear method. This method was originally proposed by Seed and his coworkers at the University of California at Berkeley, and was first coded in a one-dimensional program, SHAKE (Lysmer et al., 1972). The program has been shown to be successful in describing the response of level ground during earthquakes, and clearly influenced the future developments of dynamic response analysis in engineering practice (Finn, 1981). The one-dimensional model was later generalized to 2-D and 3-D versions. QUAD4, is the 2-D version chosen for the dynamic analysis in this research, and is based on the linear equivalent approach. The following section will describe the equivalent linear method.

##### 4.4.1. The Equivalent Linear Method

The fundamental assumption of this method is that the dynamic response of the soil is clearly a nonlinear hysteretic response, which can be approximated quite satisfactorily by a damped elastic model (visco-elastic). Seed et al., 1986 consider this

particularly true when there are no residual displacements involved and if the soil is under a reasonably symmetrical loading. For this kind of condition the response can be determined mainly by shear modulus and soil damping. The properties must be chosen correctly in order to get good results, and an iterative procedure is considered to adjust the soil properties to the shear strain level achieved in each finite element.

One of the disadvantages of this method is that since the final analysis is elastic permanent deformations cannot be calculated. The computed strains are more likely to have no relation with the field values, and they are only used to derive the strain compatible properties. However the stresses derived from these strains are assumed to be representative of the stresses in the ground, the accelerations are also assumed to be reasonably representative of stresses in the field (Finn, 1981). Comparisons between this method and "true" non-linear methods have agreed reasonably well in one-dimensional analysis (Finn et al., 1977 and Finn, 1981). Another disadvantage of this method is that it is a total stress analysis, therefore it cannot directly take into account the effects that increasing pore pressures have on the soil stiffness. Comparison studies on the response of saturated sandy sites, using one-dimensional analysis, indicated that the total stress analysis tends to overestimate the dynamic response when porewater pressures exceed about 30 % of the overburden pressure (Finn et al. 1978). These comparative studies have been carried out for one-dimensional models, but for 2D there are no convincing comparative studies of true non-linear and equivalent linear models (Finn, 1981). The major drawback of this method is that permanent deformations can not be computed, but since for this research we are only interested in the computation of dynamic shear stresses, the model was considered reasonable.

Several authors have pointed out the importance of a realistic estimation of the dynamic properties in order to obtain a good prediction of the dynamic soil response (Prakash and Puri, 1981, Hardin and Drnevich, 1972). "The response predicted by the analyses will change *proportionately* to, and is no more accurate than, the values used for the soil properties" (Hardin and Drnevich, 1972). "The process of obtaining representative

values for the critical soil properties is probably the most difficult part of the design study” (Richart, Hall and Woods, 1970). The following sections give some guidelines on how to estimate these properties and the main factors that affect them.

#### 4.4.2. Shear Modulus for Sands

Recognizing the importance of the shear modulus in the seismic response of a soil deposit, it is necessary to define them as well as possible. Several studies on dynamic properties have shown that the dominant factors affecting shear modulus in cohesionless soils are strain amplitude, confining pressure and void ratio (or relative density,  $D_r$ ) (Hardin and Drnevich, 1972, Seed and Idriss, 1970, Faccioli and Resendiz, 1976 and Seed et al. 1986).

For strain amplitudes below  $10^{-4}$ , soils exhibit a nearly constant shear modulus,  $G_{\max}$  or  $G_0$ . Several equations have been proposed to estimate  $G_{\max}$ , the most important ones are the following:

- Hardin and Drnevich (1972):

$$G_{\max} = 3230 \frac{(2.973 - e)^2}{1 + e} (\sigma'_m)^{1/2}$$

where both  $G_{\max}$  and  $\sigma'_m$  (effective mean confining pressure) are in kPa. This equation was proposed for angular grained sands.

- Yoshimi, Richart, Prakash, Barkan and Ilyichev (1977):

$$G_{\max} = 6930 \frac{(2.17 - e)^2}{1 + e} (\sigma'_m)^{1/2}$$

where both  $G_{\max}$  and  $\sigma'_m$  (effective mean confining pressure) are in kPa. The above equation was derived for round-grained sands ( $e < 0.80$ ).

- Seed and Idriss, 1970:

$$G = 1000 K_2 \sqrt{\sigma'_0} \quad (\text{psf})$$

$$G = 219 K_2 \sqrt{\sigma'_0} \quad (\text{kPa})$$

where  $K_2$  is a soil modulus coefficient which accounts for the influence of the void ratio and the strain amplitude. Figure 4.1 show values of  $K_2$  for sands of different relative densities. Since  $K_2$  varies with strain Seed and Idriss's equations give the variation of the shear modulus with strain. To obtain  $G_{\max}$  Seed et al., (1986) simplified this last equation, by proposing the use of a  $K_{2\max}$  coefficient, which could be estimated using a correlation of in situ shear wave velocity with SPT N values, and knowing that shear wave velocity can be related to the shear modulus using the well known equation of wave propagation in elastic medium,  $G_{\max} = \frac{\gamma}{g} V_s^2$ . Seed et al, 1985 obtained the following expression for the

$K_{2\max}$  coefficient:

$$K_{2\max} \cong 20(N_1)_{60}^{1/3}$$

Using this coefficient in the previous equation for the shear modulus it is possible to estimate  $G_{\max}$ .

For large cyclic deformations, sand exhibits a hysteretic non-linear behavior. Figure 4.2 shows typical curves of the variation of the secant modulus normalized with respect to  $G_{\max}$ , with strain. From this figure we can see how the shear modulus decreases monotonically at about a strain of  $10^{-4}$ , this strain defines the limit of linear behavior.

#### 4.4.3. Damping ratios for Sands

Several studies have pointed out that the main factors affecting the damping ratio are the strain level induced and the effective confining pressure (Hardin and Drnevich, 1972 and Seed and Idriss, 1970). Figure 4.3 shows the influence of the confining pressure.



From this figure it can be seen that the curves vary within a relatively small range, but for practical purposes a representative curve of damping ratio versus shear strain can be selected. Figure 4.4 shows the range of damping ratio of sands and an average curve.

#### **4.5. The Dynamic Model used in this research**

##### **4.5.2. Program Description**

The program used in this research was QUAD4TB (1993), an upgraded version of Quad4, originally developed at the University of California, Berkeley in the early 70's by Seed and his coworkers (Idriss et al., 1973). This program was used to carry out all the dynamic numerical analysis presented in this thesis, hence it is desirable to present a brief description of its main characteristics and features.

QUAD4TB is basically a finite element analysis program for plane soil structures subjected to horizontal earthquake excitation at the base. It uses the equivalent linear method, described in the previous section, and incorporates strain compatible Rayleigh damping and shear modulus in all elements. The integration of the differential equations of motion is done using the direct step-by-step integration method. The modeling of the soil structure can be done using triangular and quadrilateral finite elements. It is important to point out that the program performs only a total stress analysis, therefore no information regarding pore pressures can be estimated. A more detailed description of the program is presented in Appendix D.

##### **4.5.2. Modeling and Lessons Learned**

Two input files are required to do the numerical analysis, one is the file with the earthquake record information and the other file has all the information regarding the soil structure to be modeled, i.e. soil properties, finite element mesh information and boundary conditions information. Creating the actual input files is quite straight forward.

During the early stages of this research considerable effort was expended to verify the accuracy of the generated output. Solutions were compared with those obtained from other programs like SHAKE91 (Idriss and Sun, 1992). Through this learning process the advantages and disadvantages of this program were identified.

The results are very sensitive to the boundary conditions used in the finite element mesh. Figure 4.5 shows a typical finite element mesh used in the analyses, and the boundary conditions selected. A parametric study was carried out to study how sensitive the response was to the initial soil properties used. From this study it was concluded that the response is almost directly proportional to the initial values of the shear modulus used, and that the damping factor could affect considerably the acceleration profile along the deposit. Therefore the results presented in chapter 5 of this thesis are not rigorously applicable for other geometries, boundary conditions and soil properties. Therefore, the results provide only a guide to the extent of the zones of no shear stress reversal for similar geometries.

Once the geometry and soil properties have been defined for the soil structure it is possible to change the earthquake record that excites the base of the mesh. In this study a real earthquake record was not used in an effort to decrease the number of variables involved. Therefore, a uniform synthetic record was used. The only variable was the peak acceleration. This acceleration can be readily scaled to any value by just changing a scaling factor. This feature of the program allowed several runs to be made, for each geometry, with various values of maximum acceleration.

The output files give the maximum average stresses ( $\sigma_x$ ,  $\sigma_y$ ,  $\tau_{xy}$ ) for each element, after each iteration. Maximum accelerations, after each iteration, are also recorded for each nodal point of the mesh. There is also an option in the program in which one can obtain a complete stress history for any specified element during the shaking. For the purpose of this research only the maximum horizontal shear stresses were required, so that when compared to the initial static shear stresses on the same plane, it was possible to

determine if there was shear stress reversal. Results of the dynamic analysis are summarized in the next chapter.

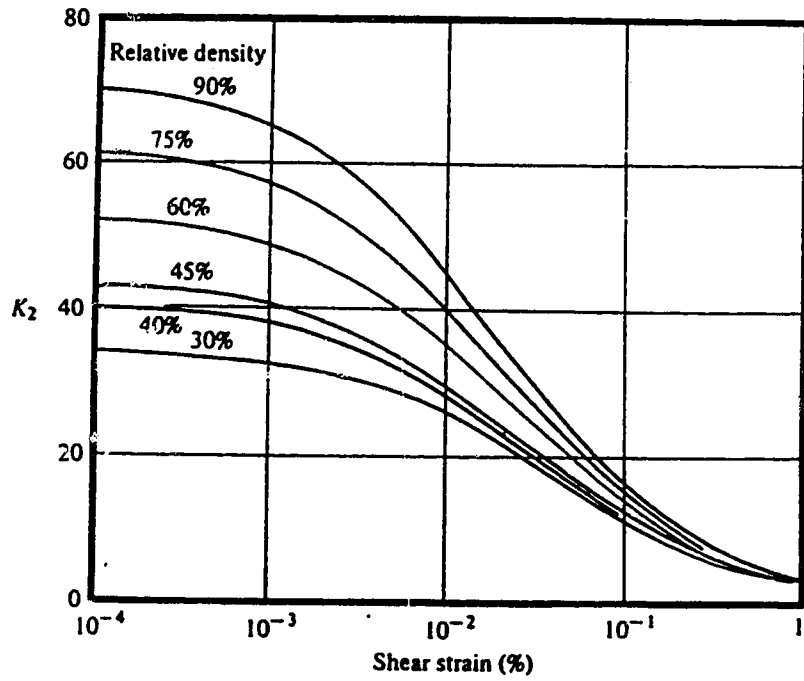


Figure 4.1  $K_2$  for different sands, after Seed and Idriss (1970)

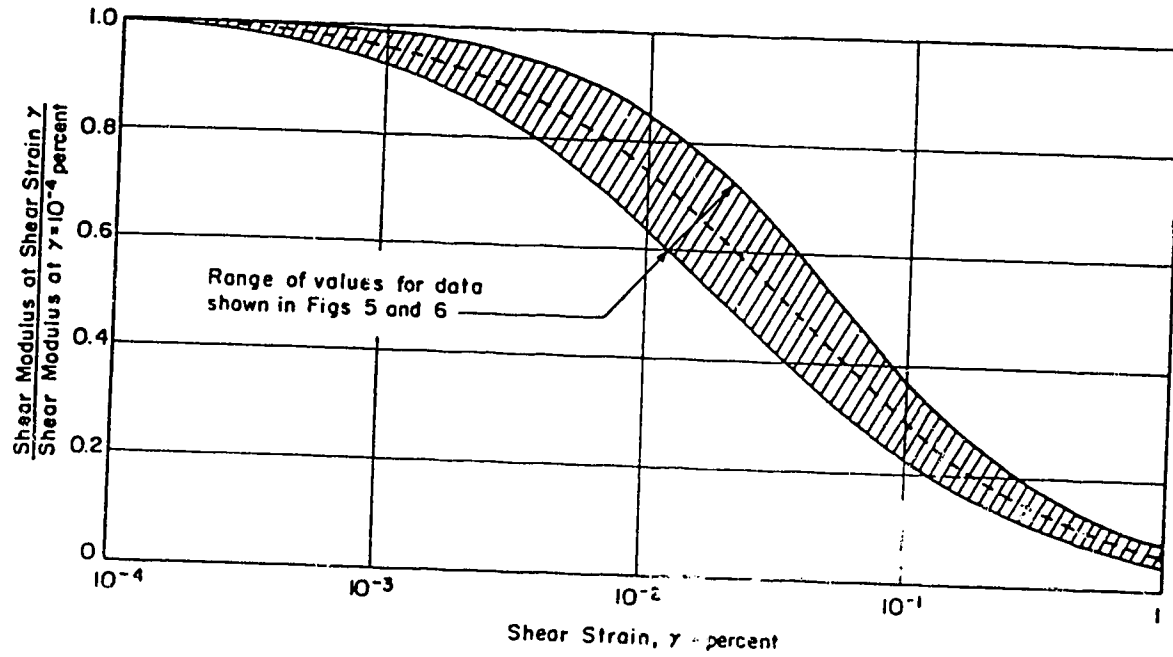
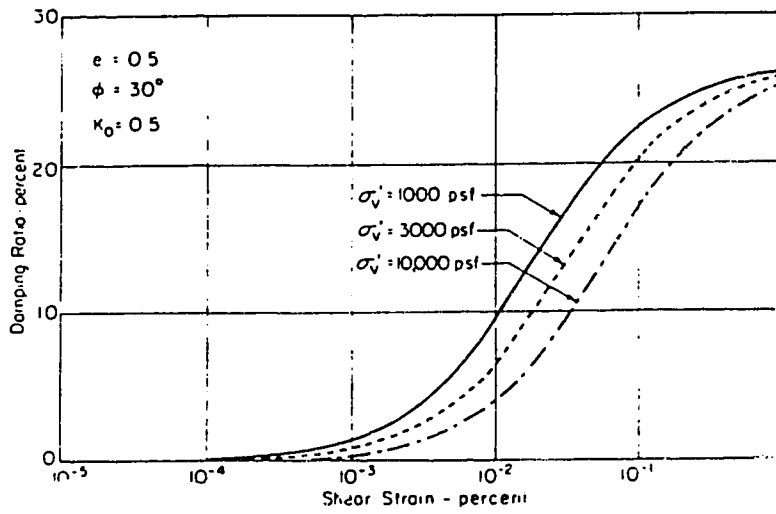
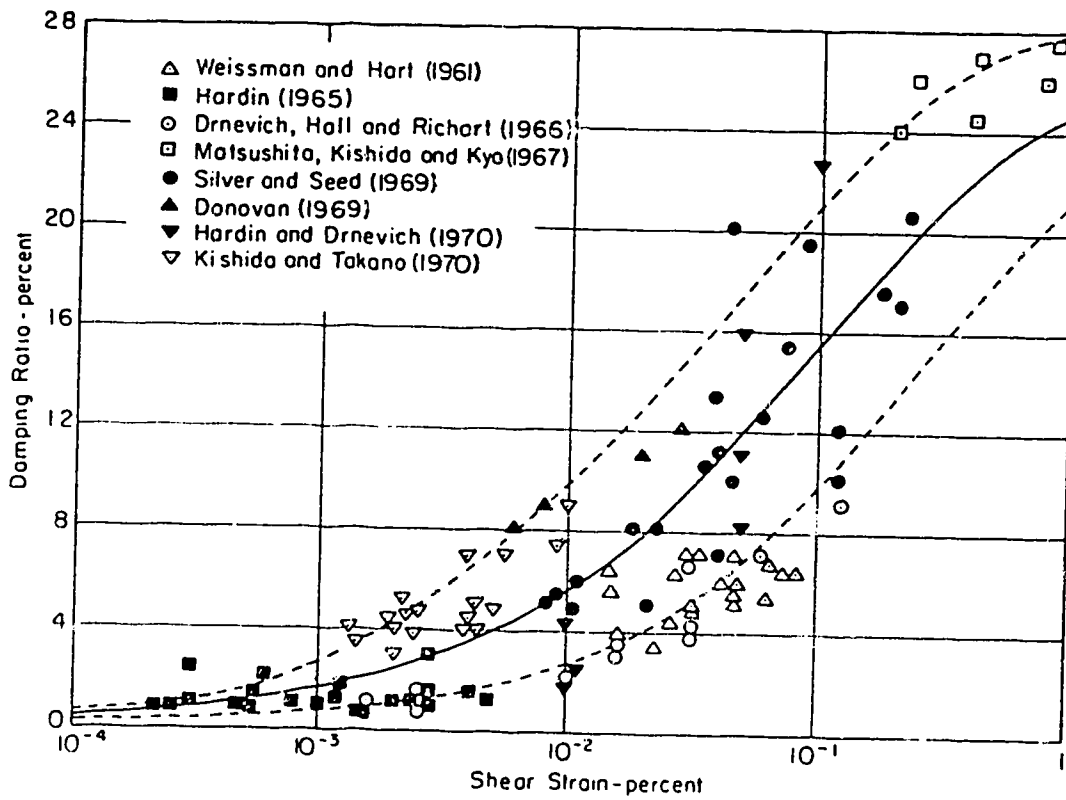


Figure 4.2  $G/G_{max}$  versus  $\gamma$  curves for sands, after Seed and Idriss (1970)



**Figure 4.3 Influence of confining pressure on the damping ratio, after Seed and Driss (1970)**



**Figure 4.4 Damping ratio versus shear strain for sands**

STEEP SLOPE 20 Degrees, H=10m

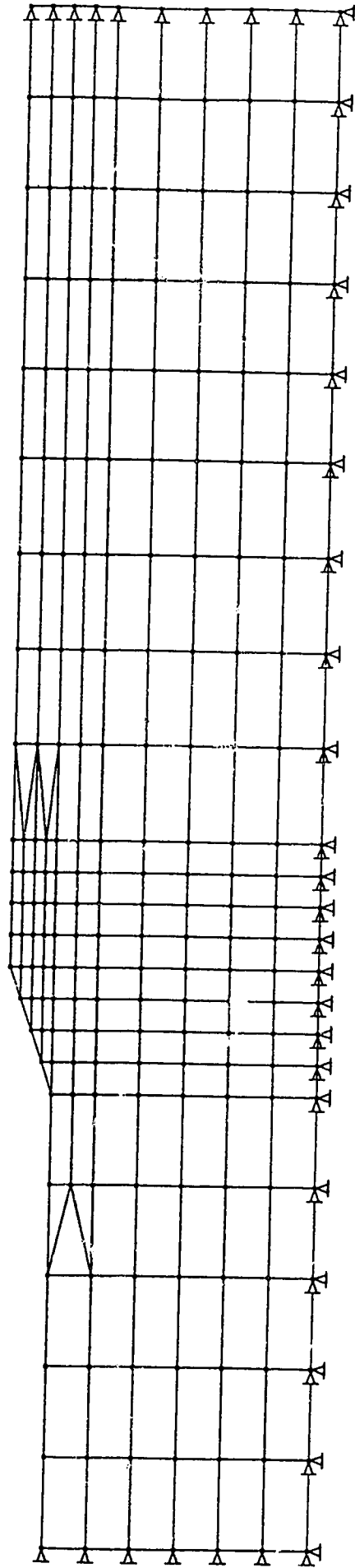


Figure 4.5 Typical finite element mesh used in the analyses



## Chapter 5

### Results

#### 5.1. Introduction

Chapter 4 briefly presented and discussed the models and programs used for the numerical analyses carried out in this research. The analysis procedure consists of two steps: 1) the determination of the initial static shear stresses and 2) the computation of the dynamic shear stresses induced by the earthquake loading. These analyses have been carried out for two types of slope geometries, an infinite slope and the finite slope. In this chapter a summary is presented of the most relevant results, especially those results that are of concern in defining the zones where no shear stress reversal occurs. For each type of geometry different slope angles were analyzed in order to cover the normal range of slope angles encountered in the field.

The first part of this chapter will summarize the input data utilized in both types of analysis. The rest of the chapter will focus on the zones of no shear stress reversal for both geometries.

#### 5.2. Summary of Input Data

##### 5.2.1. The Earthquake Record

Several variables come into consideration when choosing the earthquake motion for a dynamic analysis, as explained in chapter 4. The earthquake motion, usually represented by the acceleration history, is defined by three parameters. These are the period,  $T$ , the duration,  $D$  and the peak acceleration,  $a_{max}$ . In order to reduce the number of variables involved, for all the analyses, the values of the period,  $T$  and the duration,  $D$  have been fixed. The only variable used was the peak acceleration,  $a_{max}$ . Figure 5.1 shows the acceleration record used for all the dynamic analysis carried out in this thesis.

## 5.2.2. Soil Properties

### 5.2.2.1. Properties used in the static analyses

For the static analyses the “Switch on gravity” approach was used, therefore the results (regarding stresses not deformations) are not sensitive to the values used for the deformation properties (e.g. elastic modulus, E) or the stress-strain relationship. The main properties affecting the computation of the insitu stresses, are the unit weight,  $\gamma$  and Poisson’s ratio,  $\nu$ . All the deposits analyzed had the same average values for these properties:

$$\begin{aligned}\gamma &= 19.8 \text{ kN/m}^3 \\ \therefore \gamma' &= 10 \text{ kN/m}^3 \\ \nu &= 0.3\end{aligned}$$

All the analyses considered that the slope was completely submerged, therefore the effective unit weight,  $\gamma'$  was used.

### 5.2.2.2. Properties used in the Dynamic Analyses

Chapter 4 described which soil properties were required in order to perform a dynamic analysis using the equivalent linear method. For every deposit analyzed the shear stiffness was increased with depth (or indirectly the shear wave velocity). This was done to simulate the increase in shear modulus with increasing overburden pressure. Figure 5.2 shows the soil properties used for the 30 degree finite slope, 20 meters high. All the other slopes analyzed had a similar variation of the soil properties with depth.

Besides the properties shown in figure 5.2 it was also necessary to specify the reduction of shear modulus (in terms of the ratio  $G/G_0$ ) and the damping ratio as a function of shear strain. The curves selected for the analyses were based on the curves published by Seed and Idriss (1970) and Idriss (1990), and are shown in figures 5.3a and 5.3b respectively.

A sensitivity analysis was carried out to evaluate the influence of the initial values of the dynamic soil properties on the seismic response. From this analysis it was concluded that very special attention should be given to the selection of values for the dynamic soil properties, and that the stresses computed are almost directly proportional to the values of these properties. A summary of this sensitivity analysis is presented in Appendix B.

In the following sections the results obtained in the numerical analyses for each of the types of slopes studied will be presented.

### **5.3. Stress Reversal For Infinite Slopes**

To determine the depth of the zone of shear stress reversal in an infinite slope two basic steps have been considered. First the in-situ static shear stresses which depend on the effective vertical stress and the inclination of the slope were calculated. Secondly the dynamic shear stresses induced by the earthquake were estimated. The dynamic stresses are influenced by many factors such as: the characteristics of the earthquake (i.e. peak acceleration, fundamental period, and duration), characteristics of the soil deposit such as insitu stresses, deformation characteristics (stiffness, stiffness degradation after first cycle of dynamic loading), damping, natural period, resonance conditions, etc.

Once the static and dynamic stresses have been determined it is possible to evaluate the location of shear stress reversal. In the following sections, guidelines are given on how to estimate both the static and dynamic stresses for infinite slopes and how to calculate the depth of the zone of shear stress reversal.

#### **5.3.1. Static Shear Stresses**

A submerged infinite slope inclined an angle  $\beta$ , is shown in figure 5.4. For a slice of this slope it is possible to calculate the stresses acting at a given depth. The stresses acting along the bottom of the slice (plane parallel to the slope) are the following:

- Shear stress parallel to slope:

$$\tau_s = z \gamma' \sin \beta \cos \beta \dots\dots\dots(5.1)$$

- Normal effective stress on surface parallel to slip:

$$\sigma'_n = z \gamma' \cos^2 \beta \dots\dots\dots(5.2)$$

From equation 5.1 it is clear that the static shear stresses increase linearly with depth. In order to evaluate correctly the occurrence of shear stress reversal it is necessary to compare the static and dynamic stresses acting on the same plane. Commonly the stresses on a horizontal plane are used for comparison. Therefore, the above shear stress need to be transformed to the horizontal plane. Figure 5.5 shows the Mohr circles of stress for three different values of  $K_0$ . From this figure the following general equation for the shear stresses acting on the horizontal plane is obtained;

$$\tau_{xy} = K_0 z \gamma' \tan \beta \dots\dots\dots(5.3)$$

### 5.3.2. Dynamic Shear Stresses

#### 5.3.2.1. Simplified approach

Before performing a more rigorous computer analysis, a preliminary estimate of the dynamic stresses induced by an earthquake can be made, using the simplified equation proposed by Seed and Idriss, (1971). The stresses obtained from this equation are only applicable for level ground conditions, but it can be a guide to estimate the magnitude of the dynamic stresses induced in gently sloping ground. Equation 5.4 shows Seed and Idriss's simplified equation.

$$\tau_{cyc} = 0.65 (a_{max}/g) z \gamma' r_d \dots\dots\dots(5.4)$$

where  $a_{max}$  is the maximum acceleration at the ground surface,  $r_d$  equals a stress reduction factor allowing for the deformability of the soil, which takes a value less than unity. Iwasaki et al. (1978) recommended the following empirical formula for  $r_d$  :

$$r_d = 1 - 0.015z \dots \dots \dots (5.5)$$

where the depth,  $z$  is in meters. Combining equations 5.4 and 5.5 we obtain the following expression:

$$\tau_{cyc} = 0.65 (a_{max}/g) z \gamma (1-0.015z) \dots \dots \dots (5.6)$$

Equation 5.3 shows how the static shear stresses increase linearly with depth, and are a function of the unit weight of the soil, the coefficient of earth pressure  $K_o$  and the inclination of the slope. On the other hand, the cyclic stresses, given by equation 5.6, have a parabolic relation with depth, increasing fast at shallow depths and at a slower rate at larger depths. Therefore, if the peak ground acceleration is large, the cyclic stresses near the surface will be larger than the static stresses, allowing shear stress reversal to occur. The zone of shear stress reversal will extend to a certain depth (*Depth of Zone of Shear Stress Reversal*) which will basically depend on the peak ground acceleration and the slope inclination. For a given peak ground acceleration there is a certain *critical slope angle* for which there will be no shear stress reversal anywhere. The expressions for the depth of the zone of shear stress reversal and the critical slope angle are the following:

- Depth of Zone of Stress Reversal:

Condition for Stress Reversal to occur:  $\tau_{cyc} > \tau_{xy}$

$\therefore 0.65 (a_{max}/g) z \gamma (1-0.015z) > K_o z \gamma' \tan \beta$

from this expression:

$$Z_{\text{Reversal}} \leq \frac{1}{0.015} \frac{K_o \gamma' \tan \beta}{\left(0.65 \cdot 0.015 \cdot \frac{a_{\text{max}}}{g} \cdot \gamma\right)}$$

simplifying:

$$Z_{\text{Reversal}} \leq 66.7 - \frac{102.6 \cdot K_o \cdot \tan \beta}{\frac{\gamma}{\gamma'} \cdot \frac{a_{\text{max}}}{g}} \quad (5.7)$$

- Critical Angle:

From equation 5.7 if  $Z_{\text{Reversal}}$ , the depth of the zone of stress reversal, is equal to zero it is possible to obtain the following expression for the critical slope angle:

$$\tan \beta_{\text{crit}} = (0.65 \times (a_{\text{max}}/g)) / (K_o \gamma' / \gamma)$$

$$\beta_{\text{crit}} = \tan^{-1} \left[ \frac{0.65 \cdot \frac{a_{\text{max}}}{g} \cdot \frac{\gamma}{\gamma'}}{K_o} \right] \quad (5.8)$$

Figures 5.6 and 5.7 show the depths of shear stress reversal for  $K_o=0.5$  and 1, respectively. These figures provide an estimate of the order of magnitude for these depths. The estimate is better for smaller slope angles since they are closer to the level ground conditions for which equation 5.4 was originally developed.

### 5.3.2.2. Computer analyses using Quad4TB

In order to evaluate how good the estimates are, using the simplified approach described in the previous section, several finite element analyses were carried out. The

dynamic stresses were calculated for four slope angles 5°, 10°, 15° and 30°. For each slope angle several runs were made varying the peak acceleration at the base of the mesh. In total 22 runs were made. Figures 5.8 shows the finite element mesh used in the analyses of the 5° slope. With slight changes in the ordinates of the nodes of the upper portion of this mesh the meshes for the other slope angles were obtained. Table 5.1 shows the soil properties used in the analyses:

**Table 5.1 Soil Properties Infinite Slope Analysis**

Layer	Soil Type	Depth (m)	$\gamma$ (kN/m <sup>3</sup> )	Go (MPa)	G/Go vs $\gamma$ curve	Initial Damping
1	Sand	0 - 18	20	50	Seed & Idriss (1970)	0.05
2	Sand	18 - 33	20	85	Seed & Idriss (1970)	0.05
3	Sand	33 - 40	20	100	Seed & Idriss (1970)	0.05

Figure 5.9 shows a typical set of results from the dynamic analysis; in this particular figure the variation of the dynamic shear stresses with depth, for the 5° slope are shown. The corresponding static stresses, for both  $K_0$  conditions, are also plotted. At the depth where the dynamic stresses intercept the static stresses define the depth of the zone of shear stress reversal. It is important to point out that for each run performed the surface acceleration was recorded in order to compare the results with the simplified approach, since the simplified approach was based on surface acceleration. The results corresponding to the 22 analyses carried out are presented in Appendix C. In some of the runs no shear stress reversal occurs. Figures 5.10 and 5.11 compare the results from the simplified approach with the results using Quad4 for  $K_0=0.5$  and 1.0, respectively. From these figures it can be seen that the simplified approach underestimates the depth of shear stress reversal for slope angles greater than 10°, for the case of  $K_0=0.5$ . For  $K_0=1.0$ , the discrepancies become considerable at angles greater than 5°. The greater the slope angle the greater the error using the simplified approach. Using the dynamic analyses results approximate curves to estimate the depth of shear stress reversal can be developed. These

curves are shown in figures 5.12 and 5.13 for the cases of  $K_0=0.5$  and  $K_0=1.0$ , respectively.

## 5.4. Shear Stress Reversal for Finite Slopes

### 5.4.1. Introduction

In the previous section results concerning infinite slopes were presented. In practice, slopes can not always be treated as infinite. In this section results corresponding to finite slopes will be presented.

Three slopes angles ( $\beta = 10^\circ, 20^\circ$  and  $30^\circ$ ) were studied, and for each slope angle four slope heights were analyzed ( $H = 5$  m, 10 m, 20 m and 50 m). This gives a total of 12 different geometries studied. For each geometry different peak accelerations were used for the exciting motion applied at the base of the model. The goal of this part of the study was to obtain for each slope the contours defining the zones of no shear stress reversal, within the body of the slope, for the different  $a_{max}$  applied at the base. A total of 57 dynamic analysis were carried out to obtain these contours.

### 5.4.2. Static Analysis

For the purpose of obtaining the zones where no shear stress reversal occurs, it is necessary to calculate the initial static shear stresses acting on the horizontal plane,  $\tau_{xy}$ . Figures 5.14, 5.15 and 5.16 show the stress contours for the insitu stresses for the 30 degrees,  $H=20$  m finite slope obtained using Sigma-W<sup>®</sup>. Figures 5.14 and 5.15 show the contours of  $\sigma'_x$  and  $\sigma'_y$  respectively. These contours in the horizontal surface areas far from the slope are equal to the unit weight times the depth (for  $\sigma'_y$ ) and times  $K_0$  (for  $\sigma'_x$ ). This provides confidence with the results obtained from the static analysis. For the definition of the zones of no shear stress reversal we only need the  $\tau_{xy}$  contours, Figures 5.17 through 5.27 show these contours for the other slopes studied.



### 5.4.3. Dynamic Analysis

The dynamic analyses were carried out using the same finite element meshes used in the static analyses. The nodes at the base of the mesh, are used by the program as the nodes where the earthquake motion is applied. The boundaries at each side of the slope were chosen to be sufficiently far (at least 2 times H) to avoid undesired influence of these on the computed dynamic stresses.

The peak acceleration profile at the base was uniform since, as explained above, these nodes were points of excitation. However the peak acceleration profile at the surface of the mesh was variable. This complicates the determination of the contours of the zones of no shear stress reversal as a function of the surface acceleration. The surface acceleration profile, depends on many factors, due to the geometric changes in the surface, due to the variation of the natural period of the soil columns (which are a function of the depth to bedrock and the dynamic properties), etc.

The depth to bedrock, from the toe of the slope, was chosen to be 60 meters for all the analyses presented here. Different depths to bedrock will affect the length of wave propagation and the seismic response will be affected by this. The next section illustrates how much this depth affects the dynamic stresses and the surface acceleration profile for the finite slope of 30 degrees angle,  $H = 20$  m.

### 5.4.4. Influence of the Depth to Bedrock

To evaluate the influence of the depth of the bedrock ( $H_B$ ) in the analyses, the 30°,  $H = 20$  m finite slope was selected. Three cases were studied  $H_B = 40$  m,  $H_B = 60$  m and  $H_B = 80$  m. All these cases were analyzed for only one acceleration record corresponding to  $a_{max} = 0.2$  g.

Figure 5.28 shows the influence that the depth to bedrock has on the curve of acceleration versus depth at the middle of the slope. The accelerations decrease with increasing depth to bedrock, suggesting that the attenuation factor is larger for higher columns of sand (i.e. longer natural periods). This effect can also be seen in figure 5.29 where the surface acceleration profiles are shown for each depth to bedrock considered. Again the attenuation of accelerations is higher for deeper bedrock. Also the surface acceleration is higher at the toe (smaller height of column of sand) than beyond the crest (20 meters more of sand, i.e. longer natural period). The crest acceleration values are close to the corresponding toe acceleration values for bedrock 20 meters deeper. Within the slope, the acceleration profile is variable, decreasing initially until it reaches a minimum approximately at the mid slope point, from this point onwards it increases until it reaches the crest point, where it stops increasing. This figure shows how important the two dimensional effects can be in the seismic response of a soil deposit, and it also shows the complexity of the problem due to the variables involved.

Figure 5.30 shows the influence that the depth to bedrock has on the mid-slope shear stress profile. From this figure the stresses increase with decreasing depth to bedrock (i.e. less attenuation), but the variation is not so pronounced compared to the accelerations case.

The purpose of this subsection was to point out that the results presented in this chapter are applicable only for a depth to bedrock equal to 60 meters, and that results can only be considered as an estimate for other conditions.

#### 5.4.5. Definition of the Zones of No Shear Stress Reversal

Using the results from the static and dynamic analyses described in the previous sections, the contour of the zone where there is no shear stress reversal (*No Reversal Zone*) can be defined. If for a given element of the finite element mesh the average dynamic shear stress, computed in the dynamic analysis, is smaller than the corresponding

static shear stress, this element belongs to this *No reversal zone*. By doing this comparison procedure for all the elements of the mesh it is possible to estimate the approximate shape of the *No reversal zone*. The smaller the dynamic stresses induced the larger the *no reversal zone* should be. The steeper the slope the higher the initial static shear stresses in the slope, and therefore the larger the *no reversal zones* compared to less steep slopes.

The dynamic shear stresses computed by Quad4TB are part of the output file generated by the program. These stresses are calculated for each element, and are saved as a regular text file, which can be imported into any spread sheet software. The comparison process described above was done using a spread sheet. As a result of the comparison process the spread sheet would only list the elements where no shear stress reversal occurred and would also show the degree of shear stress reversal, expressed by a ratio between the dynamic shear stress and the static shear stress ( $R = \tau_{dyn} / \tau_{stat}$ ).

As mentioned before, a total of 57 analyses were carried out. For each of these analysis the comparison process was done and therefore a no shear stress reversal contour was obtained. For some geometries the static stresses were so small that the peak accelerations had to be very small to actually obtain zones of no reversal. Figures 5.31 through 5.42 show the contours obtained for each finite slope analyzed.

#### 5.4.6. Discussion of Results

For a gentle slope of  $10^\circ$ , and slope heights less than 50 m for base accelerations higher than 0.1 g the zone of no reversal is very small or essentially non-existent, and is usually located at the crest of the slope. For slope heights greater than 50 m a considerably larger zone of no shear stress reversal occurs underneath the slope. For small bedrock accelerations ( $< 0.1$  g) larger zones of no shear stress reversal, are expected. It is interesting to note that there is a pattern where the zones tend to start from the crest and as the acceleration decreases the zones get larger extending towards the toe and underneath the slope

For an intermediate slope angle, such as  $20^\circ$  a similar trend is found, but now the initial shear stresses are larger, therefore higher accelerations are required at the base to generate a similar size of zones of no shear stress reversal. For a height of 5 m a very small zone of no shear stress reversal is observed at the crest, remaining the same size for the whole range of accelerations covered (0.1g - 0.5g). For slope heights between 10 and 20 m a considerable zone of no shear stress reversal is observed underneath the slope. For the 50 m high slope the static shear stresses are so high that the zones of no shear stress reversal extend all the way to the bedrock and throughout the slope. Here the zones of reversal are only on the horizontal sections beyond the toe and crest of the slope.

The final case studied was a steep slope of  $30^\circ$ . For this slope angle a major zone of no shear stress reversal exists beneath the slope. The higher slopes showed larger zones increasing in size as the height increased.

The consequences of having a central portion of no shear stress reversal within a slope could be important for deposits of medium to dense sands, where cyclic mobility could predominate. However, cyclic liquefaction can occur in the level ground at the toe of a slope resulting in large deformations during the cyclic loading.

## **5.5 Comparison of Results**

### **5.5.1 Introduction**

The direct comparison of the results presented in the previous sections of this chapter with other calculations or analyses carried out for sloping sand structures was not possible. This is mainly due to the fact that liquefaction assessment studies generally do not differentiate between cyclic liquefaction and cyclic mobility. Therefore, they do not approach the problem from the perspective of occurrence of shear stress reversal or not,

but rather follow the conventional simplified methods which tries to incorporate the influence of the initial static shear stress by using a correction factor such as  $K_{\alpha}$ .

Sunaka et al. (1988) carried out an effective stress analysis of a  $30^{\circ}$  - 15 meter high slope, the authors defined liquefaction as the condition of zero effective stress. The study showed that a considerable portion underneath the slope did not liquefy. Their results compared with Seed's conventional procedure showed that Seed's method overestimates the liquefaction potential of the deposit, predicting liquefaction everywhere underneath the slope. Several 2D studies similar to that of Sunasaka et al. (1988) have been presented, but they do not give any guideline regarding the zones of no shear stress reversal.

The liquefaction assessment study of Duncan Dam study had sufficient data available to back-calculate the zones of no shear stress reversal. The following will present a comparison of results from this study and that of Duncan Dam.

### 5.5.2 Duncan Dam Study

Duncan Dam is located on the Duncan river approximately 8 km north of Kootenay lake in southeastern British Columbia. The dam is a zoned earthfill embankment 39 m in height with relatively flat upstream and down stream slopes. Figure 5.43 shows a typical dam section. The results presented in this section were obtained from the liquefaction assessment and seismic stability studies done by BC Hydro under the Dam Safety Program. A detailed description of Duncan Dam and the liquefaction assessment studies carried out can be found in Byrne et al. (1993).

Figure 5.43 shows the different units of soils composing the foundation of Duncan Dam. Unit 3c was considered to be the major concern in the liquefaction assessment study, and consisted of a uniform fine sand ( $D_{50} = 0.2$  mm) with a fines content of about

5%. The relative density of the unit 3c sand was indicated to be about 30% to 35% beneath the dam toe and 55% to 60% beneath the dam crest (Plewes et al., 1993).

In order to evaluate the liquefaction potential of the foundation soils at Duncan Dam several analysis were carried out by BC Hydro. A static analysis was carried out to evaluate the initial stresses and values of  $\alpha$  in the foundation soils. They were calculated at the end of construction and for maximum reservoir conditions. The dynamic analyses performed were one dimensional, and used the computer code SHAKE (Lysmer et al., 1972). For these analyses the Helena Earthquake ( $a_{max}=0.12$  g) was used as input motion at the base of the soil column. The cyclic stress ratio, CSR, was computed continuously for the full depth of fill and foundation materials, a detailed description of the results obtained is given by Pillai and Stewart, 1993).

In order to obtain the zones where no shear stress reversal occurred we must compare the values of  $\alpha$  with the CSR values and wherever  $\alpha$  exceeds the value of the CSR we have no shear stress reversal. The above can be explained further with the following expression for the factor of safety against shear stress reversal (FSR):

$$FSR = \frac{\tau_{static}}{\tau_{dynamic}} = \frac{\frac{\tau_{static}}{\sigma'_v}}{\frac{\tau_{dynamic}}{\sigma'_v}} = \frac{\alpha}{CSR}$$

Figure 5.44 shows the zones of no shear stress reversal obtained in the foundation soils, for maximum reservoir conditions. This last figure can be compared to the zones obtained using the curves from Quad4 presented in chapter 4, keeping in mind that these curves were obtained using a homogeneous slope of sand and there was no simulation of the maximum reservoir condition (this last factor may change quite considerably the initial distribution of static stresses). In order to compare the extent of the zone of no reversal, shown in figure 5.44, for a dam with variable slope inclination (3 slopes 2:1, 5:1 and 8:1),

two approaches were considered. One was to superpose the results of each of the slopes composing the dam and the second approach was to approximate the whole face of the dam to a single average slope angle of 17 degrees. Both results are shown in figure 5.45.

We can see that the extent of the zones of no stress reversal, using the different approaches, are quite similar. They both show a considerable zone underneath the downstream slope where no shear stress reversal occurs. This could be very important for post-earthquake stability analyses. Figures 5.46 and 5.47 show the areas of liquefaction, calculated by Pillai and Salgado (1993). It should be noted that liquefaction was predicted mainly where no shear stress reversal occurred. This is particularly true for figure 5.47 where the liquefaction potential was based on Seed's correction factor method, rather than for figure 5.46 where lab results on undisturbed samples were used to estimate the liquefaction extent.

The fact that a large portion of the predicted zones of liquefaction falls within the zone of no shear stress reversal, represents that cyclic mobility would occur in this zone. Therefore, this zone would present small strains, unless the soil is in loose state being then collapse liquefaction an important issue. This example illustrates the importance of the occurrence of shear stress reversal or not, and the influence it could have in the design or risk assessment of any real problem.

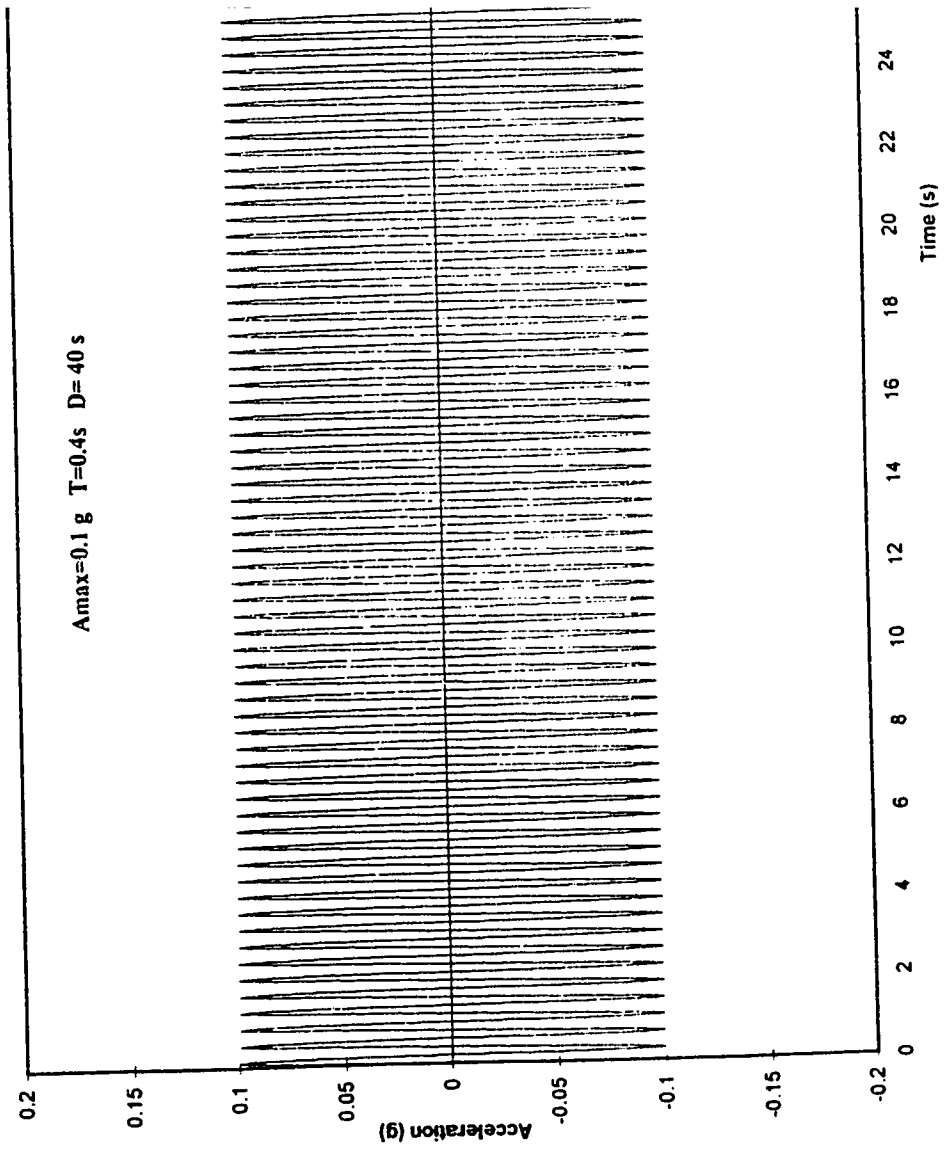


Figure 5.1 Typical Acceleration Record U



Finite Slope 30 degrees, H=20 m

Dynamic Properties

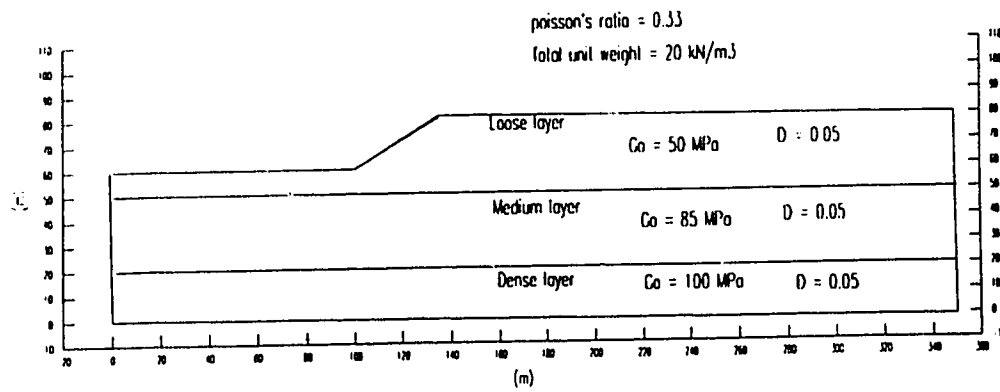
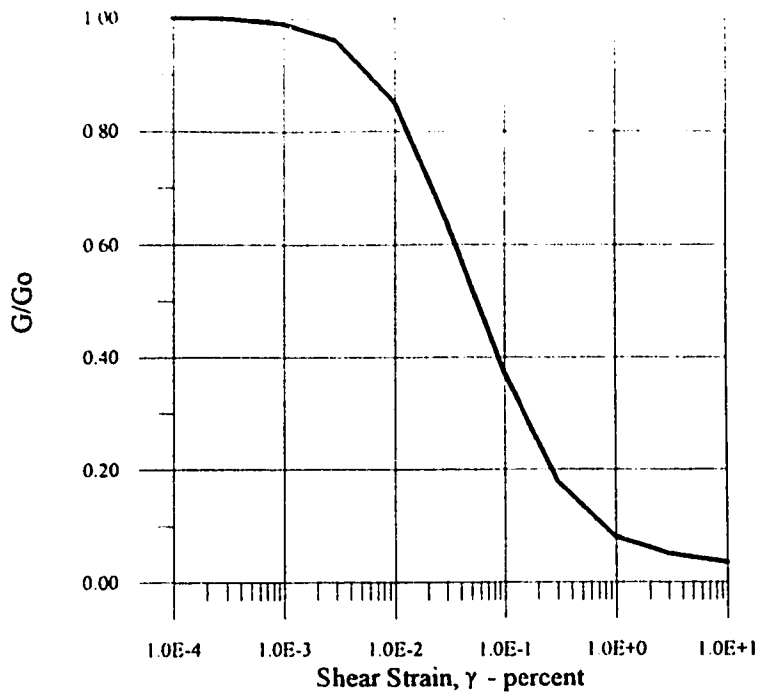
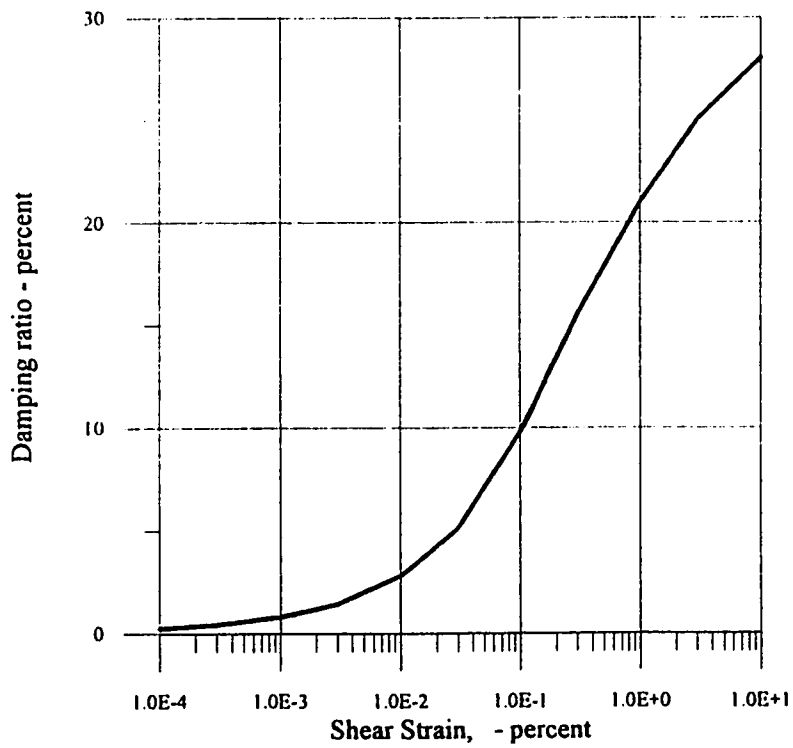


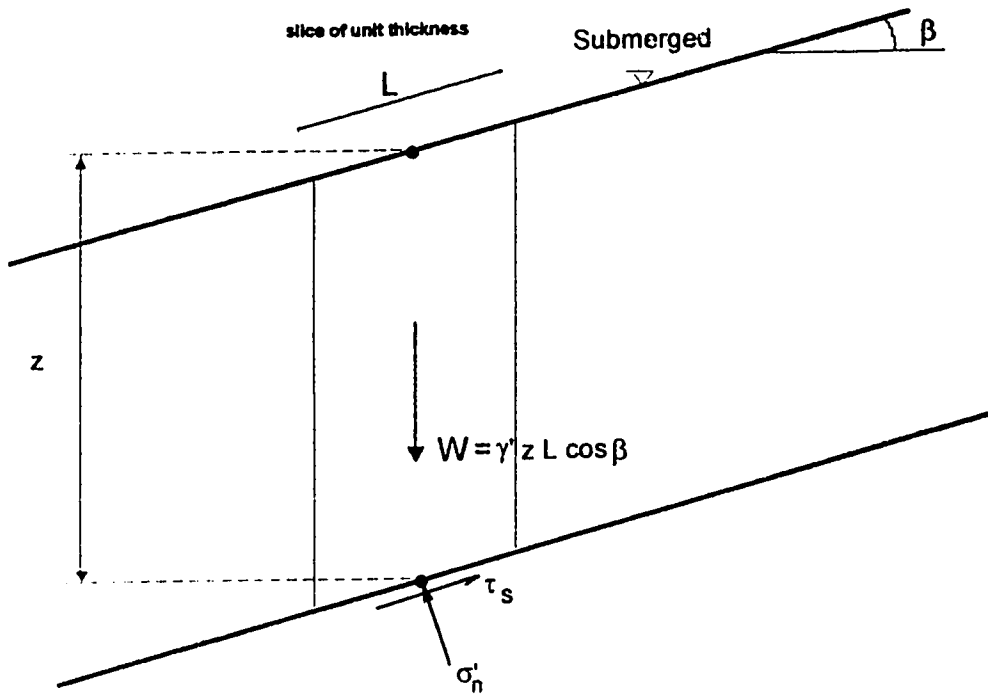
Figure 5.2 Dynamic Properties used for the 30°, H= 20 m Finite Slope



**Figure 5.3a. Variation of The Shear Modulus with Shear Strain**



**Figure 5.3b. Variation of The Damping Ratio with Shear Strain**



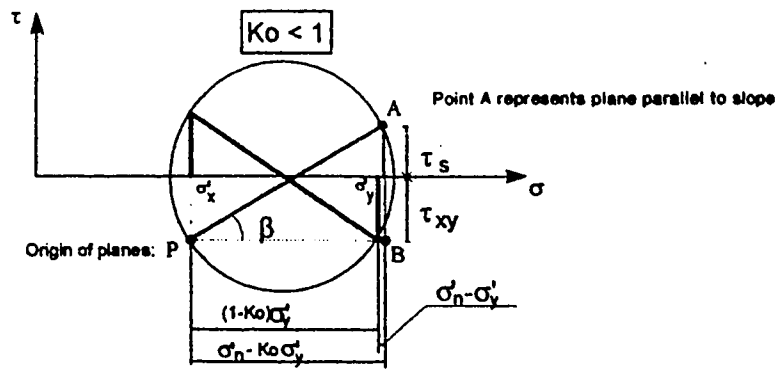
$$\Sigma F_y = 0: \quad \gamma' z L \cos \beta = \sigma'_n L \cos \beta + \tau_s L \sin \beta$$

$$\Sigma F_x = 0: \quad \sigma'_n L \sin \beta = \tau_s L \cos \beta$$

From the above equations:

$\sigma'_n = \gamma' z \cos^2 \beta$ $\tau_s = \gamma' z \sin \beta \cos \beta$
---

Figure 5.4 Stresses in a Submerged Infinite Slope



NOTE: Triangle PAB:  $\tan \beta = (\tau_s + \tau_{xy}) / (\sigma_n - K_o \sigma_y')$  [1]

but  $\sigma_n = \sigma_y' \cos^2 \beta$  [2]

$\tau_s = \sigma_y' \sin \beta \cos \beta$  [3]

[2] and [3] in [4], and rearranging:  $\tau_{xy} = K_o \sigma_y' \tan \beta$  [4]

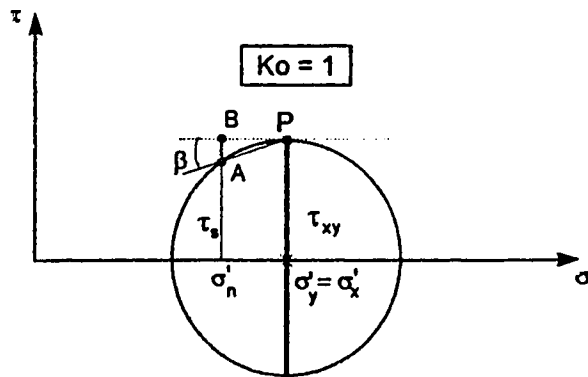
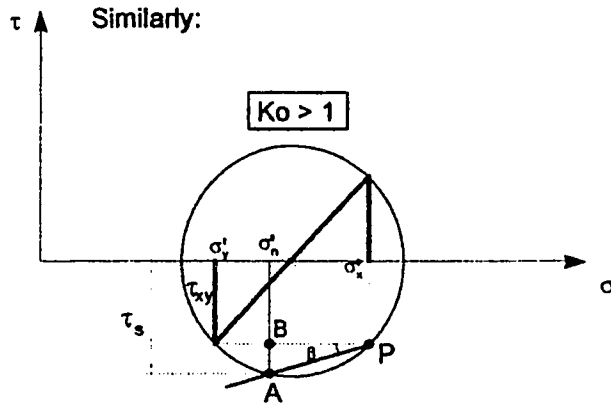
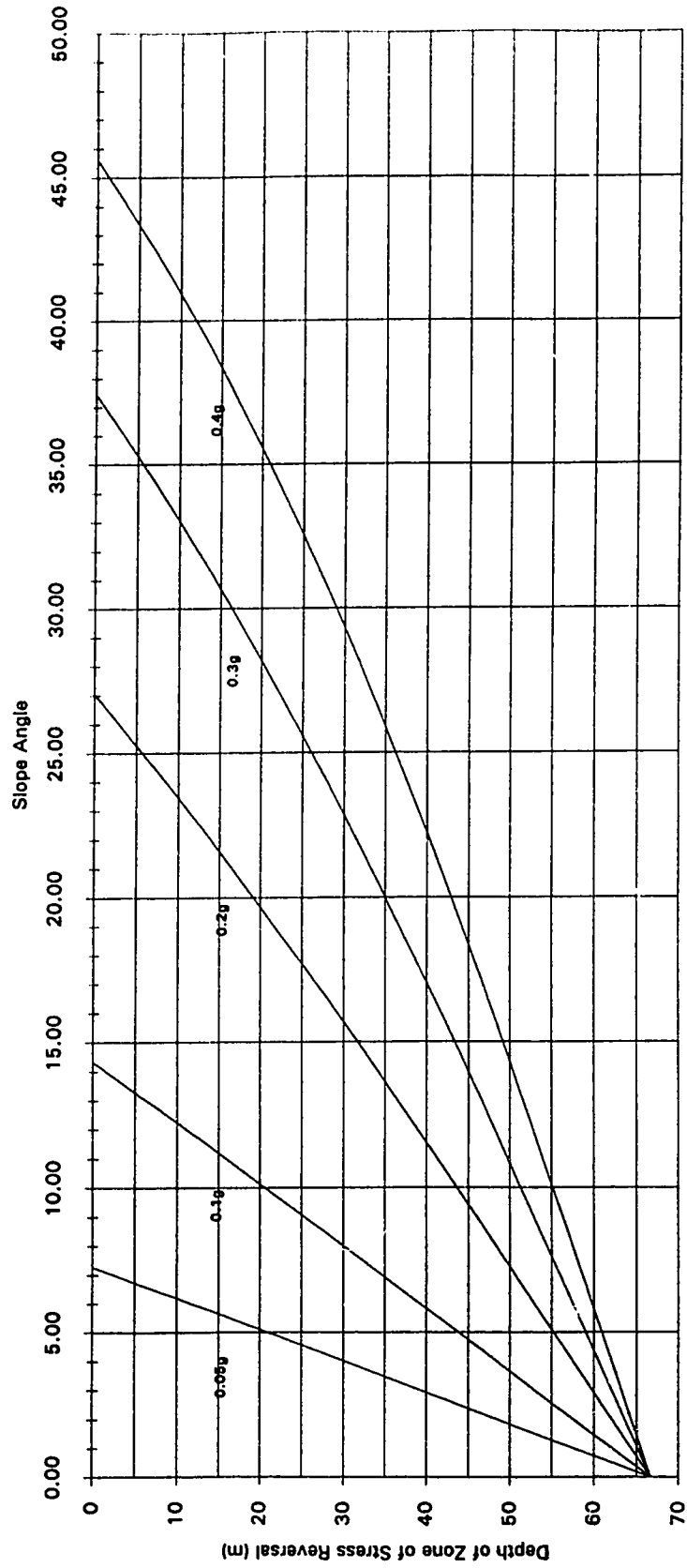


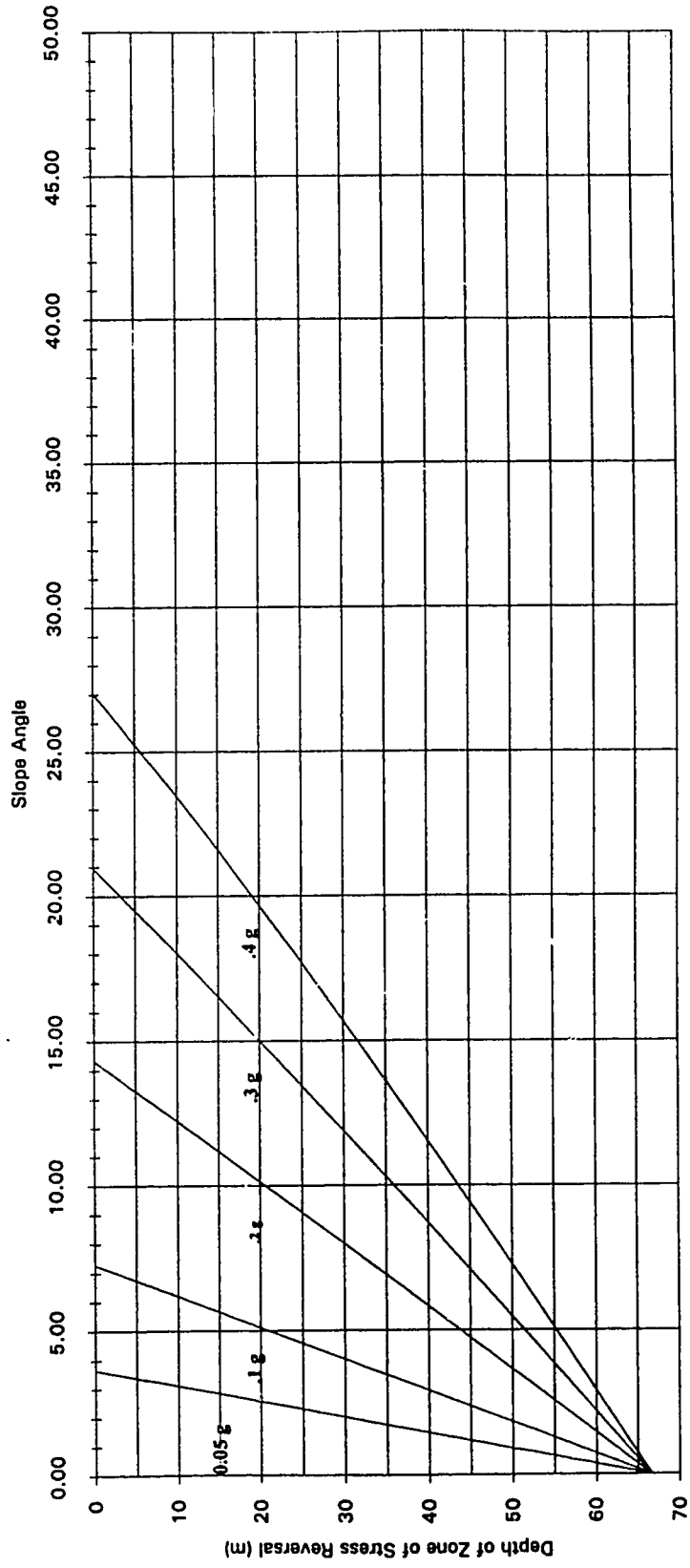
**Figure 5.5 Shear stress in the horizontal plane for an Infinite Slope Condition**

**Figure 5.6 Depth of Zone of Stress Reversal - Simplified Approach (Ko=0.5)**



**Note: Accelerations are peak surface accelerations**

**Figure 5.7 Depth of Zone of Stress Reversal - Simplified Approach (Ko=1.0)**



**Note: Accelerations are peak surface accelerations**

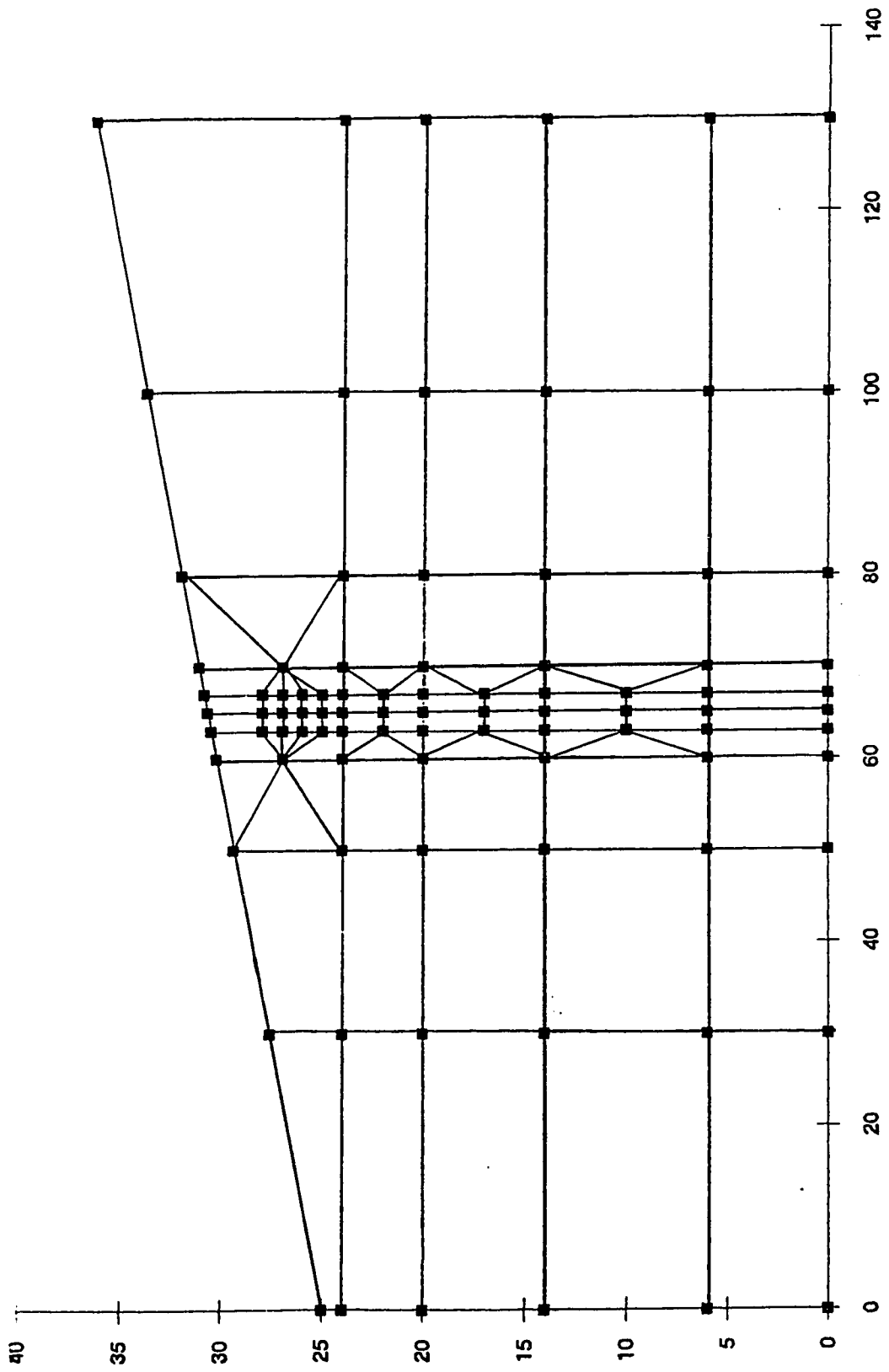


**Figure 5.8 Finite Element Mesh used for dynamic analyses in Infinite Slopes**

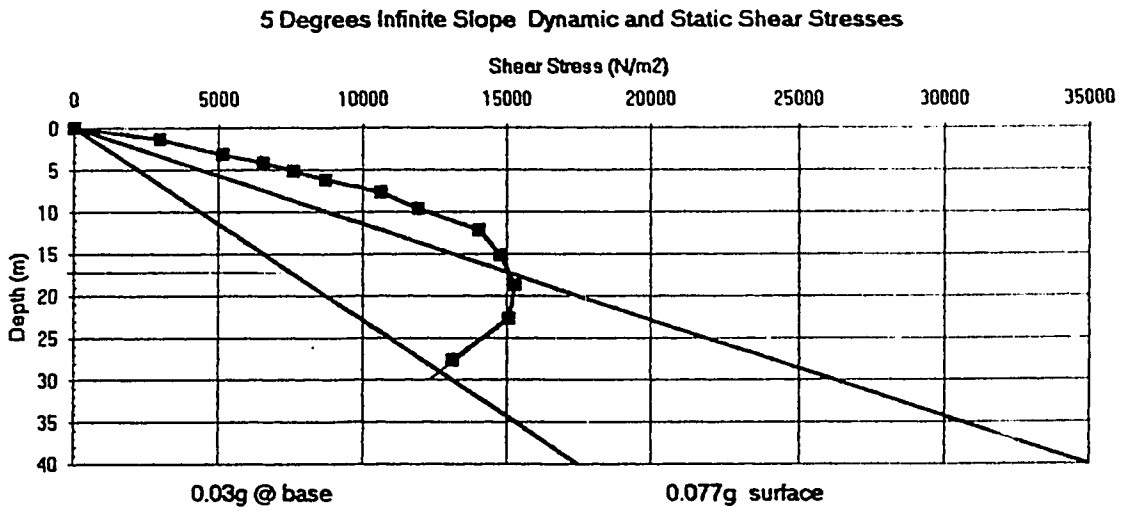


**Figure 5.9 Typical Dynamic Analysis Results in Infinite Slope Geometry**



**Figure 5.10 Comparison of Results between the Simplified Approach and Quad4 (Ko=0.5)**

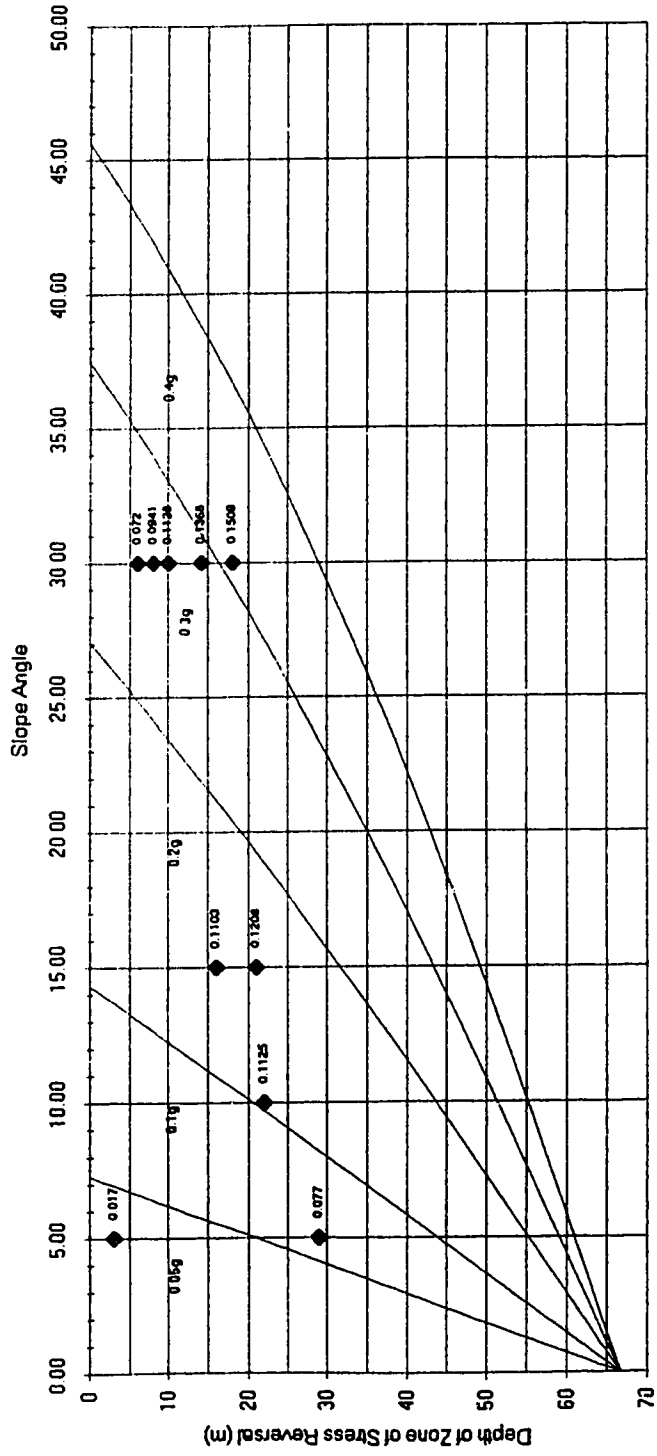


**Figure 5.11 Comparison of Results between the Simplified Approach and Quad4 (Ko=1.0)**

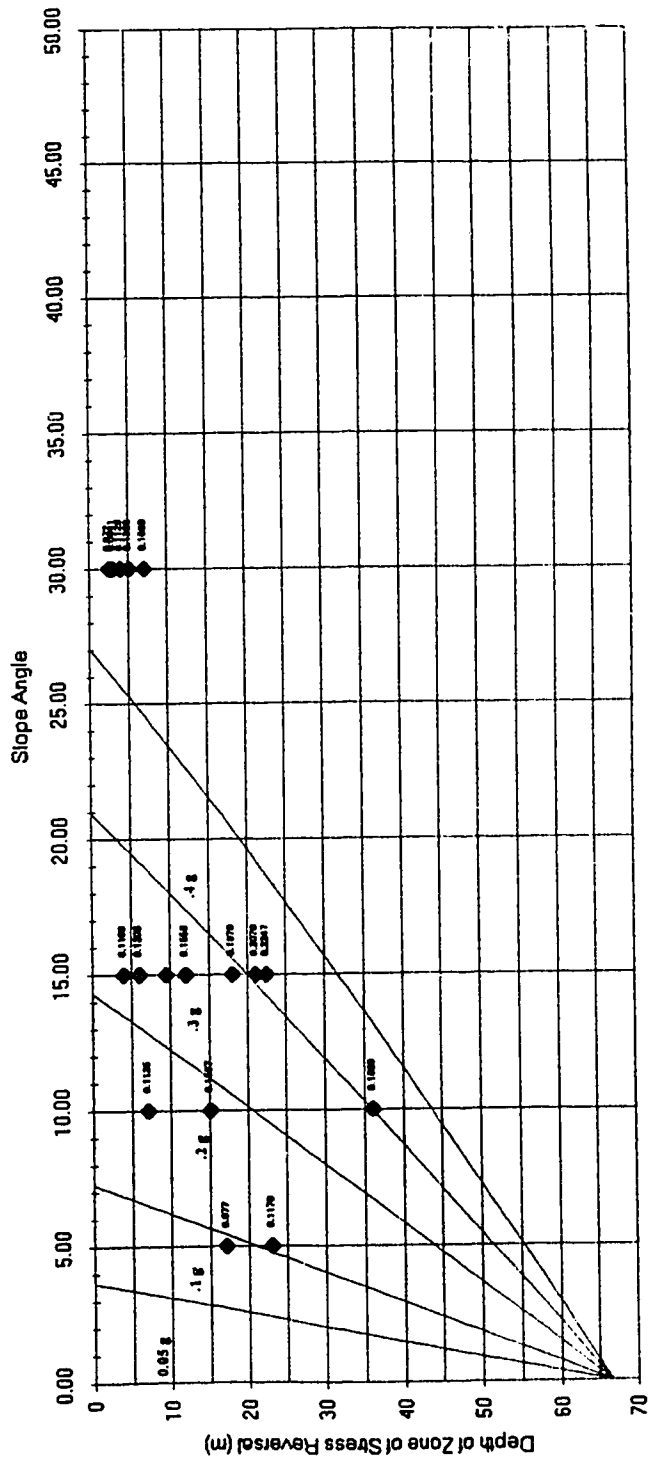


**Figure 5.12 Curves to obtain the Depth of the Zone of Stress Reversal ( $K_0=0.5$ )**

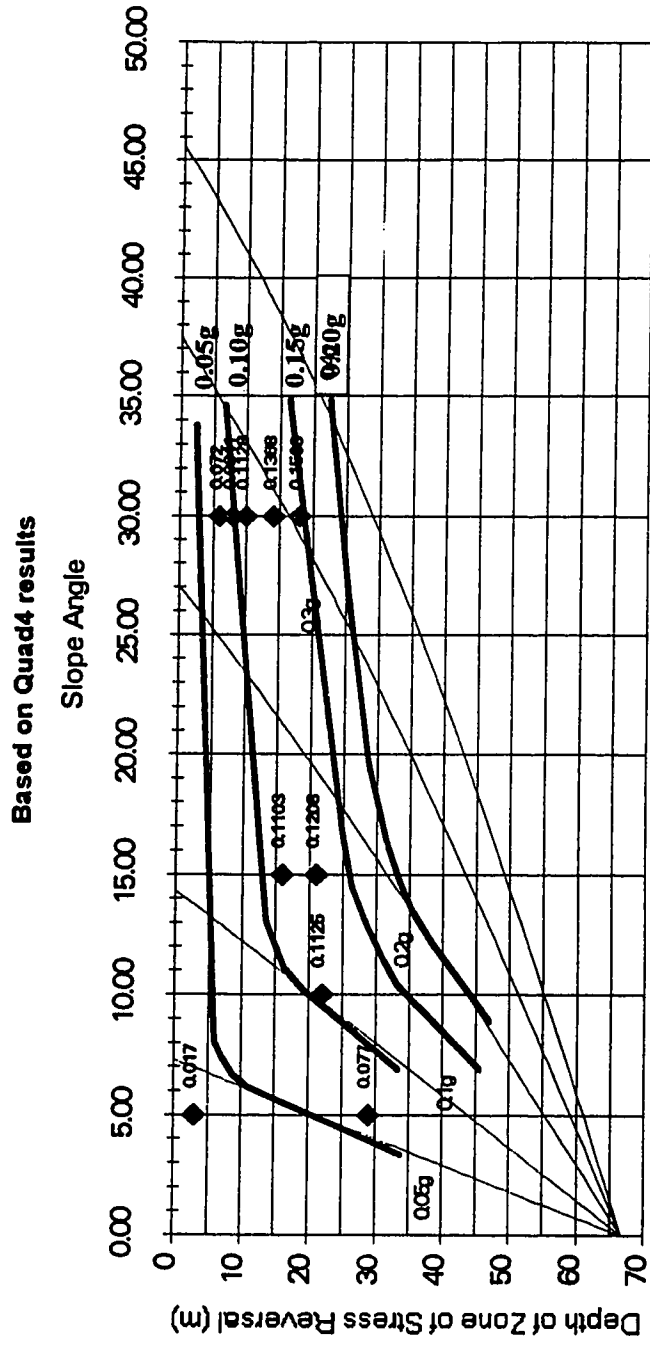
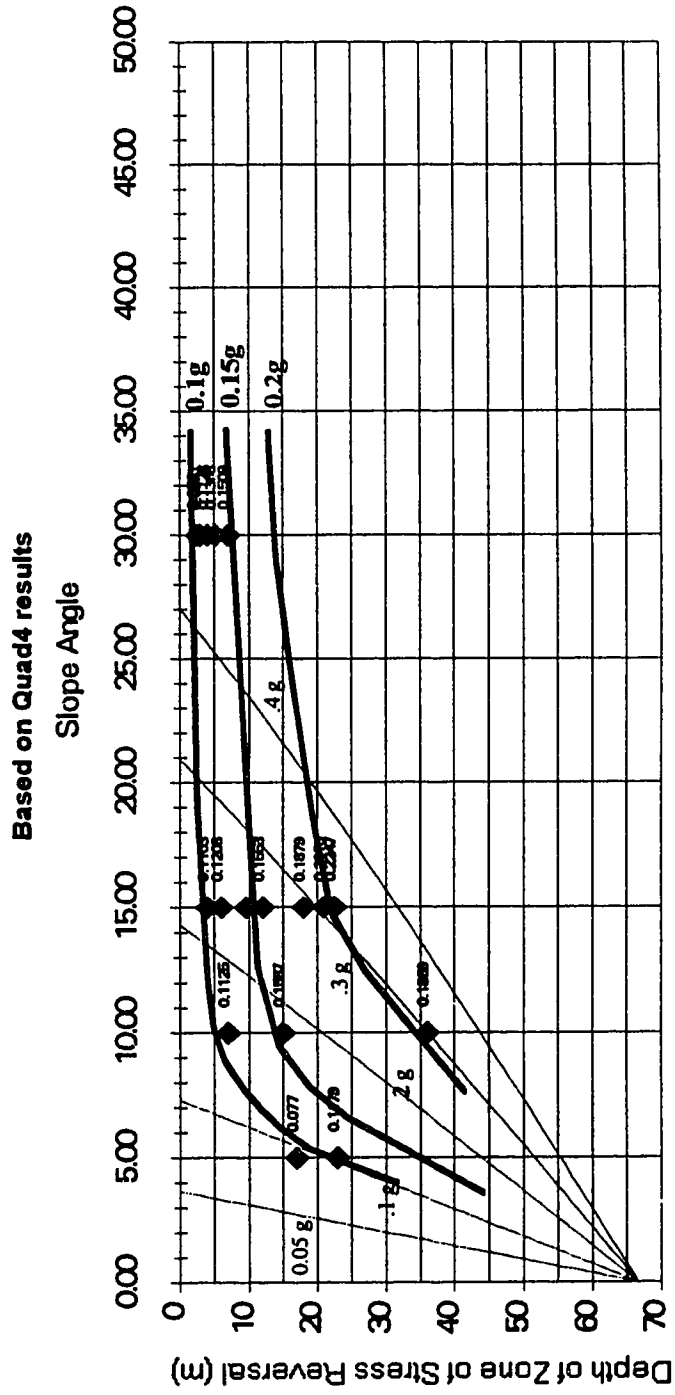


**Figure 5.13 Curves to obtain the Depth of the Zone of Stress Reversal ( $K_0=1.0$ )**



Finite Slope 30 degrees, H=20 m

$K_0=1.0$

Sigma-X (kPa) contours

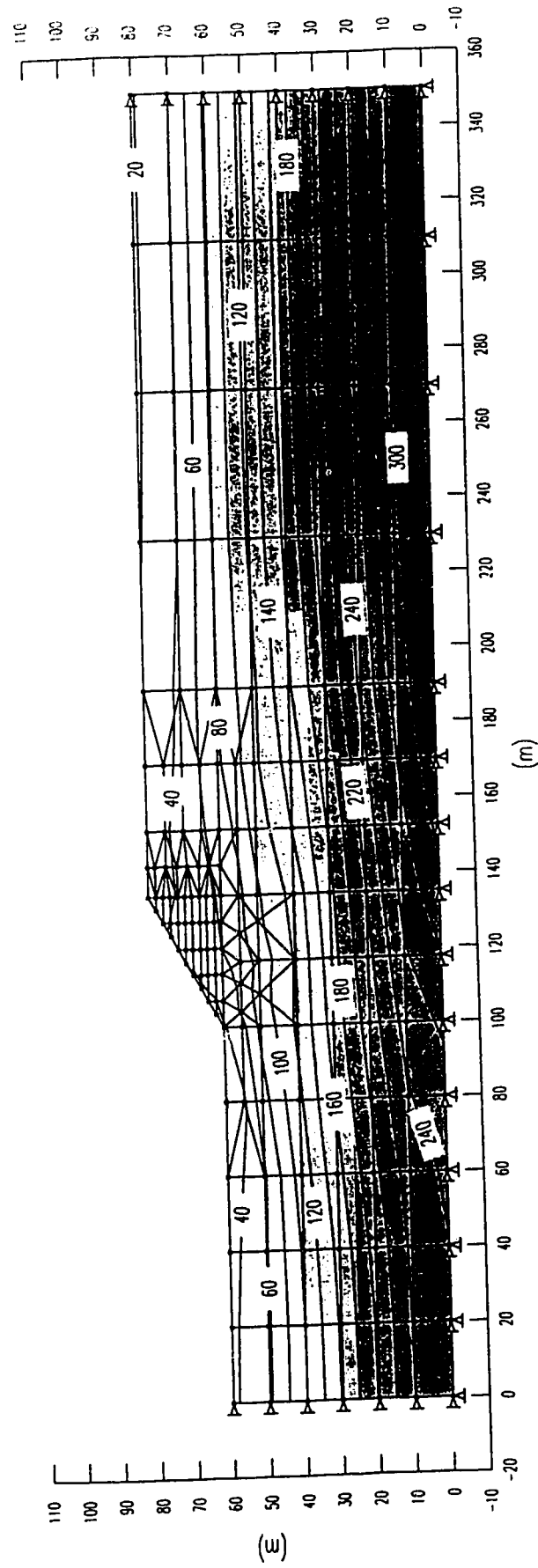


Figure 5.14 Initial Stresses for the 30°, H=20 m finite slope -  $\sigma_x$  contours

Finite Slope 30 degrees, H=20 m

Sigma-y contours (kPa)

$K_0=1.0$

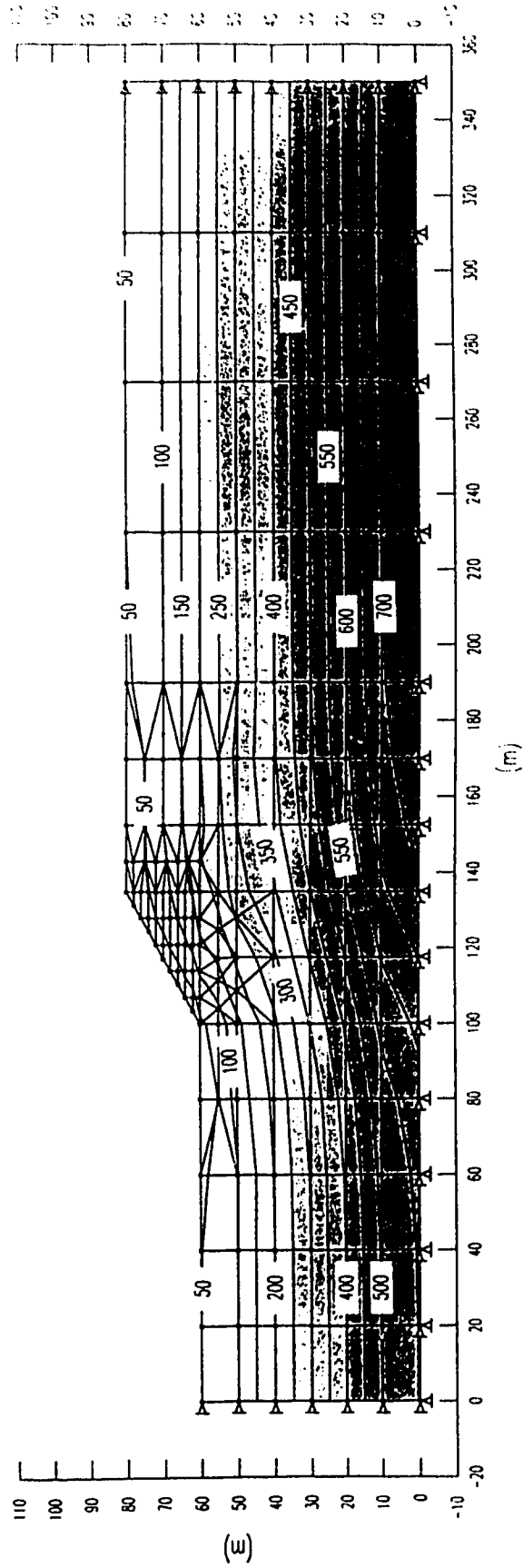
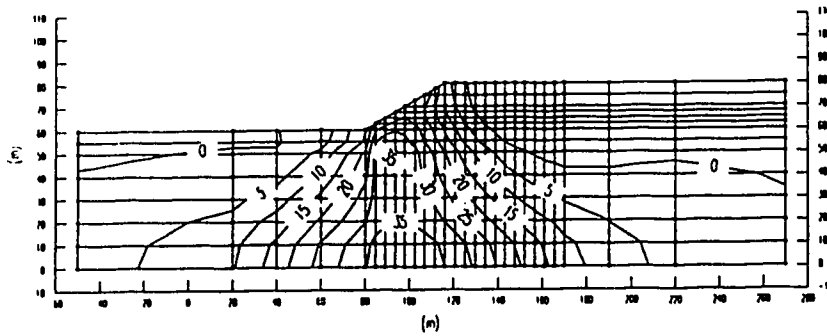


Figure 5.15 Initial Stresses for the 30°, H=20 m finite slope -  $\sigma_y$  contours

Finite Slope 30 degrees, H=20 m

$\tau_{xy}$  (kPa)



**Figure 5.16 Initial Stresses for the 30°, H=20 m Finite Slope -  $\tau_{xy}$  contours**

Finite Slope 10 degrees, H=5m

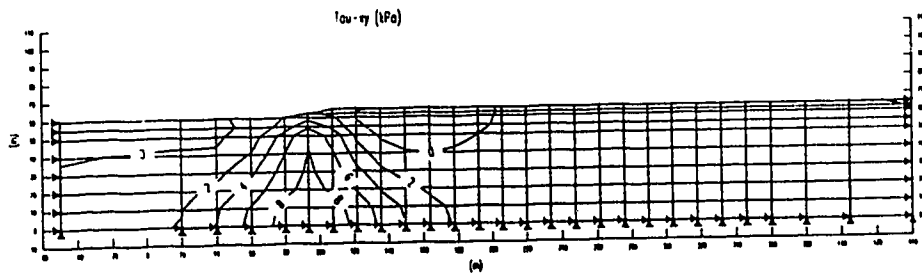


**Figure 5.17 Initial Stresses for the 10°, H=5 m Finite Slope -  $\tau_{xy}$  contours**



Finite Slope 10 degrees, H=10m

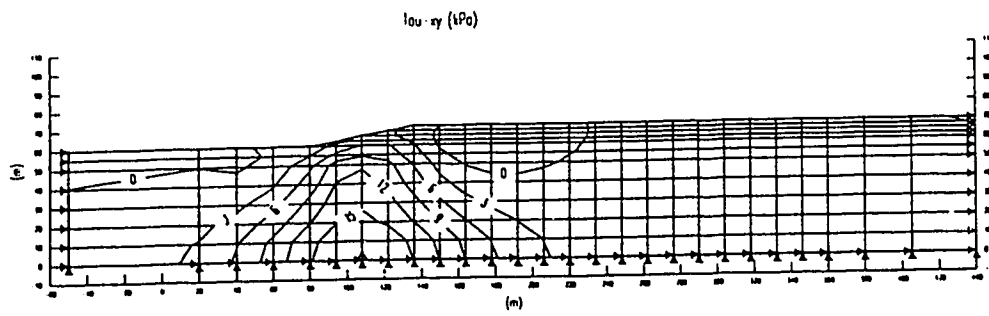


**Figure 5.18 Initial Stresses for the 10°, H=10 m Finite Slope -  $\tau_{xy}$  contours**

Finite Slope 10 degrees, H=20m

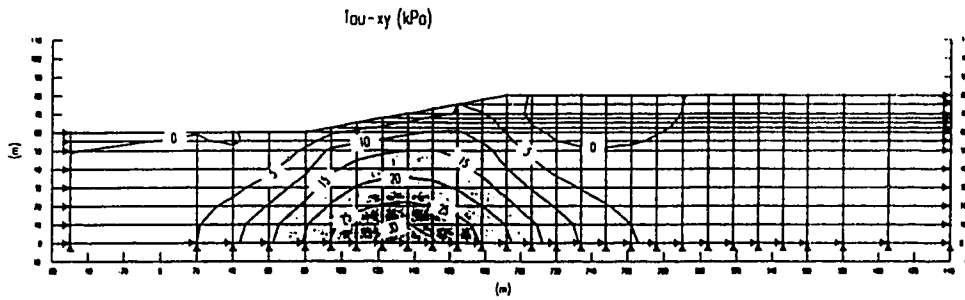
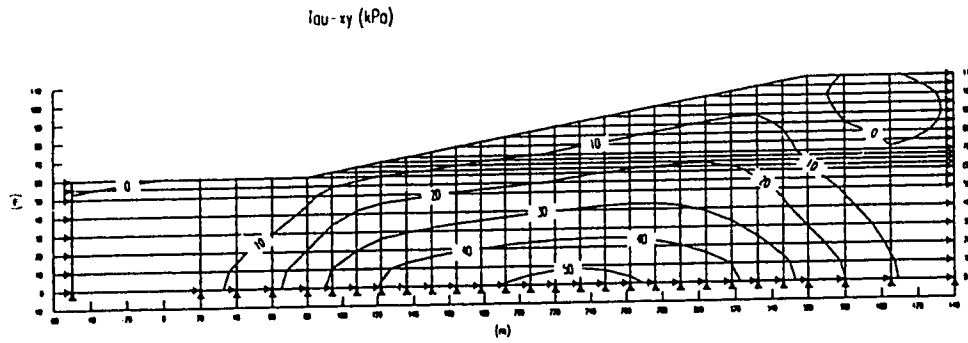
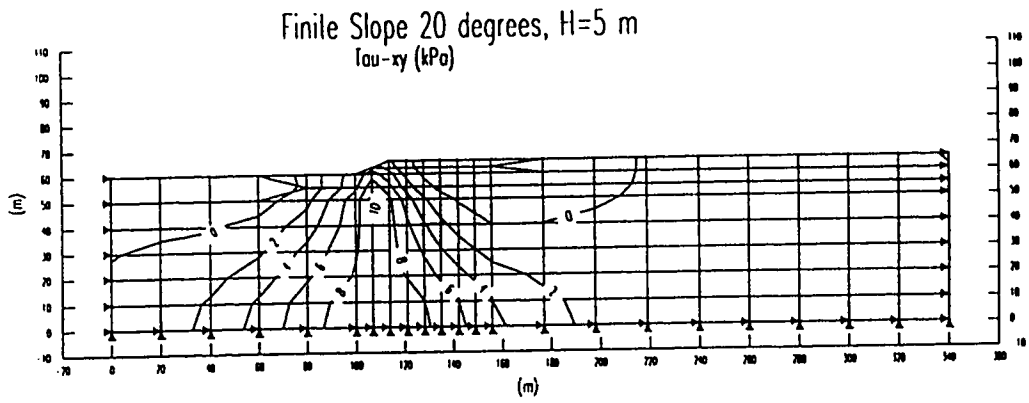


Figure 5.19 Initial Stresses for the 10°, H=20 m Finite Slope -  $\tau_{xy}$  contours

Finite Slope 10 degrees, H=50 m



**Figure 5.20 Initial Stresses for the 10°, H=50 m Finite Slope -  $\tau_{xy}$  contours**



**Figure 5.21 Initial Stresses for the 20°, H=5 m Finite Slope -  $\tau_{xy}$  contours**

FINITE SLOPE 20 Degrees, H=10m

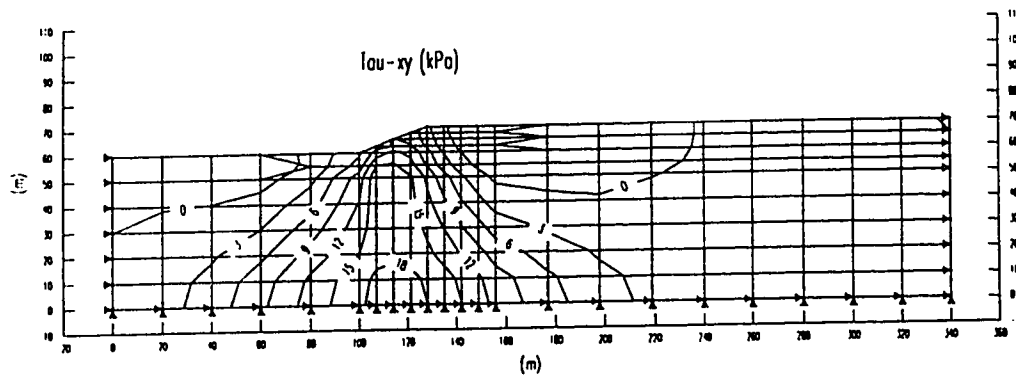


Figure 5.22 Initial Stresses for the 20°, H=10 m Finite Slope -  $\tau_{xy}$  contours

FINITE SLOPE 20 Degrees, H=20m

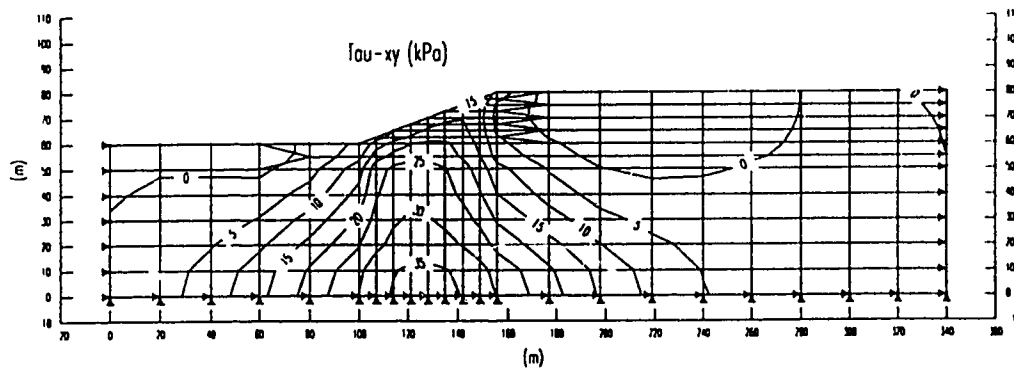


Figure 5.23 Initial Stresses for the 20°, H=20 m Finite Slope -  $\tau_{xy}$  contours

FINITE SLOPE 20 Degrees, H=50m

$\tau_{xy}$  (kPa)

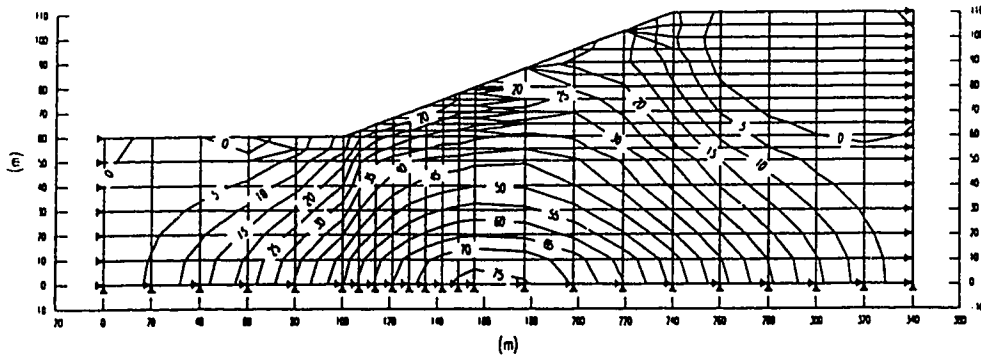
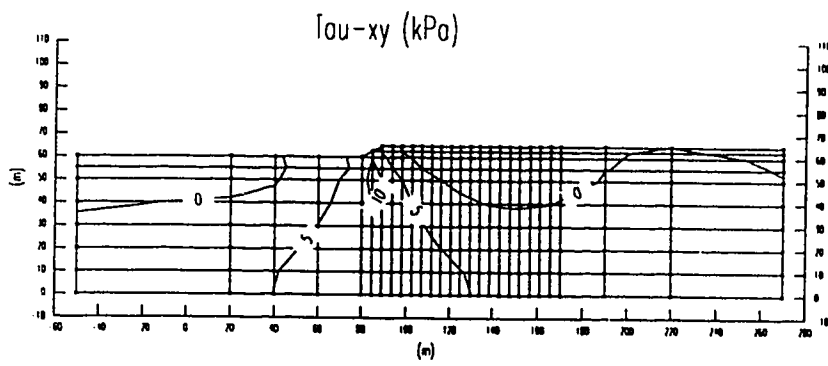


Figure 5.24 Initial Stresses for the 20°, H=50 m Finite Slope -  $\tau_{xy}$  contours

Finite Slope 30 degrees, H=5m



**Figure 5.25 Initial Stresses for the 30°, H=5 m Finite Slope -  $\tau_{xy}$  contours**



Finite Slope 30 degrees, H=10m

$\tau_{xy}$  (kPa)

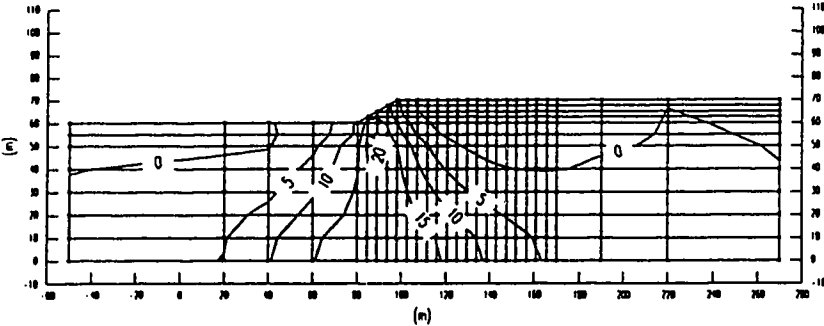
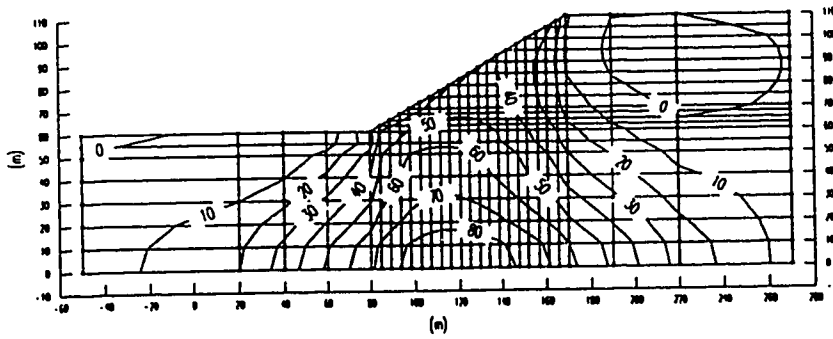


Figure 5.26 Initial Stresses for the 30°, H=10 m Finite Slope -  $\tau_{xy}$  contours

Finite Slope 30 degrees, H=50 m  
 $\tau_{xy}$  (kPa)



**Figure 5.27 Initial Stresses for the 30°, H=50 m Finite Slope -  $\tau_{xy}$  contours**

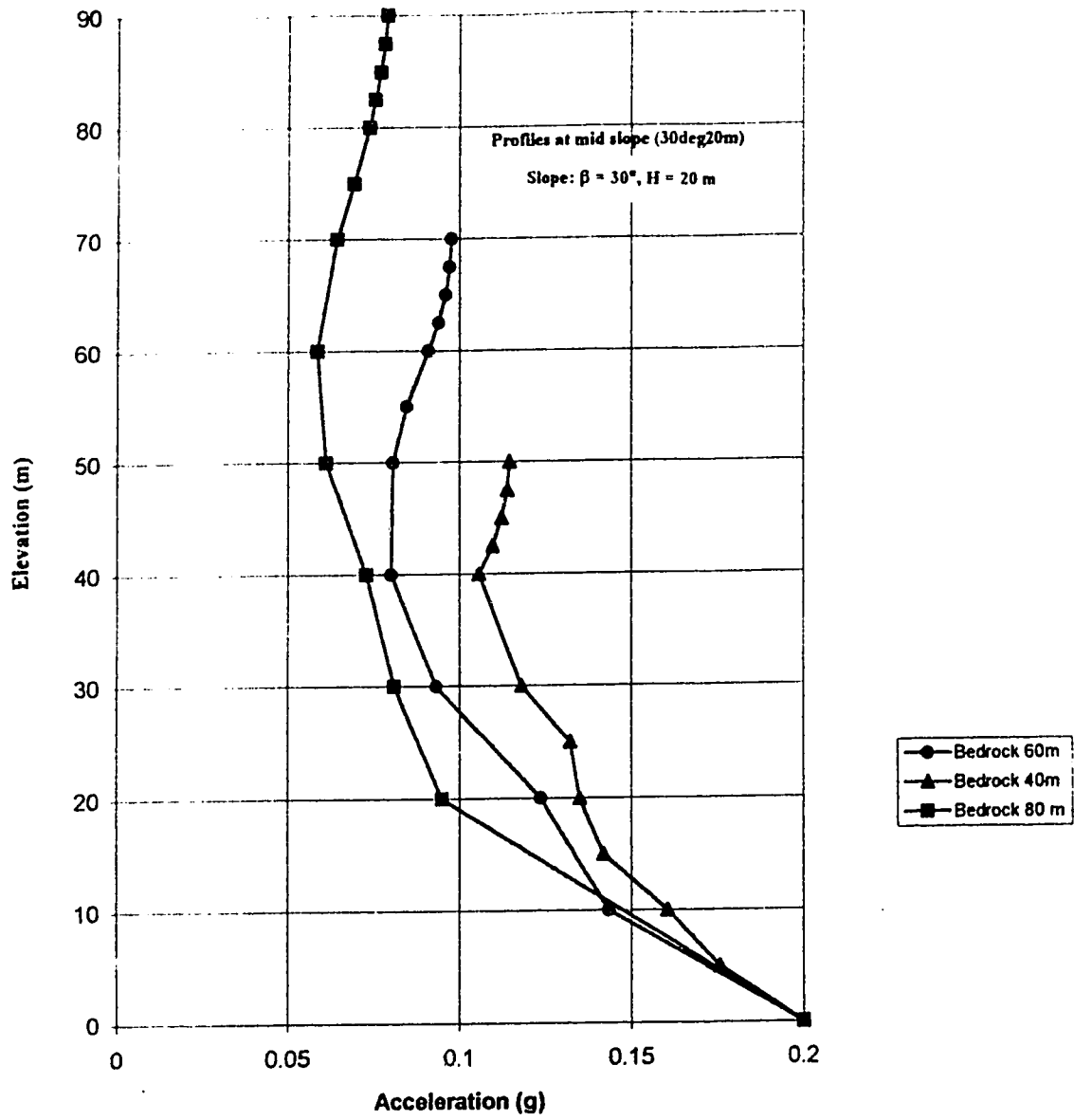


Figure 5.28 Influence of Bedrock Depth on the Acceleration Profile

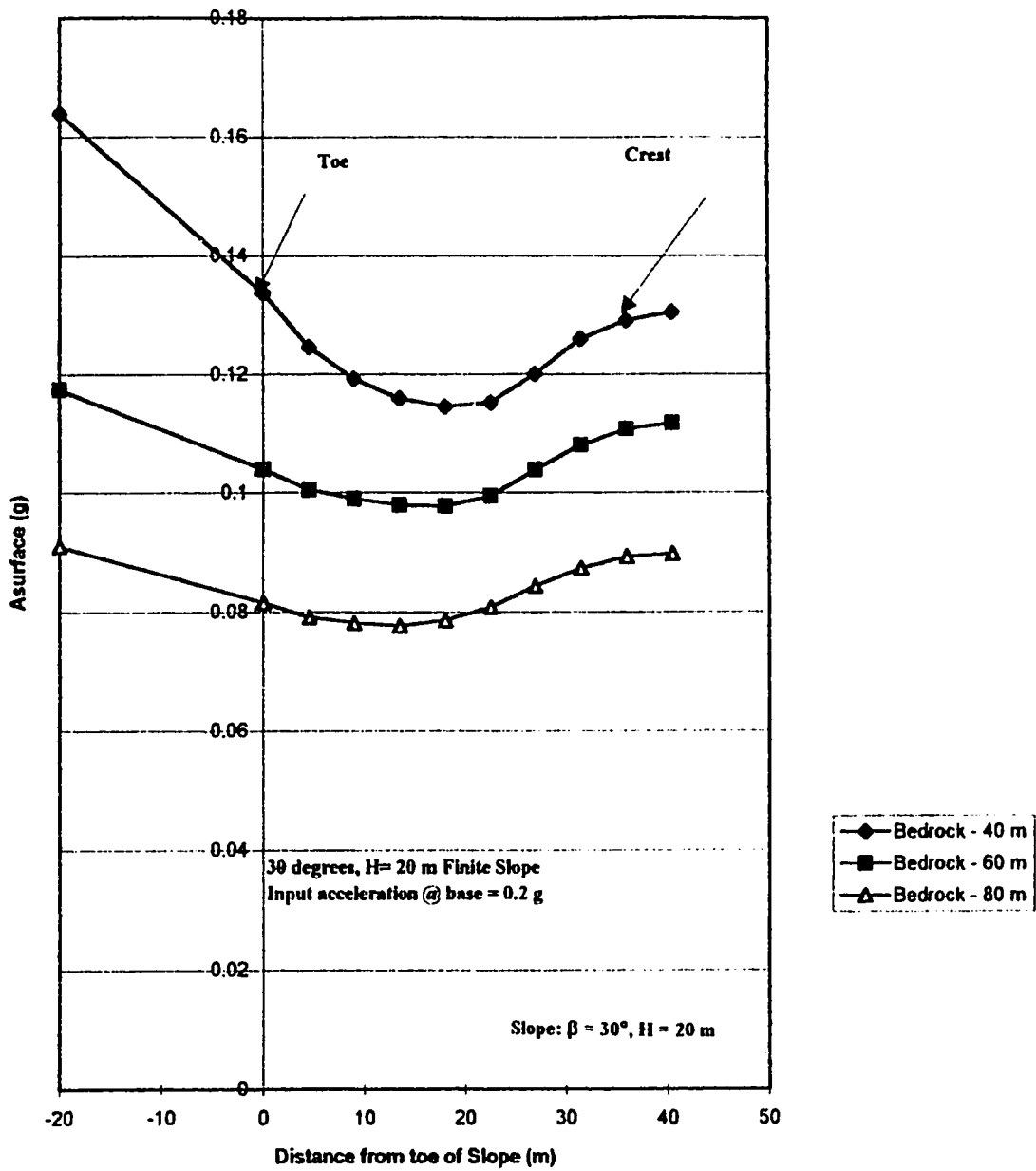
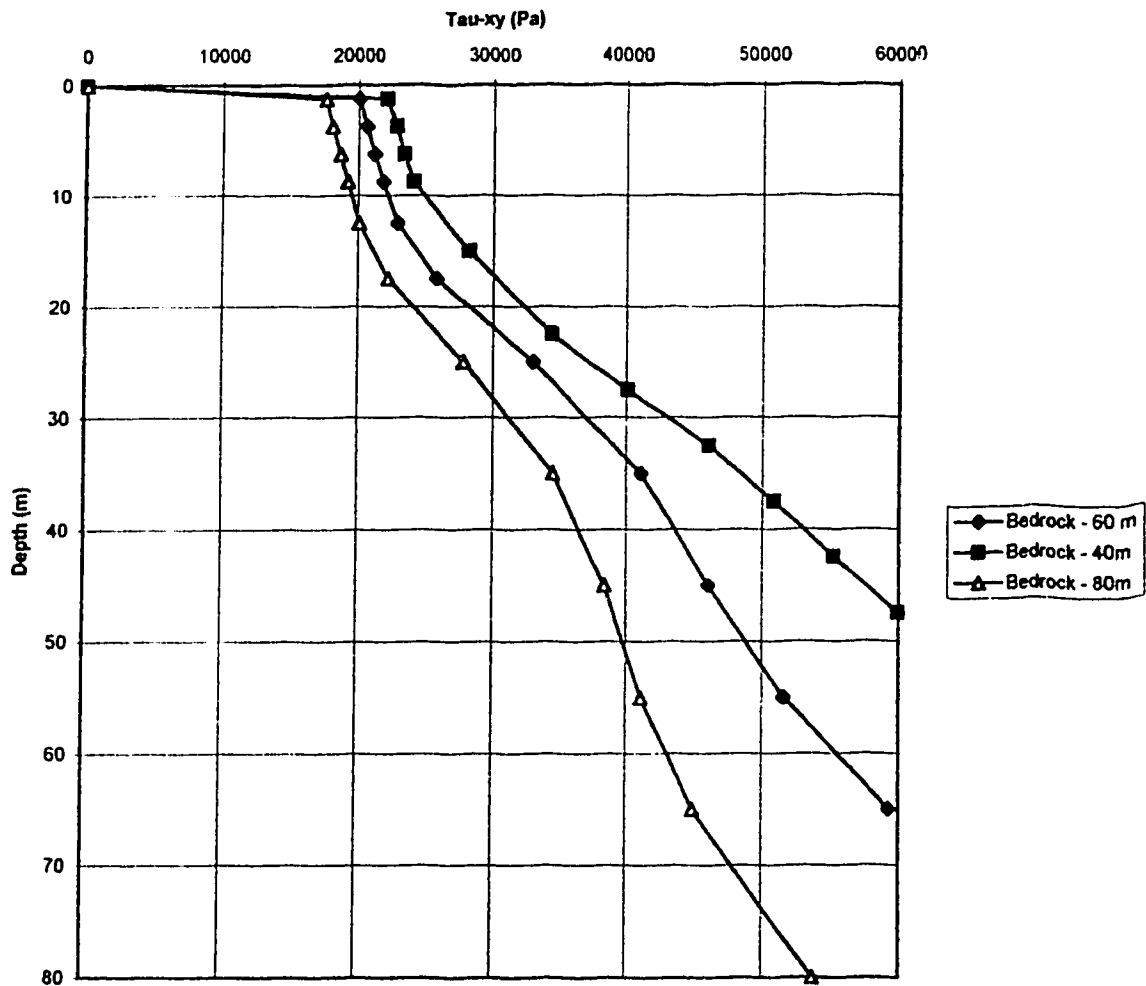


Figure 5.29 Influence of the Depth of Bedrock in the Surface Acceleration Profile



Note: Slope 30 degrees, H=20 m  
 Shear stress profile for the midslope.

Figure 5.30 Influence of Bedrock Depth on the Shear stresses Profiles

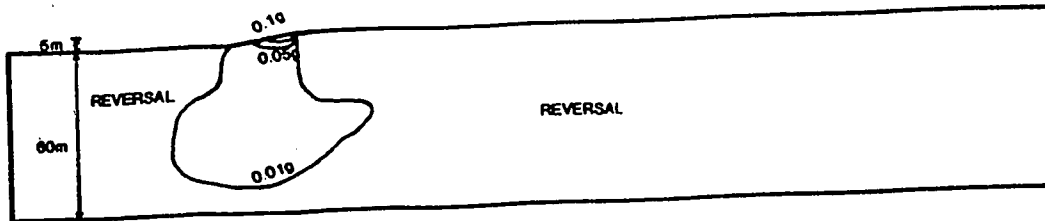


Figure 5.31 Zones of No Shear Stress Reversal, Finite Slope  $10^\circ$ ,  $H = 5$  m

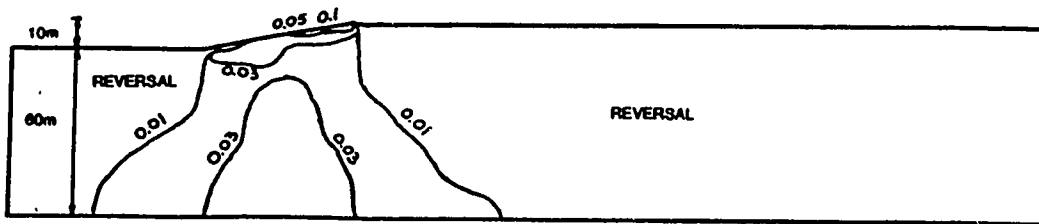


Figure 5.32 Zones of No Shear Stress Reversal, Finite Slope 10°, H = 10 m

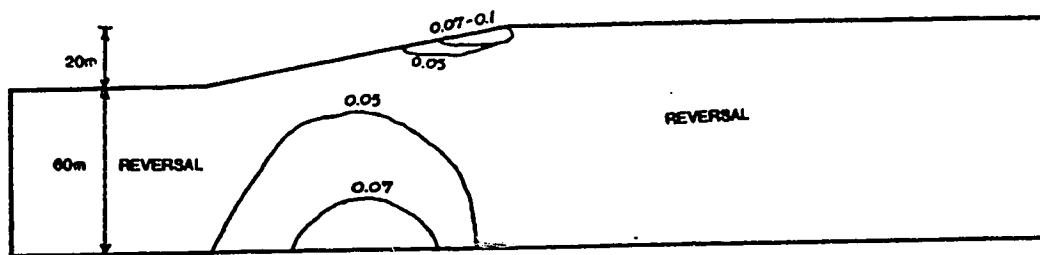


Figure 5.33 Zones of No Shear Stress Reversal, Finite Slope  $10^\circ$ ,  $H = 20$  m



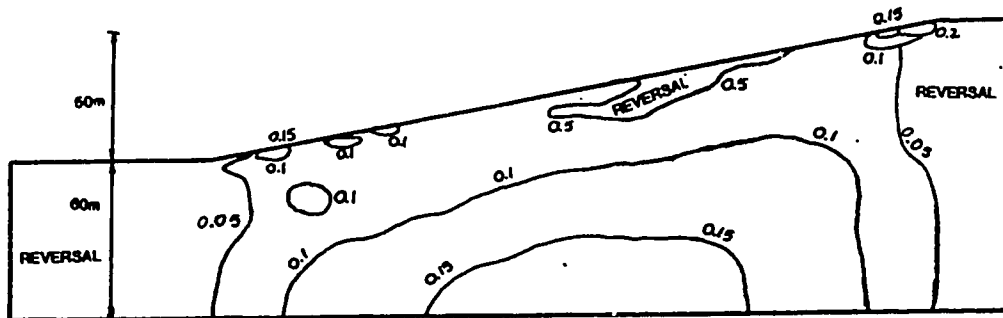


Figure 5.34 Zones of No Shear Stress Reversal, Finite Slope  $10^\circ$ ,  $H = 50$  m

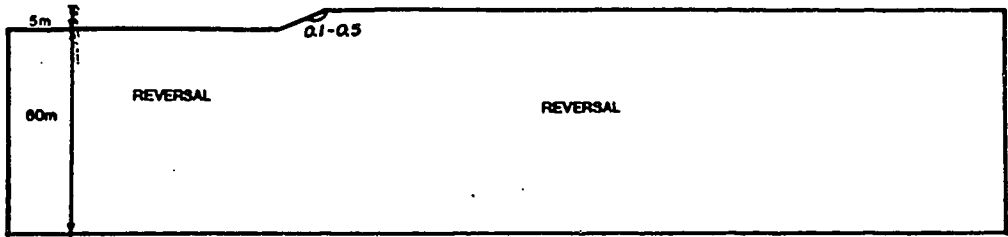


Figure 5.35 Zones of No Shear Stress Reversal, Finite Slope 20°, H = 5 m

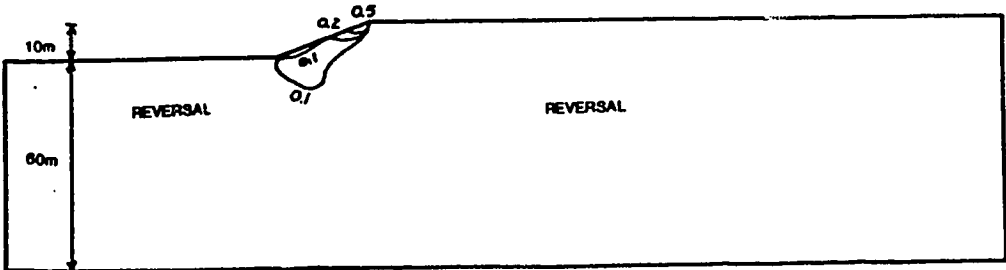


Figure 5.36 Zones of No Shear Stress Reversal, Finite Slope 20°, H = 10 m

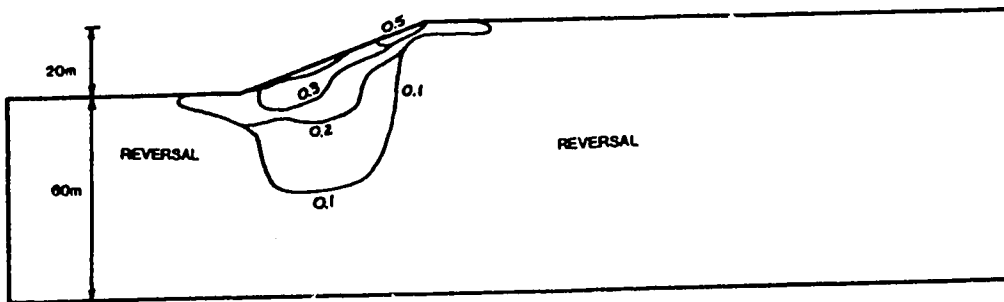


Figure 5.37 Zones of No Shear Stress Reversal, Finite Slope 20°, H = 20 m

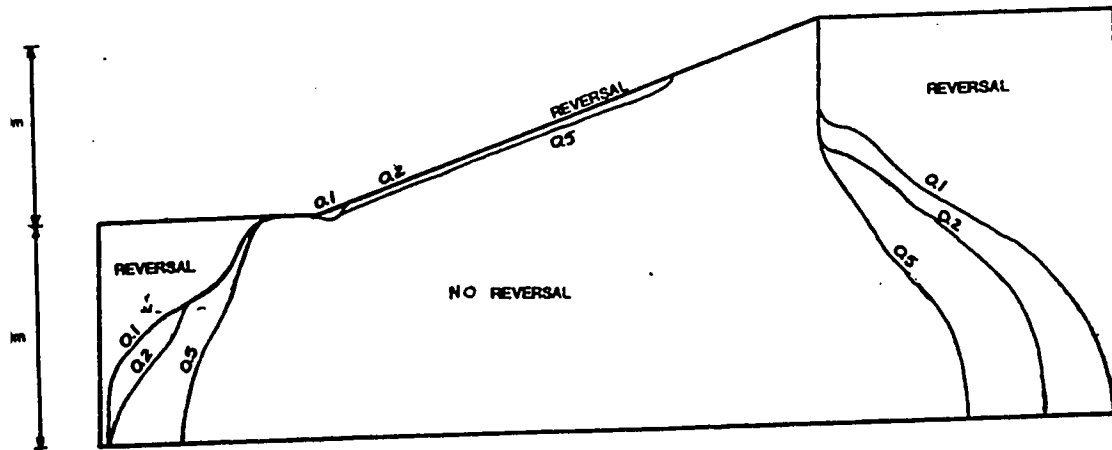


Figure 5.38 Zones of No Shear Stress Reversal, Finite Slope 20°, H = 50 m

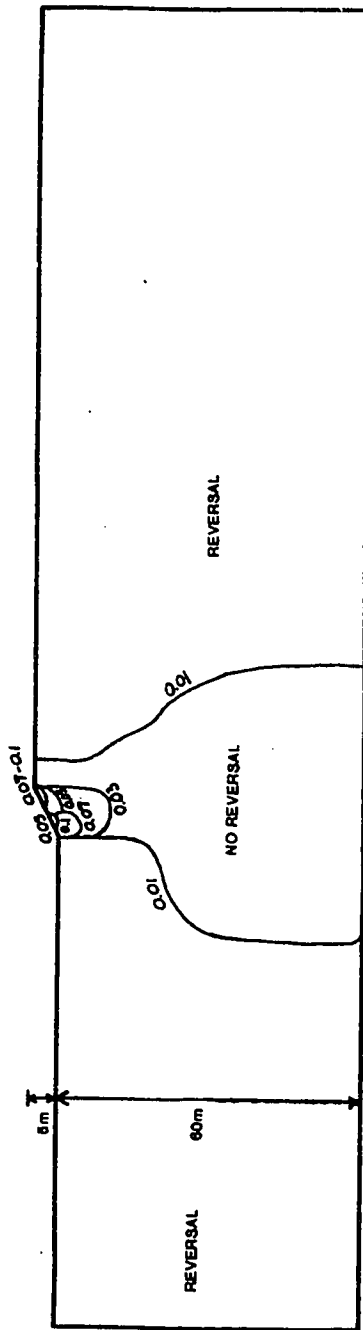


Figure 5.39 Zones of No Shear Stress Reversal, Finite Slope  $30^\circ$ ,  $H = 5 \text{ m}$

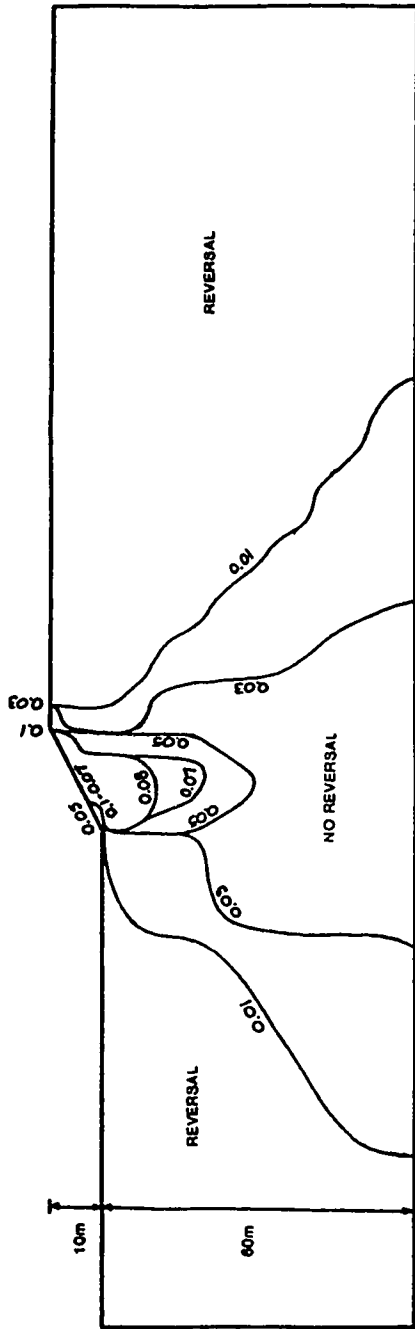


Figure 5.40 Zones of No Shear Stress Reversal, Finite Slope 30°, H = 10 m

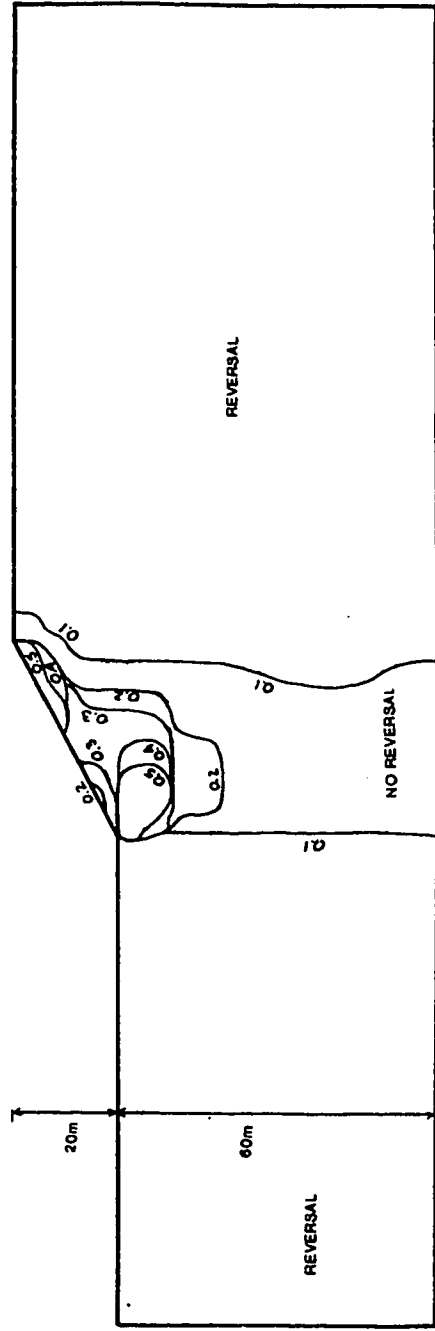


Figure 5.41 Zones of No Shear Stress Reversal, Finite Slope 30°,  $H = 20$  m.

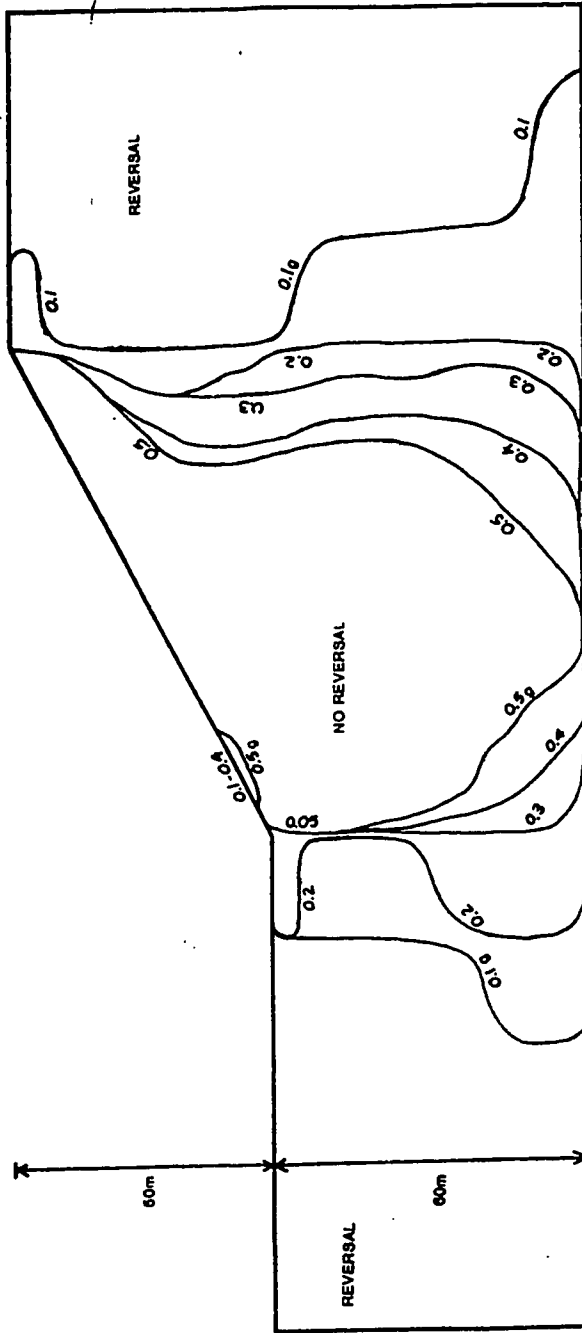


Figure 5.42 Zones of No Shear Stress Reversal, Finite Slope  $30^\circ$ ,  $H = 50$  m

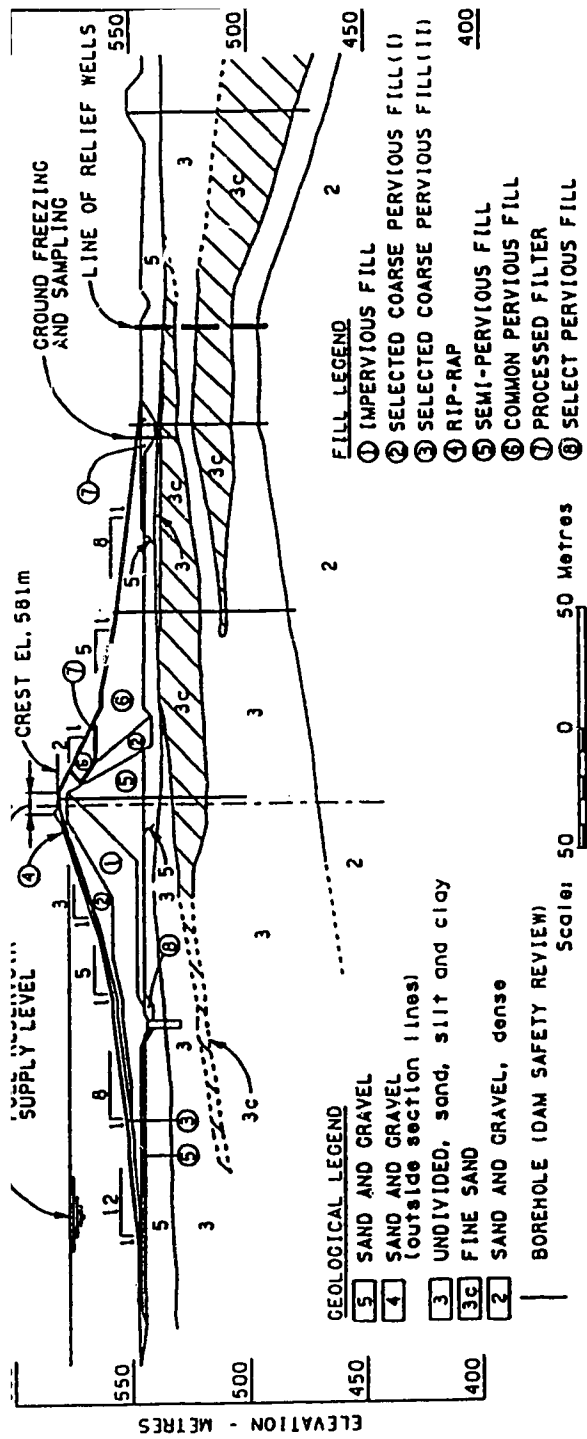
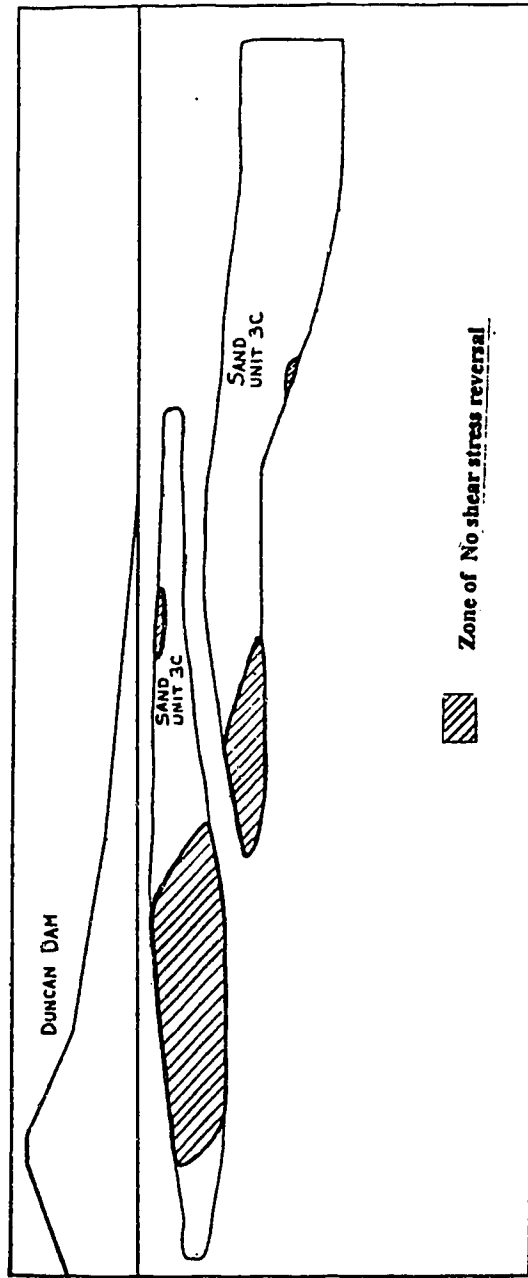


Figure 5.4\$ Typical cross section and foundation of Duncan Dam (adapted from Pillai and Stewart, 1993)



Figure 5.44 Zones of No Shear Stress Reversal for Maximum Reservoir Conditions  
Based on Report No. H2599 results ( $A_{max}=0.13g$ )



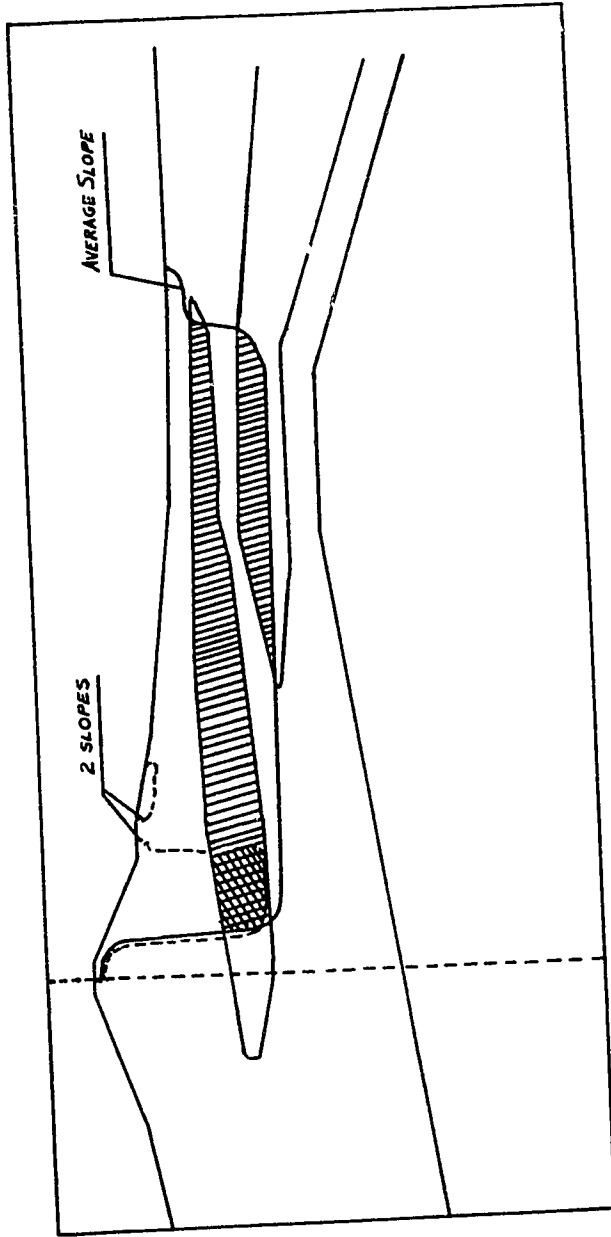
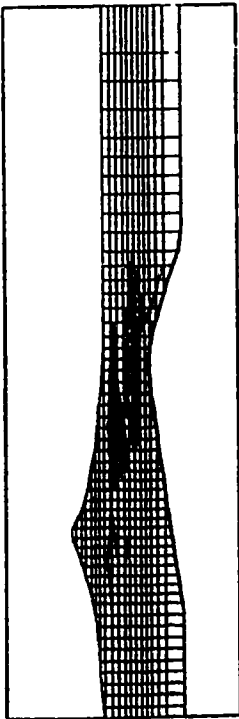


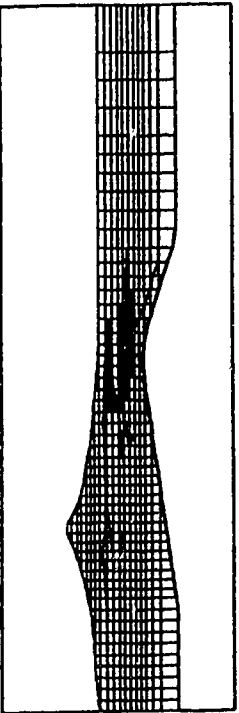
Figure 5.45 Zones of No Shear Stress Reversal - Simplified Approach

TRIGGERING ANALYSIS (PGA = .12g)

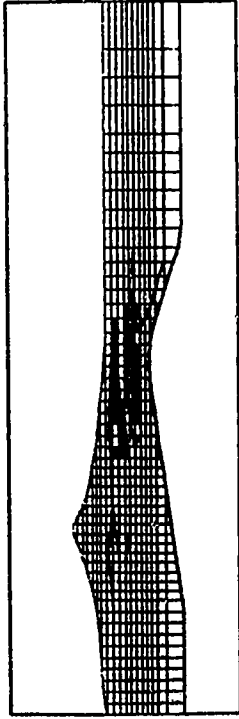
CRR = .14 ; FSL = 1.3 ; Kaipha < 1 (LC-EE1)



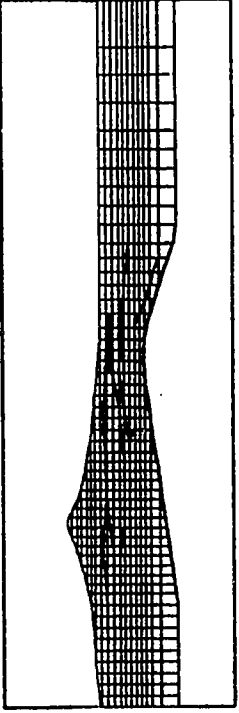
CRR = .14 ; FSL = 1.3 ; Kaipha = 1 (LCASE2)



CRR = .14 ; FSL = 1.1 ; Kaipha < 1 (LC-EE3)



CRR = .14 ; FSL = 1.1 ; Kaipha = 1 (LCASE4)



CRR = Cyclic Resistance Ratio

FSL = Factor Safety Against Liquefaction

LEGEND



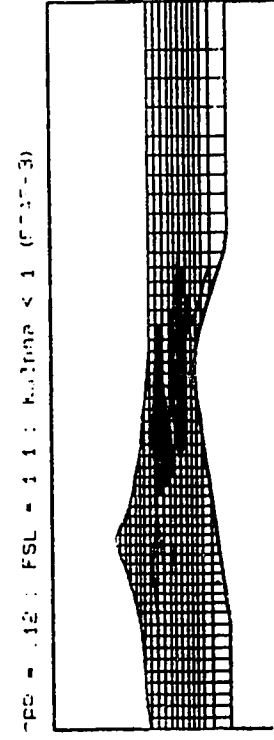
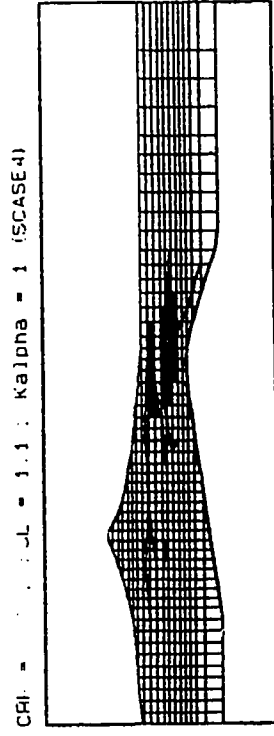
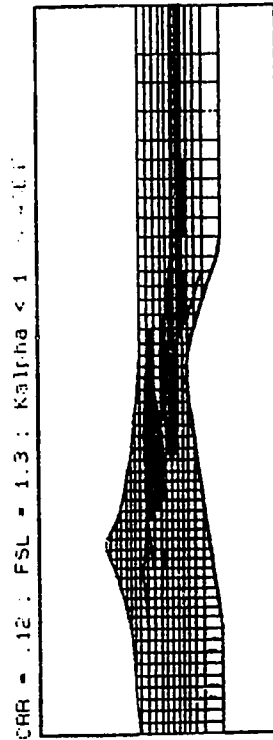
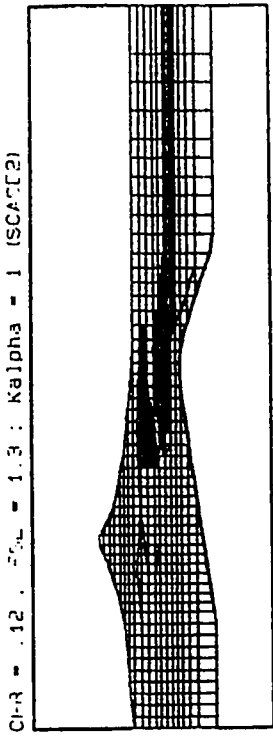
UNLIQUEFIED SOIL



LIQUEFIED SOIL

Figure 5.46 Liquefaction Extent - Lab Method (after Pillai and Salgado, 1993)

# TRIGGERING ANALYSIS (PGA = .12g)



CRR = CYCLIC RESISTANCE RATIO  
 FSL = FILLING SOIL AGAINST LIQUIDATION

## LEGEND



UNLIQUEFIED SOIL



LIQUEFIED SOIL

Figure S.47 Liquefaction Extent - Seed's Method (after Pillai and Salgado, 1993)

## Chapter 6

### Conclusions

A review of the current methods for evaluation of liquefaction used in practice when dealing with sloping ground under cycling loading, reveals limitations. The current empirical correction factor  $K_\alpha$  has been reviewed. The existing correlation charts that use relative density as a fundamental parameter, are inappropriate and show considerable scatter. The use of an alternative parameter, is required to explain more accurately the influence of the initial static shear stress on the liquefaction resistance of sands. Pillai (1991) suggested the use of the state parameter  $\psi$ . His hypothesis has been evaluated with the available limited data, and although still there was scatter in the results, the trends appeared more appropriate. Clearly further research is required to evaluate the influence of  $\alpha$  on the cyclic resistance ratio.

Lab results show a clear difference in response if no shear stress reversal takes place. If no shear stress reversal occurs in medium dense to dense sands, deformations are generally small. When shear stress reversal occurs, deformations can be very large due to the cyclic softening as the soil approaches zero effective stress. For very loose sands, cyclic loading can trigger collapse and flow liquefaction with resulting large deformations. Therefore it is important to identify the zones where no shear stress reversal on horizontal planes takes place for a given slope and earthquake loading.

Two dimensional static and dynamic analyses have been carried out to identify regions within different sloping soil deposits, where no shear stress reversal occurs, due to different earthquake loadings. Slopes ranging from 5m to 50 m in height and from 10 to 30 degrees in slope angle have been studied. Static finite element analyses were carried out for each geometry, in order to compute the insitu stresses. The dynamic shear stresses were calculated using a dynamic finite element model. The magnitude of these stresses were evaluated for different sizes of earthquakes. Due to the number of variables and considerations involved in the analyses, the results of this thesis are only strictly applicable

for the geometries and soil properties used in the analyses. Therefore, they can only be considered as an estimate for other conditions different from the used. Further analyses, with other soil properties and geometries could help complement the results from this thesis.

From the calculated stresses the zones where no shear stress reversal on horizontal planes were defined. A review of existing cyclic laboratory data, clearly shows two distinctive types of response of sands under cyclic loading, depending primarily on the initial conditions and whether shear stress reversal takes place during loading. Hence, for the regions of soil, within a slope, where no shear stress reversal takes place the response during earthquake loading would be different. Therefore these results provide a useful guideline to optimize liquefaction designs in sloping grounds.

## REFERENCE LIST

- Alarcón-Guzmán, A., Leonards, G.A. and Chameau, J.L. (1988), " Undrained Monotonic and Cyclic Strength of Sands", J.G.E.D., A.S.C.E., V.114, No. 10, pp. 1089-1109.
- Atkinson, J.H. and Bransby, P.L. (1978), "The Mechanics of Soils, an Introduction to Critical Soil Mechanics" McGraw-Hill, London, England.
- Basham, P.W., Weichert, D.H., Anglin, F.M., and Berry, M.J. (1985), "New Probabilistic strong seismic ground motion maps of Canada" Bulletin of the Seismological Society of America, 75: 563-595.
- BC Hydro (1993), "DUNCAN DAM - Liquefaction Assessment and Seismic Stability", Report No. H2599, Dam Safety Investigations, BC Hydro Hydroelectric Engineering Division.
- BC Hydro (1993), "DUNCAN DAM - Report on Laboratory Testing on Foundation Soils", Report No. GEO 1/91, Dam Safety Investigations, BC Hydro Hydroelectric Engineering Division.
- Been, K. and Jefferies, M.G. (1985), "A State parameter for Sands", Geotechnique 35, no.2, pp. 99-112.
- Been, K., Jefferies, M.G. and Hachey, J. (1991), "The Critical State of Sands", Geotechnique, No.41(3), pp. 365-381.
- Castro, G. (1969), "Liquefaction of Sands", Harvard Soil Mechanics No. 81, Harvard University, Cambridge, MA.
- Castro, G. (1975), "Liquefaction and Cyclic Mobility of Saturated Sands", ASCE Journal of Geotechnical Engineering Division. v.101, No.6, pp. 551-569.
- Castro, G. and Poulos, S.J. (1977), "Factors affecting liquefaction and Cyclic Mobility", ASCE, Journal of Geotechnical Engineering Division. v.103, No.6, pp. 501-516.
- Castro, G., Poulos, S.J., France, J.W. and Enos, J.L. (1982), "Liquefaction Induced by Cyclic Loading," Report by Geotechnical Engineers, Inc., to the National Science Foundation, Washington, D.C. 80pp.
- Chern, J.C. (1985), "Undrained Response of Saturated Sands with emphasis on Liquefaction and Cyclic Mobility," Ph.D. Thesis, The University of British Columbia, Vancouver, B.C., January, 1985.
- Clough, R.W. and Chopra, A.K. (1966), "Earthquake Stress Analysis in Earth Dams", JGED, ASCE, v. 92, No.2, pp. 197-211.

- Cook, A.R., Malkus, D.S. and Plesha, M.E. (1989), "The Concepts and Applications of Finite Element Analysis", John Wiley & Sons, 3ed. 630p.
- Cunning, J.C. (1994), "Shear wave velocity measurement of cohesionless soils for evaluation of in-situ state", M.Sc. Thesis, University of Alberta, Edmonton, Alberta.
- Das, B.M. (1983), "Fundamentals of Soil Dynamics". Ed. Elsevier. 399p.
- Duke, C.M. and Leeds, D.J. (1963), "Response of soils, Foundations, and Earth Structures to the Chilean Earthquakes of 1960" Bulletin of the Seismological Society of America, vol. 53, No. 2, February, 1963.
- Faccioli, E. and Reséndiz, D. (1976), "Soil Dynamics: Behavior including liquefaction", Chpt. 4 Seismic Risk and Engineering Decisions (Lomnitz, C. and Rosenblueth, E. eds), Elsevier.
- Finn, W.D.L. (1981), "Dynamic Analysis of Soil Structures", Proceedings Implementation of Computer Procedures And Stress-Strain Laws in Geotechnical Engineering (Desai, C.S. and Saxena, S.X. Eds.), Illinois, V.1 pp. 3-27.
- Finn, W.D.L. (1981), "Liquefaction Potential: Developments Since 1976", International Conference on Recent Advances in Geotechnical Earthquake Engineering and Soil Dynamics, St. Louis, MO, 655 - 681.
- Finn, W.D.L. and Bhatia, S.K. (1981), "Prediction of Seismic Porewater Pressures", Proceedings 10th. I.C.S.M.F.E., v. 3, PP. 201-206.
- Finn, W.D.L. and Byrne, P.M. (1976), "Liquefaction Potential of Mine Tailings Dams", Proceedings, Twelfth International Conference on Large Dams, Mexico City, v. 1, pp. 153-176.
- Finn, W.D.L., Lee, K.W. and Martin, G.R. (1977), "An effective stress model for Liquefaction.", Journal of Geotechnical Engineering Division, ASCE, vol 103, No.6, pp. 517-533.
- Finn, W.D.L., Lee, K.W. and Martin, G.R. (1977), "An Effective Stress Model For Liquefaction", J.G.E.D., A.S.C.E., V.103, No. 6 pp. 517-533.
- Finn, W.D.L., Lee, K.W. and Martin, G.R. (1978), "Comparison of Dynamic Analyses for Saturated Sands", Proc. Spec. Conference on Earthquake Engineering and Soil Dynamics, ASCE, v.1, pp. 472-491.
- Finn, W.D.L., Pickering, D.J. and Bransby, P.L. (1971), "Sand Liquefaction in Triaxial and Simple Shear Tests", Journal of the Soil Mechanics and Foundation Division, A.S.C.E., V.97, No. SM4, Proc. Paper 8039, pp. 639-659.



- Fukutake, K., Ohtsuki, A., Sato, M. and Shamoto, Y. (1990), "Analysis of saturated Dense Sand-Structure System and Comparison with results from Shaking Table Test", *Earthquake Engineering and Structural Dynamics*, V.19, pp. 977-992.
- Ghaboussi, J. and Dikmen, S.U. (1978), "Liquefaction Analysis of Horizontally Layered Sands", *J.G.E.D., A.S.C.E.*, V.103, No. 3, pp. 341-356.
- Ghaboussi, J. and Dikmen, S.U. (1984a), "Effective Stress Analysis of Seismic Response and Liquefaction: Theory", *J.G.E.D., A.S.C.E.*, V.110, No. 5, pp. 628-643.
- Ghaboussi, J. and Dikmen, S.U. (1984b), "Effective Stress Analysis of Seismic Response and Liquefaction: Case Studies", *J.G.E.D., A.S.C.E.*, V.110, No. 5, pp. 645-658.
- Hardin, B.O. and Drnevich, V.P. (1972) " Shear Modulus and Damping in soils: design equations and curves", *JSMFD, ASCE*, v.98(7), pp. 667-692.
- Heidebrecht, A.C., Basham, P.W., Rainer, J.H. and Berry, M.J. (1983), "Engineering applications of new probabilistic seismic ground-motion maps of Canada", *Canadian Journal of Civil Engineering*, V.10, No. 4, pp. 670-680.
- Housner, G.W. and Jennings, P.C. (1964), " Generation of artificial earthquakes" *J.Eng. Mech. Div., Proc. ASCE*, 90, (EM1), pp. 113-150.
- Hyodo, M., Murata, H., Yasufuku, N, and Fujii, T. (1991), "Undrained Cyclic Shear Strength and Residual Shear strain of Saturated sand by cyclic triaxial tests", *Soils and Foundations*, v.31, No. 3, pp. 60-76.
- Hyodo, M., Tanimizu, H., Yasufuku, N, and Murata, H.(1994), "Undrained Cyclic and Monotonic Triaxial Behaviour of Saturated Loose Sand", *Soils and Foundations*, v.34, No. 1, pp. 19-32.
- ICOLD (1983), "Seismicity and Dam Design", *Bulletin* 46.
- ICOLD (1989), "Selecting Seismic Parameters for Large Dams. Guidelines", *Bulletin* 72.
- Idriss, I.M. (1990), "Response of Soft soil sites during earthquakes", *Proceedings H.B. Seed Memorial Symposium*, V.2, pp. 273-289.
- Idriss, I.M. and Sun, J.I. (1992), "SHAKE91 A Computer Program fro Conducting Equivalent Linear Seismic Response Analyses of Horizontally Layered Soil Deposits", *University of California, Davis, CA.*
- Idriss, I.M., Lysmer, J., Hwang, R. and Seed, H.B. (1973),"Quad-4. A Computer Program for Evaluating the Seismic Response of Soil Structures by Variable Damping Finite Elements" Report no. UCB/EERC 73-16, *University of California, Berkeley.*

- Ishihara, K. (1993), "Liquefaction and Flow failure during earthquakes", 33rd Rankine Lecture, *Geotechnique*, V. 43, No. 3, pp. 351-415.
- Ishihara, K., Verdugo, R. and Acacio, A.A. (1991), "Characterization of Cyclic Behaviour of Sand and Post-Seismic Stability Analyses," Proc. 9th Asian Regional Conference on Soil Mechanics and Foundation Engineering, v.2, pp. 45-67.
- Iwasaki, T., Tatsuoka, F., Tokida, K. and Yasuda, S. (1978), "A Practical Method for Assessing Soil Liquefaction Potential Based on Case Studies at Various Sites in Japan", Proc. 2nd. International Conference on Microzonation for Safer Construction, Research and Application. vol. 2, pp. 885-896.
- Konrad, J-M (1993), "Undrained response of loosely compacted sands during monotonic and cyclic compression tests", *Geotechnique* 43, no.1, pp. 69-89.
- Lee, K. and Seed, H.B. (1967), "Dynamic strength of Anisotropically Consolidated Sand", *Journal of Soil Mechanics and Foundations Division*, v.93, no. SM5, pp. 169-190.
- Lee, K.L. and Chan, K. (1972), "Number of Equivalent Significant Cycles in Strong Motion Earthquakes", Proceedings, Int. Conf. on Microzonation, October, Seattle, Wash., vol. II, pp. 609-627.
- Lee, W.S., Robertson, P.K. and Morgenstern, N.R. (1992), "Laboratory Test Data Analysis on Dashihe Tailings Sands", Report 3-5 for SINO-CANADIAN JOINT, 59p.
- Little, T.E., Imrie, A.S. and Psutka, J.F. (1993), "Geologic and Seismic Setting pertinent to Dam Safety Review of Duncan Dam", 46th Annual Canadian Geotechnical Conference, September, Saskatoon.
- Martin, G.R., Lam, I.P., McCaskie and Tsai C. (1981), "A Parametric Study of an Effective Stress Liquefaction Model", International Conference on Recent Advances in Geotechnical Earthquake Engineering and Soil Dynamics, St. Louis, MO, pp.699-705.
- Matasovic, N. and Vucetic, M. (1993), "Cyclic Characterization of Liquefiable Sands", *Journal of Geotechnical Engineering*, ASCE, vol. 119, No. 11, pp. 1805-1822.
- McRoberts, E.C. and Sladen, J.A. (1992), "Observations on Static and Cyclic sand-liquefaction methodologies", *Canadian Geotechnical Journal*, v. 29, pp. 650-665.
- National Research Council (1985), "Liquefaction of Soils during Earthquakes," Committee on Earthquake Engineering, Report No. CETS-EE-1.
- Nemat-Nasser, S. and Takahashi, K. (1984), "Liquefaction and Fabric of Sand", *J.G.E.D., A.S.C.E.*, V.110, No. 9, pp. 1291-1306.

- Ohtsuki, A. and Itoh, T. (1987), "Two-Dimensional Effective Stress Analysis of Liquefaction of Irregular Ground including Soil-Structure Interaction", *Earthquake Engineering and Structural Dynamics*, V.15, pp. 345-366.
- Pillai, V.S. (1991), "Liquefaction Analysis of Sands: Some Interpretation of Seed's  $K_\sigma$  (Sloping Ground) and  $K_\sigma$  (Depth) Correction Factors Using Steady State Concept," *Proc. 2nd International Conference on Recent Advances in Geotechnical Earthquake Engineering and Soil Dynamics*, St. Louis, vol.2, pp. 579-587.
- Pillai, V.S. and Salgado, F.M. (1993), " Seismic Stability and Deformation Analysis of Duncan Dam", 46th Annual Canadian Geotechnical Conference, Saskatoon, Saskatchewan.
- Pillai, V.S. and Byrne, P.M. (1994), " Effect of Overburden Pressure on Liquefaction Resistance of Sand", *Canadian Geotechnical Journal*, v.31, N.1, pp. 53-60
- Pillai, V.S. and Stewart, R.A. (1993), " Evaluation of Liquefaction Potential of Foundation Soils at Duncan Dam", 46th Annual Canadian Geotechnical Conference, September, Saskatoon., p.
- Poorooshasb, H.B. (1989), " Simulation of Flow of Sand Using State Parameters," *Computers and Geotechnics*, pp. 195-218.
- Poulos, S.J. (1981), " The Steady State of Deformation", *JGED, ASCE*, v.107, GT5, pp. 553-562.
- Prakash, S. and Puri, V.K. (1981) "Dynamic properties of soils from insitu tests", *JGED, ASCE*, v.107(7), pp.943-964.
- Richart, F.E., Hall, J.R. and Woods, R.D. (1970), "Vibrations of Soils and Foundations", Prentice Hall Inc., 414 p.
- Robertson, P.K. (1993), "Design Considerations for Liquefaction", US-Japan Workshop.
- Robertson, P.K. (1994), "Suggested Terminology for Liquefaction: An Internal CANLEX Report. University of Alberta, Edmonton, Alberta.
- Rollins, K.M. (1987), "The Influence of Buildings on Potential Liquefaction Damage", Ph.D. Dissertation, University of California, Berkeley, CA.
- Rollins, K.M. and Seed, H.B. (1990), "Influence of Buildings on Potential Liquefaction Damage", *J.G.E.D., A.S.C.E.*, V.116, No. 2, pp. 165-185.
- Roscoe, K.H., Schofield, A.N., Wroth, C.P. (1958), "On the yielding of Soils", *Geotechnique*, No.8, pp. 22-53.

- Saada, A.S. (1985), "On Cyclic Testing with Thin Long Hollow Cylinders", Proceedings Session on Advances in The Art of Testing of Soils under Cyclic Conditions, ASCE, Detroit, Michigan, pp. 1-28.
- Salgado, F.M. and Pillai, V.S. (1993), " Seismic Stability and Deformation Analysis of Duncan Dam", 46th Annual Canadian Geotechnical Conference, September, Saskatoon.
- Schnabel, P.B., Lysmer, J. and Seed, H.B. (1972), "SHAKE A Computer Program for Earthquake Response Analysis of Horizontally Layered Sites", Report No. EERC 72-12, Earthquake Engineering Research Center, University of California, Berkeley.
- Schofield, A.N. and Wroth, C.P. (1968), "Critical State Soil Mechanics", McGraw-Hill, London, England.
- Sêco e Pinto, P.S. (1993), "Dynamic Analysis of embankment dams", Soil Dynamics and Geotechnical Engineering, Sêco e Pinto(ed.), Balkema, Rotterdam. pp. 159-269.
- Seed, H.B. (1968), "Landslides During Earthquakes due to liquefaction", Journal of Soil Mechanics and Foundations Division, v.94, no. SM5, pp. 1055-1122.
- Seed, H.B. (1979), "Soil Liquefaction and Cyclic Mobility evaluation for level ground during earthquakes", ASCE Journal of Geotechnical Engineering Division. v.105, No.2, pp. 201-255.
- Seed, H.B. (1983), "Earthquake Resistant Design of Earth Dams.", Proc. Symp. on Seismic Design of Embankments and Caverns, ASCE, vol. 1, pp. 41-64.
- Seed, H.B. and Idriss, I.M. (1969), "Influence of Soil Conditions on Ground Motion during Earthquakes", JSMFD, ASCE, v.95, no.1, pp. 99-137.
- Seed, H.B. and Idriss, I.M. (1970). "Soil moduli and Damping factors for dynamic response analyses" Report EERC 70-10, Earthquake Engineering Research Center., U.of California, Berkeley, Calif.
- Seed, H.B. and Idriss, I.M. (1971). "Simplified Procedures for Evaluating Soil Liquefaction Potential" Proc. ASCE, v.97, SM9, pp. 1249-1273.
- Seed, H.B. and Lee, K. (1966), "Liquefaction of Saturated Sands During Cyclic Loading", Journal of Soil Mechanics and Foundations Division, ASCE, v.92, no. SM6, pp. 105-135.
- Seed, H.B. and Martin, P.P. (1976), "Pore-Water pressure changes during Soil Liquefaction", J.G.E.D., A.S.C.E., V.102, No. 4, pp. 323-346.
- Seed, H.B., et al. (1973), "Analysis of the slides in the San Fernando dams during the earthquake of Feb. 9, 1971.", Report No. EERC-73/2, Berkeley, California.

- Seed, H.B., Idriss, I.M., Makdisi, F. and Banerjee, N. (1975a), "Representation of irregular stress time histories by equivalent uniform stress series in liquefaction analyses", report EERC 75-29, University of California, Berkeley, October, 1975.
- Seed, H.B., Lee, K., Idriss, I.M. and Makdisi, F. (1975b), "The slides in the San Fernando dams during the earthquake of Feb. 9, 1971.", *Journal of ASCE*, v.101, GT7, pp.651-689.
- Seed, H.B., Tokimatsu, K., Harder, L.F. Jr., and Chung, R.M. (1984), "The influence of SPT procedures in soil liquefaction resistance evaluations." Report No. UCB/EERC-84/15, University of California, Berkeley, CA.
- Seed, H.B., Tokimatsu, K., Harder, L.F. Jr., and Chung, R.M. (1985), "Influence of SPT procedures in soil liquefaction resistance evaluation.", *JGED, ASCE*, v.111 (12), pp. 1425-1445.
- Seed, H.B., Wong, R.T., Idriss, I.M. and Tokimatsu, K. (1986) "Moduli and Damping factors for Dynamic Analyses of Cohesionless Soils", *JGED, ASCE*, v.112 (11), pp. 1016-1032.
- Seed, R.B. and Harder, L.F. Jr. (1990), "SPT-based Analysis of Cyclic Pore Pressure Generation and Undrained Residual Strength", *Proceedings Memorial Symposium H.Bolton Seed*, v.2, pp. 351-376
- Sladen, J.A., D'Hollander, R.D., and Krahn, J. (1985), "The Liquefaction of Sands, A collapse surface approach", *Canadian Geotechnical Journal*, v.22 (4), pp. 564-578.
- Sunasaka, Y., Yoshida, H., Suzuki, K. and Matsumoto, T. (1988), "Comparison of Prediction Methods Fro Sand Liquefaction", *Numerical Methods in Geomechanics Swoboda ed., Balkema, Rotterdam*, pp. 1769-1773.
- Sunasaka, Y., Yoshida, H., Suzuki, K. and Matsumoto, T. (1988), "Comparison of Prediction Methods for Sand Liquefaction", *Numerical Methods in Geomechanics, Swoboba Ed.*, pp. 1769-1773.
- Szerdy, F. (1985), "Flow slide Failure associated with low level vibrations", Ph.D. Dissertation, University of California, Berkeley, CA.
- Vaid, Y. P. and Finn, W. D. L. (1979), "Static Shear and Liquefaction Potential", *J.G.E.D., A.S.C.E.*, V. 105, No. GT10, pp.1233 - 1246.
- Vaid, Y.P. and Chern, J.C. (1983), "Effect of Static Shear Stress on Resistance to Liquefaction", *Soils and Foundations, J.S.S.M.F.E.*, V.23, No.1, pp. 47-60.
- Vaid, Y.P. and Chern, J.C. (1985), "Cyclic and Monotonic Undrained Response of Saturated Sands", *Proceedings Session on Advances in The Art of Testing of Soils under Cyclic Conditions, ASCE, Detroit, Michigan*, pp. 120-147.

- Valera, J.E. and Donovan, N.C. (1977), " Soil Liquefaction Procedures-A Review", J.G.E.D., A.S.C.E., V.103, No. 6, pp. 607-625.
- Watanabe, T. (1966), "Damage to oil refinery plants and a building on compacted ground by the Niigata earthquake and their restoration.", Soils and Foundations, Tokyo, Japan, v.15, No. 3, pp. 27-40.
- Yegian, M.K., Ghahraman, V.G. and Harutiunyan (1994), "Liquefaction and Embankment Failure Case Histories, 1988 Armenia Earthquake", JGED, ASCE, v.120, No.3, pp. 581-596.
- Yoshimi, Y. and Oh-oka, H. (1975), "Influence of Degree of Shear Stress Reversal on the Liquefaction Potential of Saturated Sand", Soils and Foundations, J.S.S.M.F.E., V.15, No.3, pp. 27-40.
- Yoshimi, Y., Richart, F.E., Prakash, S., Balkan, D.D. and Ilyichev (1977), "Soil Dynamics and its Application to Foundation Engineering," Proc. 9th International Conference on Soil Mechanics and Foundation Engineering, Tokyo, vol.2, pp. 605-650.
- Zeghal, M. and Elgamal, A. (1994), "Analysis of Site Liquefaction using Earthquake Records", JGED, ASCE, v.120, n.6, pp. 996-1017.
- Zienkewics, O.C., Chang, C.T. and Hinton, E. (1978), "Non-linear Seismic Response and Liquefaction", Intl. Jour. for Numerical and Analytical Methods in Geomechanics, v.2, pp. 381-404.

## Appendix A - Transformation of Triaxial Laboratory Data

Not all the laboratory data presented in chapter 3, was originally expressed by their authors, in terms of CSR and  $\alpha$ . In order to be consistent and for comparison purposes, it was necessary to transform some of these data.

Data from cyclic triaxial tests is usually presented in terms of the stresses acting on a potential failure plane within the sample, i.e. a plane inclined at an angle of  $45^\circ + \phi'/2$  to the horizontal, where  $\phi'$  is the drained angle of internal friction of the soil (see figure A.1). From this figure we can deduce the following expressions, for cyclic triaxial data:

$$\alpha = \frac{\tau_{fc}}{\sigma'_{fc}}$$

$$CSR = \frac{\tau_{cyc}}{\sigma'_{fc}}$$

In the following section we will present the transformation equations used in order to express all the data in term of the above stresses.

- **Data represented in terms of  $p'$  and  $q$ :**

The data was expressed in terms of the mean principal stress,  $p' = (\sigma'_a + 2\sigma'_r)/3$ , and the deviator stress,  $q = \sigma'_a - \sigma'_r$ . The cyclic stress ratio was expressed using the following expression:

$$CSR' = \frac{q_{cyc}}{p'_c}$$

where  $q_{cyc}$  represents the cyclic deviator stress and  $p'_c$  the consolidation mean principal stress.  $\alpha$  was expressed in terms of the initial deviator stress ratio:

$$\alpha' = \frac{q_s}{p'_c}$$

The following transformation equations had to be used in order to transform the original data:

$$\alpha = \tan(45 + \phi' / 2) \times \left[ 1 - \frac{1}{1 + \frac{3q_s(1 - \sin \phi')}{6p'_c - 2q_s}} \right]$$

$$CSR = \frac{\frac{q_{cyc}}{p'_c}}{2 + \left(\frac{1}{3} - \sin \phi'\right) \cdot \frac{q_1}{p'_c}}$$

- **Data expressed in terms of  $K_c$  and  $\sigma'_{3c}$ :**

Most of the data used in this research used this form of expression for data, i.e. the use of the anisotropic consolidation ratio,  $K_c = \sigma'_1 / \sigma'_{3c}$ . Based on Figure A.1 we can obtain the following expressions of transformation:

$$\alpha = \tan(45 + \phi' / 2) \left[ 1 - \frac{1}{1 + \frac{K_c - 1}{2} (1 - \sin \phi')} \right]$$

usually the CSR is expressed as the cyclic deviator stress,  $\sigma_{dyc} = (\sigma_1 - \sigma_3)_{cyc}$  divided by the minor consolidation stress  $\sigma'_{3c}$ , the following transformation equation should be used:

$$CSR = \left[ \frac{1}{1 + \frac{K_c - 1}{2} \cdot (1 - \sin \phi')} \right] \cdot \left( \frac{\sigma_{dyc}}{2\sigma'_{3c}} \right)$$

**NOTE:** For some set of data  $\phi'$  was not available, therefore the stresses acting on the plane of  $45^\circ$  were used. The above equations were used with  $\phi' = 0$ , the influence of this on the values of CSR and  $\alpha$  is estimated to be of the order of 5 %.



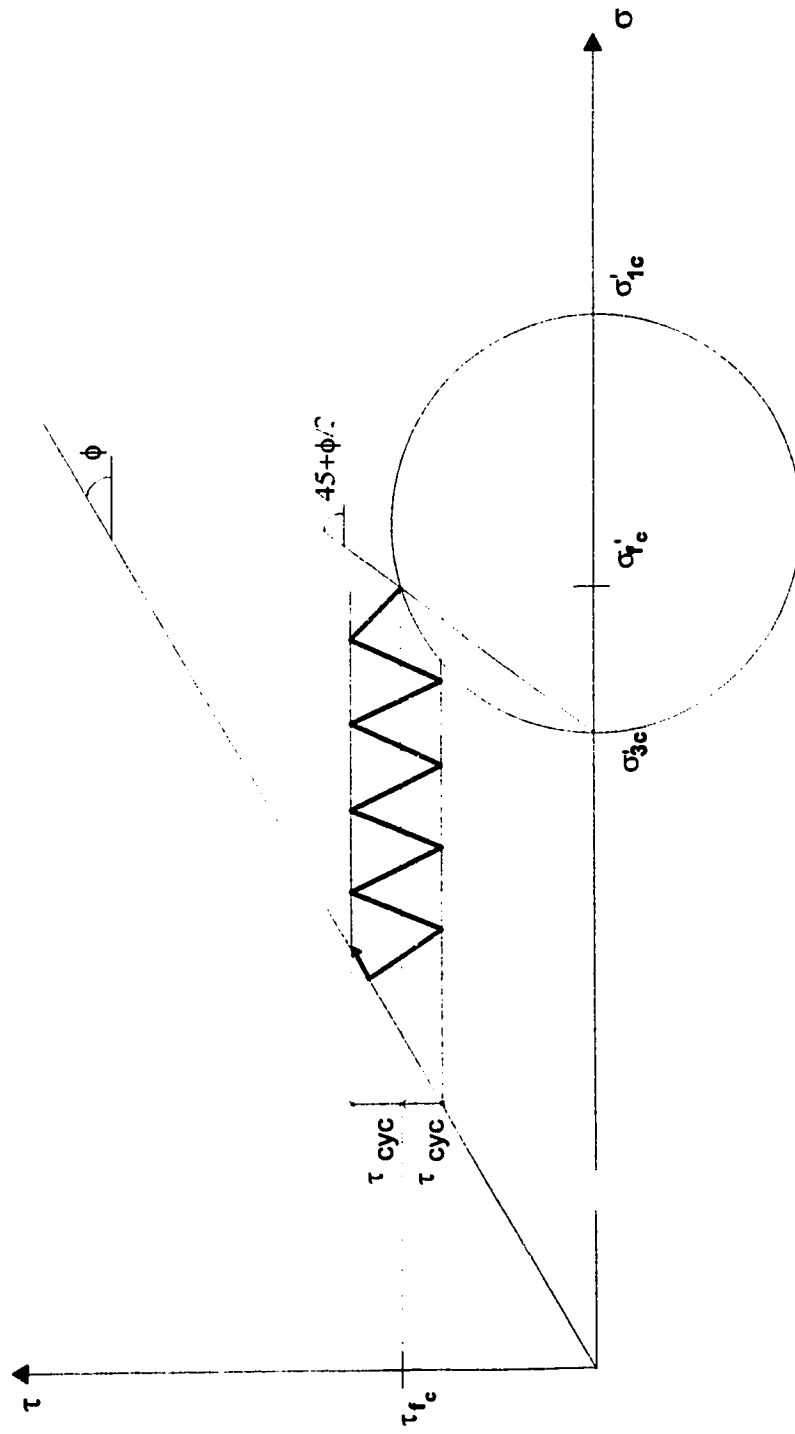


**Figure A.1 Anisotropically Consolidated - Cyclic Triaxial Test**

## Appendix B - Dynamic properties sensitivity analysis

Several authors have pointed out the importance of a realistic estimation of the dynamic properties in order to obtain a good prediction of the soil dynamic response (Prakash and Puri, 1981, Hardin and Drnevich, 1972). "the response predicted by the analyses will change *proportionately* to, and is no more accurate than, the values used for the soil properties" (Hardin and Drnevich, 1972). This appendix summarizes the results of a sensitivity analysis of the dynamic properties to evaluate how sensitive the dynamic stresses and accelerations are to the values used for them. Table B.1 shows the reference values used in the sensitivity analysis.

Table B.1 Reference values used for the sensitivity analysis

ELEVATION (m)	G <sub>max</sub> (kN/m <sup>2</sup> )	G <sub>initial</sub> (kN/m <sup>2</sup> )	γ (kN/m <sup>3</sup> )	ν	D
0 - 5	3800	3600	20	0.33	0.2
5 - 10	3700	3500	20	0.33	0.2
10 - 24	3300	3000	20	0.33	0.2
24 - 28	2600	2500	20	0.33	0.2

The program was runned three times using three sets of shear moduli: 0.1xG<sub>ref</sub>, G<sub>ref</sub> and 10xG<sub>ref</sub>. Figure B.1 shows the influence that the shear modulus has on the surface acceleration profile. Figure B.2a and B.2b show how the horizontal dynamic shear stresses computed for each element varies almost linearly with the value of shear modulus used, i.e. for  $G = 10 G_0$ ,  $\tau = 10.21\tau_0$ . It can be concluded from these results that the selection of dynamic properties should be done very carefully to avoid misleading results.

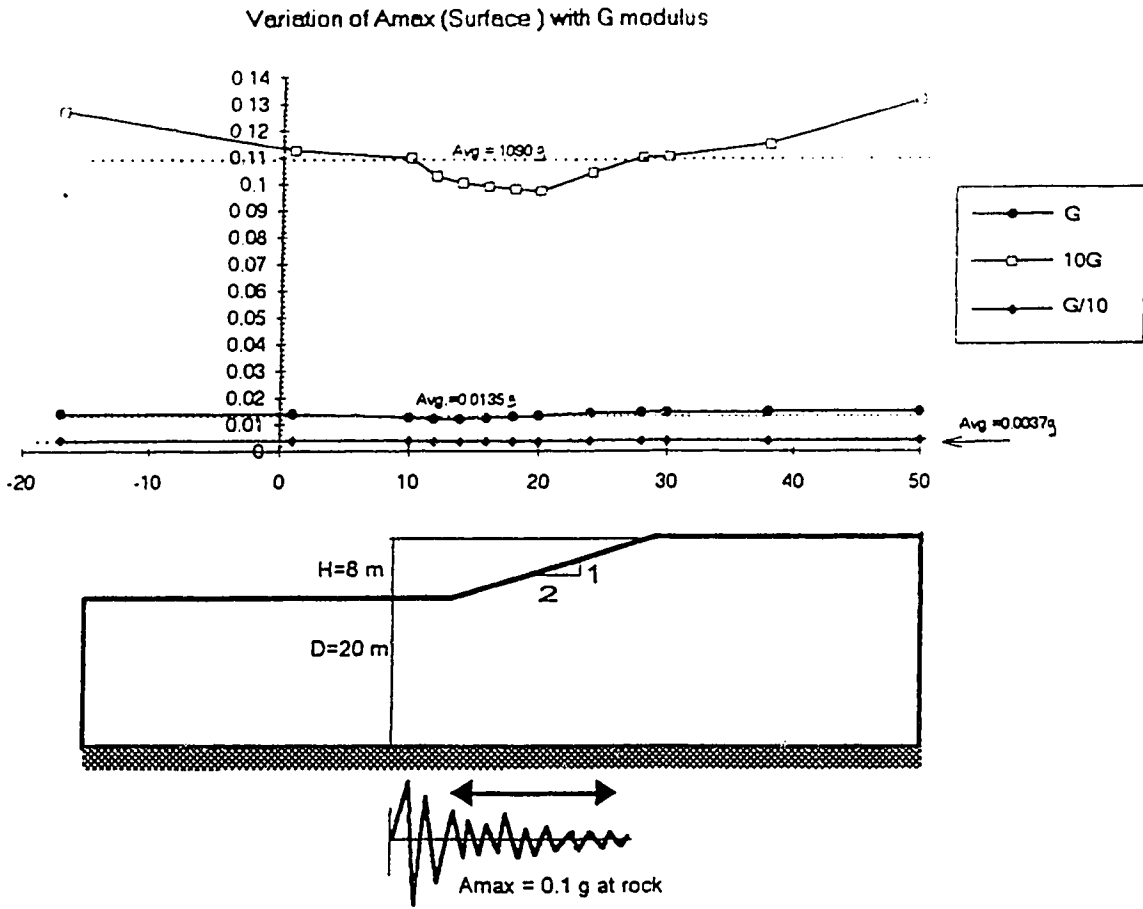


Figure B.1 Variation of Surface acceleration with the dynamic shear modulus value

(Tau-xy variation with G modulus)

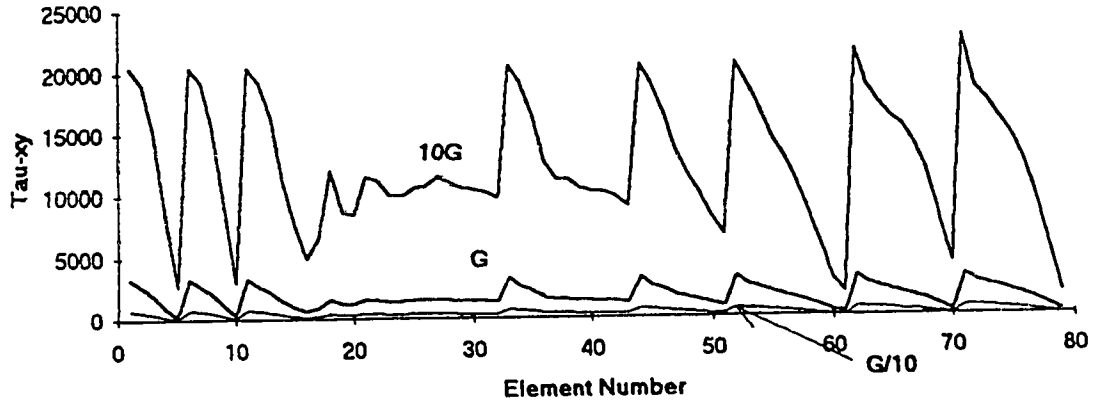


Figure B.2a  $\tau_{xy}$  variation with the dynamic shear modulus value

Variation of Dynamic Shear stresses with Gmax used

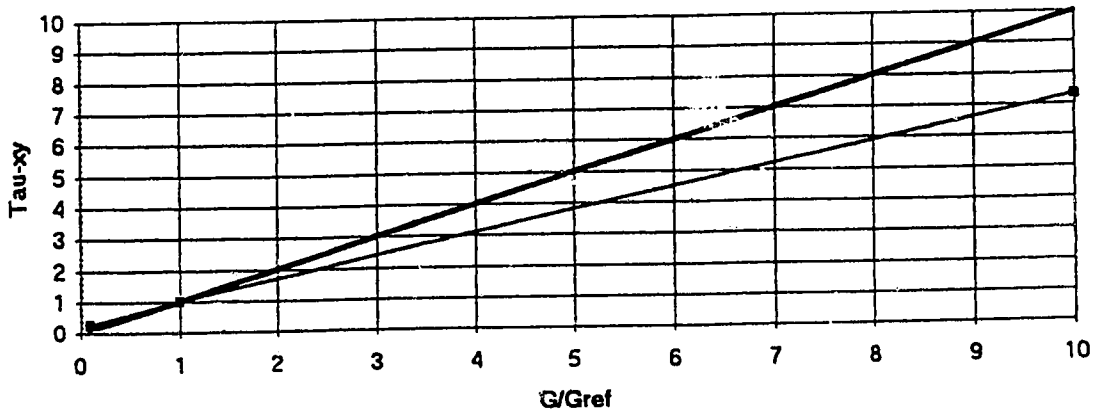
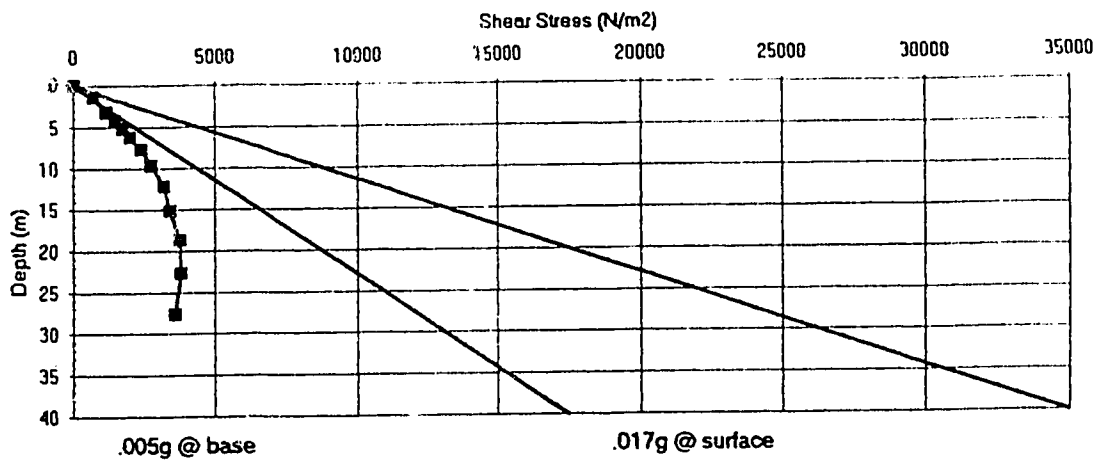


Figure B.2b  $\tau_{xy}$  ratio vs Shear modulus ratio

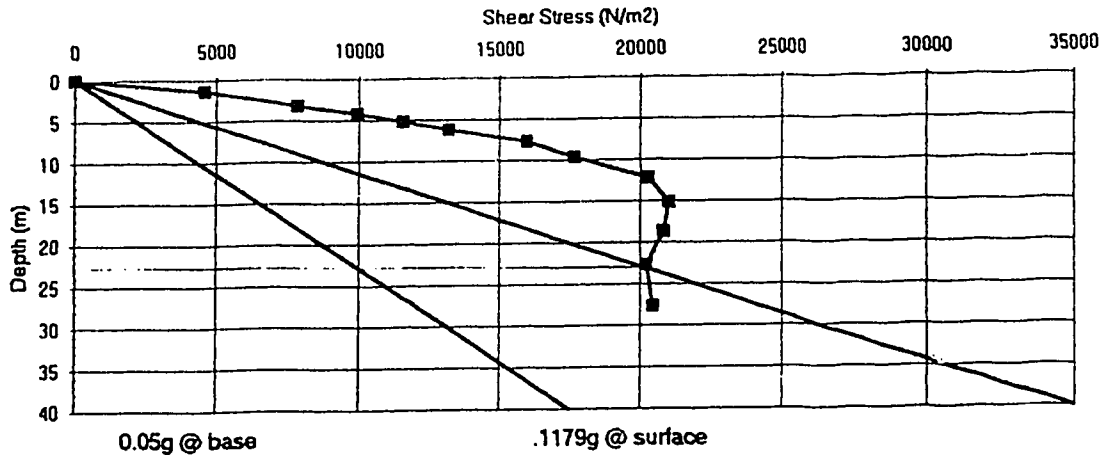
## **Appendix C - Infinite slope analyses results**

Four slope angles were analyzed for the infinite slope analysis case ( $5^\circ$ ,  $10^\circ$ ,  $15^\circ$  and  $30^\circ$ ). A total of 22 analyses were carried out. The summary plots for each of these analyses, with the dynamic and shear stresses are, contained in the following pages of this appendix.

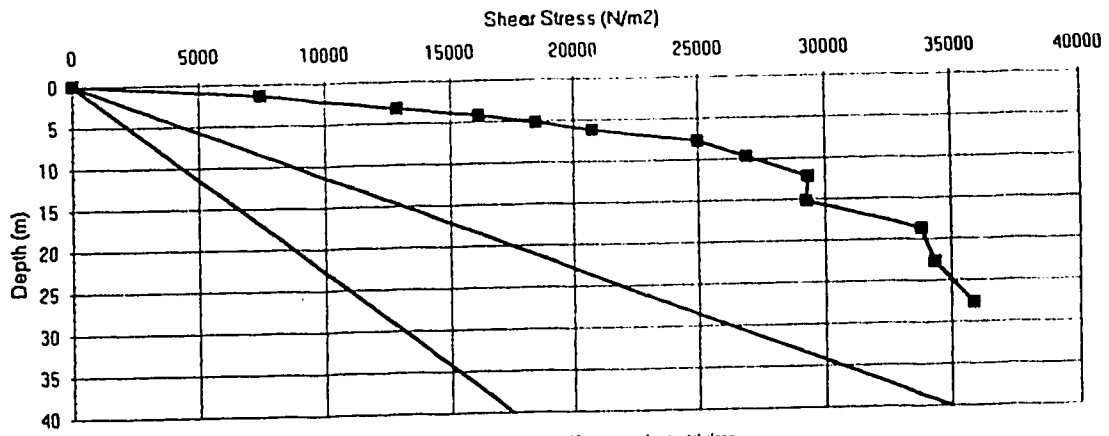
### 5 Degrees Infinite Slope Dynamic and Static Shear Stresses



### 5 Degrees Infinite Slope Dynamic and Static Shear Stresses



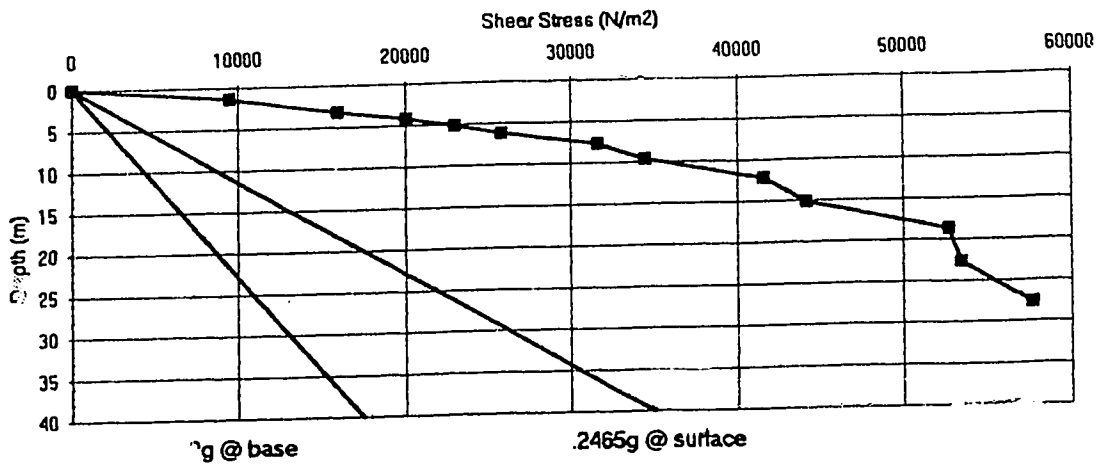
### 5 Degrees Infinite Slope Dynamic and Static Shear Stresses



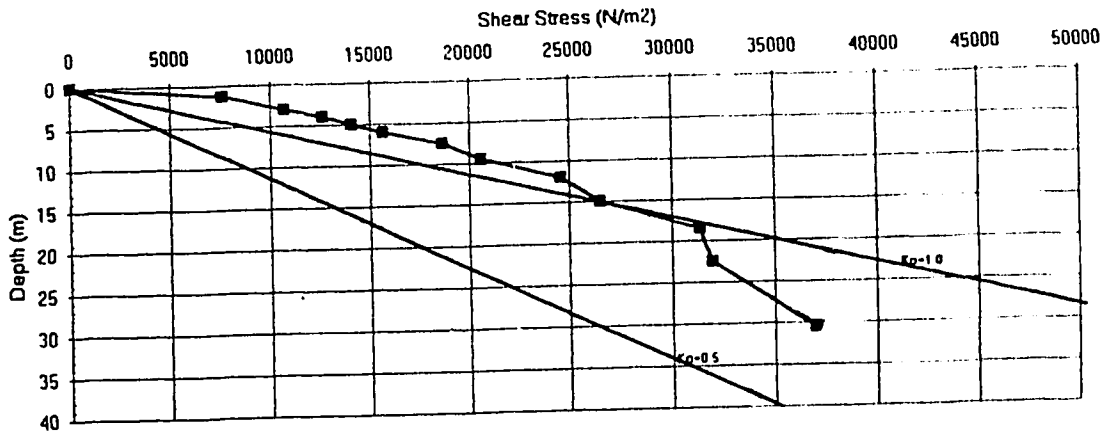
Notes: Uniform input motion  $A_{max}=0.1g$        $A_{max}$  of surface = 1518g      All stresses in horizontal plane



### 5 Degrees Infinite Slope Dynamic and Static Shear Stresses

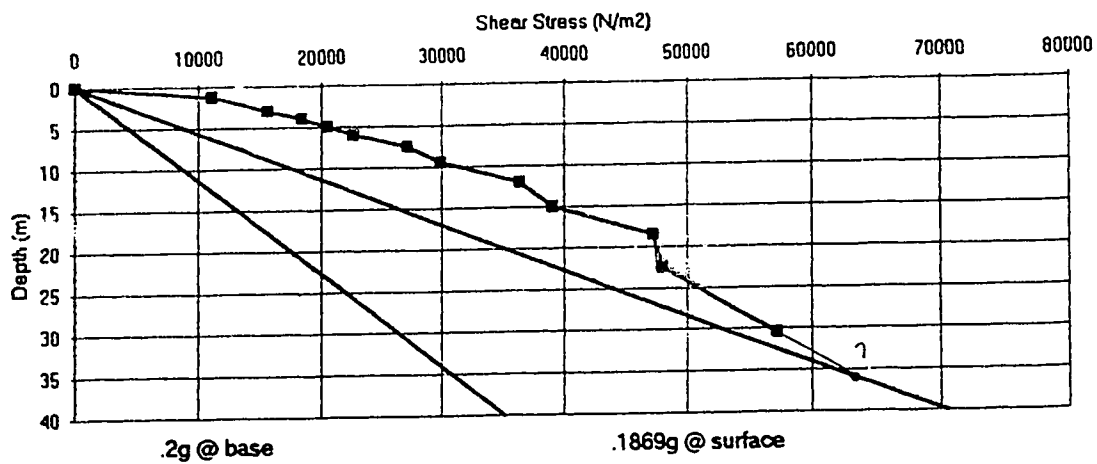


### 10 degrees Infinite Slope Dynamic and Static Shear Stresses

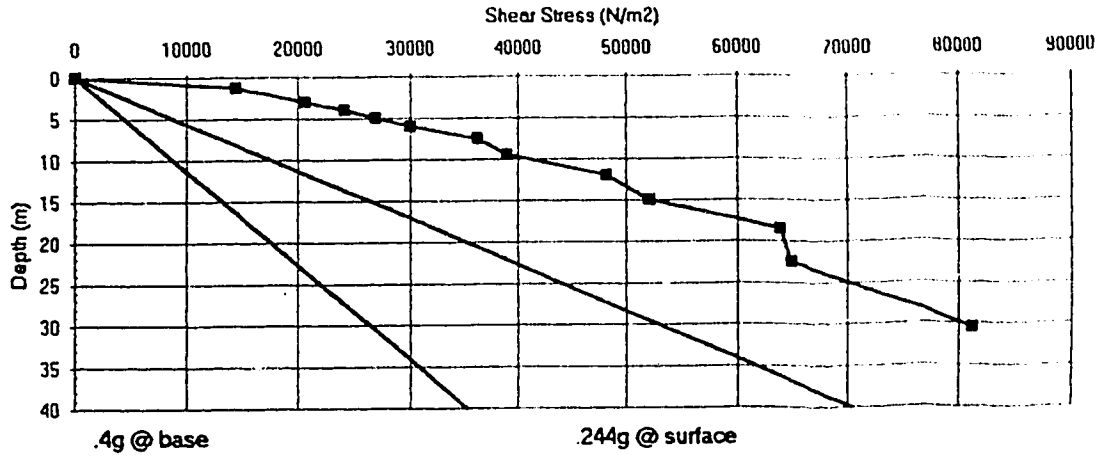


Notes: Uniform input motion  $A_{max}=0.1g$        $A_{max}$  at surface =  $1587g$       All stresses in horizontal plane

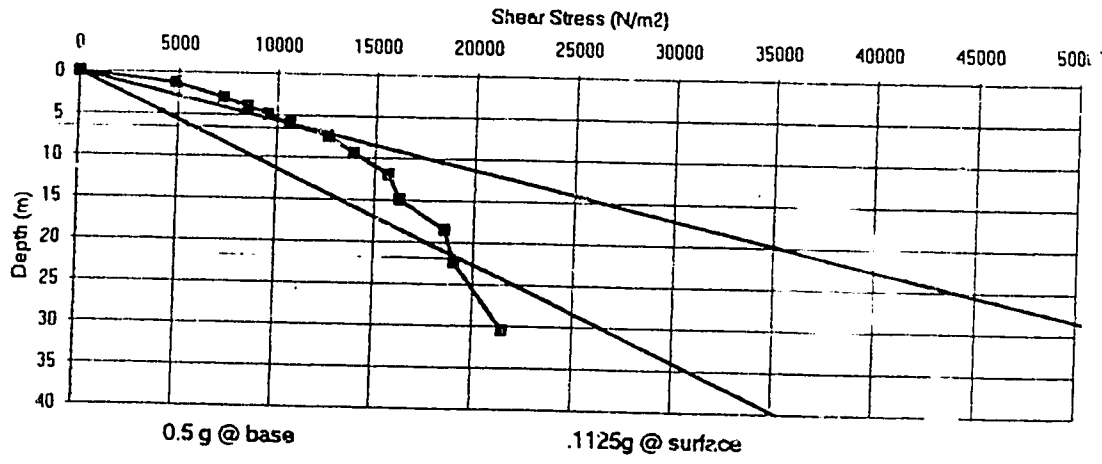
### 10 degrees Infinite Slope Dynamic and Static Shear Stresses



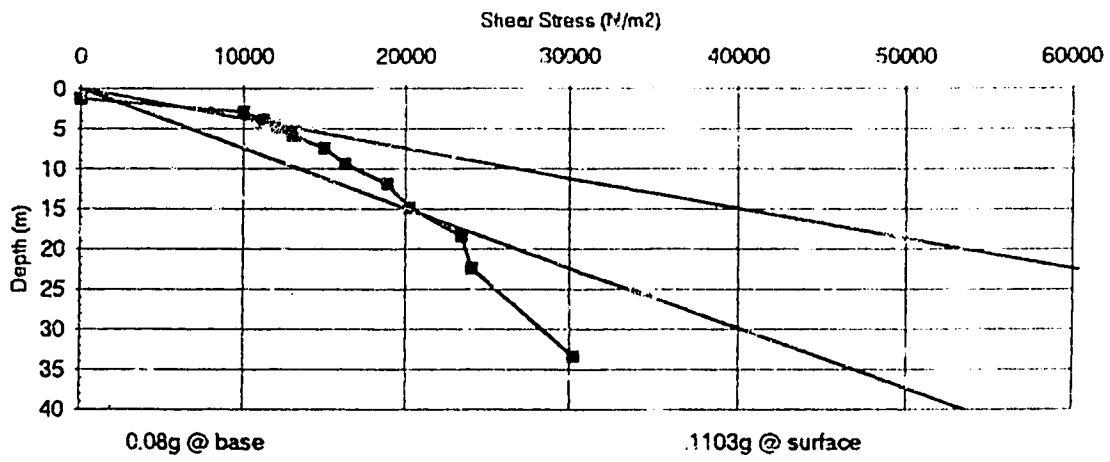
10 degrees Infinite Slope Dynamic and Static Shear Stresses



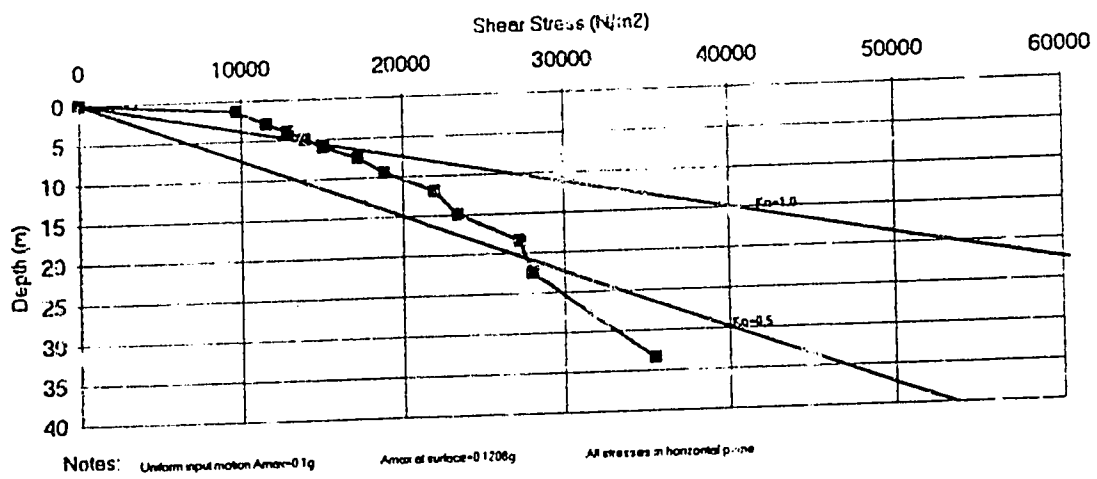
### 10 degrees Infinite Slope Dynamic and Static Shear Stresses



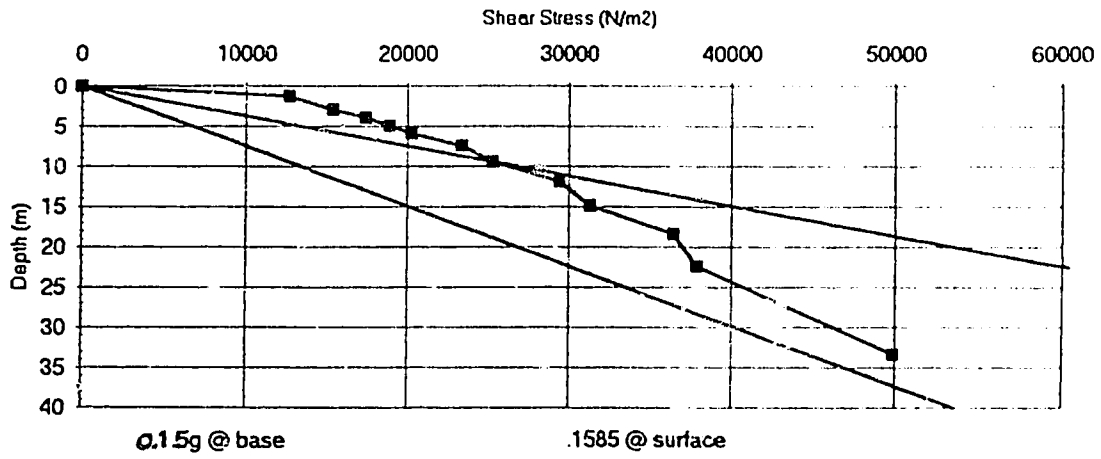
15 degrees Infinite Slope Dynamic and Static Shear Stresses



### 15 degrees Infinite Slope Dynamic and Static Shear Stresses

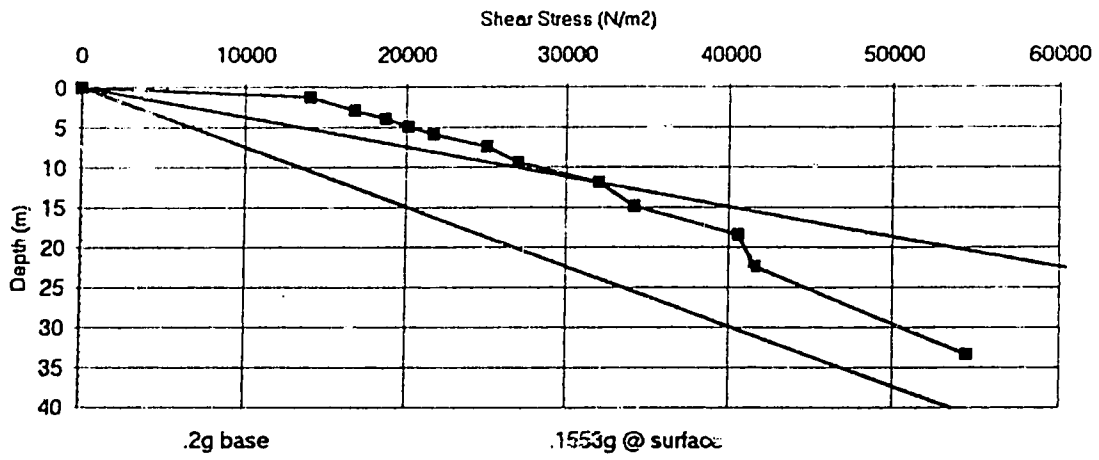


15 degrees Infinite Slope Dynamic and Static Shear Stresses

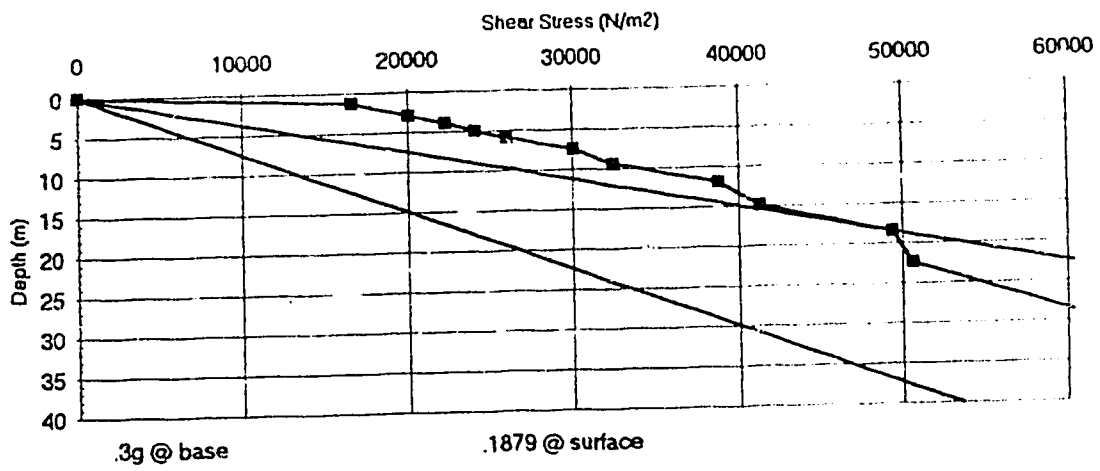




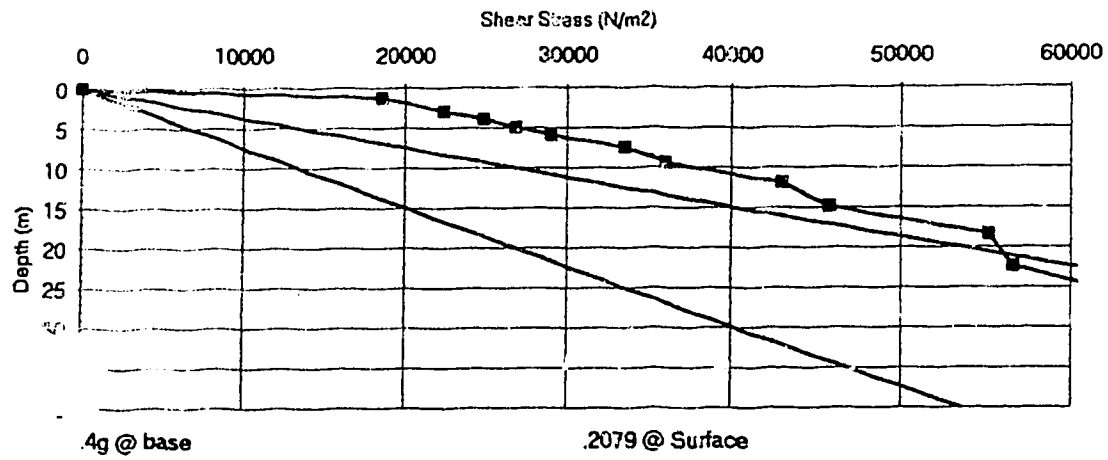
### 15 degrees Infinite Slope Dynamic and Static Shear Stresses



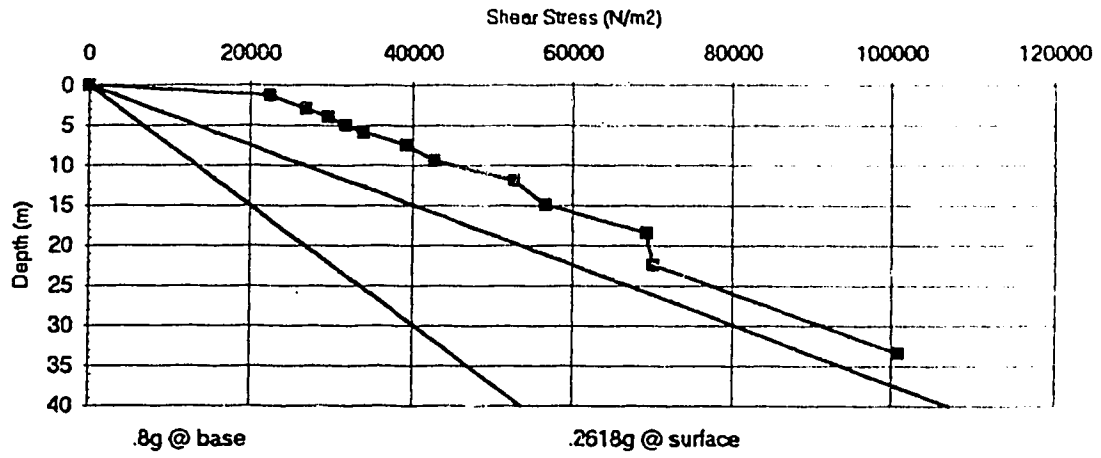
### 15 degrees Infinite Slope Dynamic and Static Shear Stresses



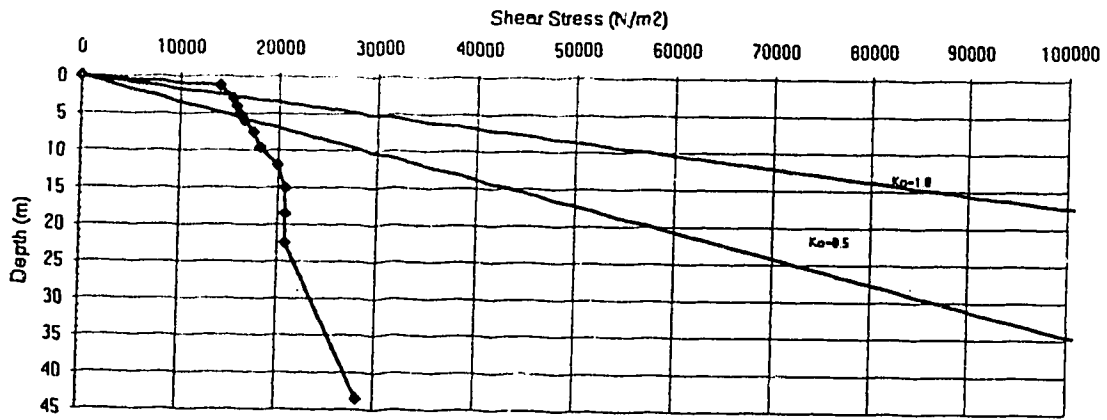
### 15 degrees Infinite Slope Dynamic and Static Shear Stresses



### 15 degrees Infinite Slope Dynamic and Static Shear Stresses

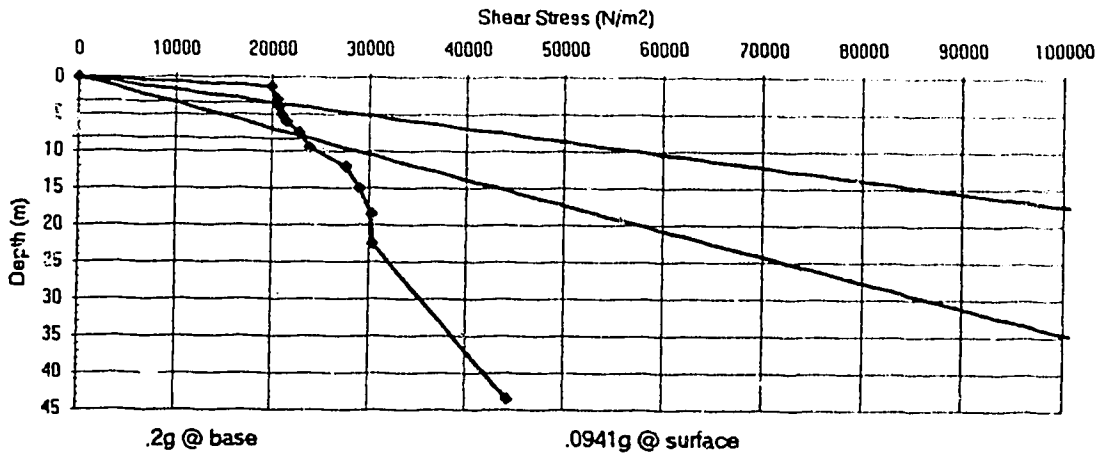


### 30 degree Infinite Slope Dynamic and Static Shear Stresses

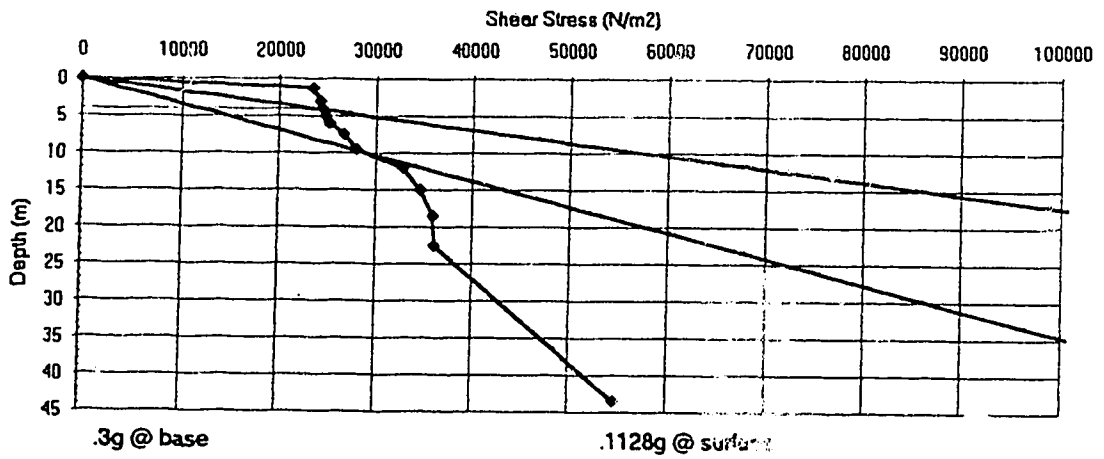


Notes: Uniform input motion  $A_{max}=0.1g$        $A_{max}$  at surface  $=0.072g$       All stresses are in horizontal plane

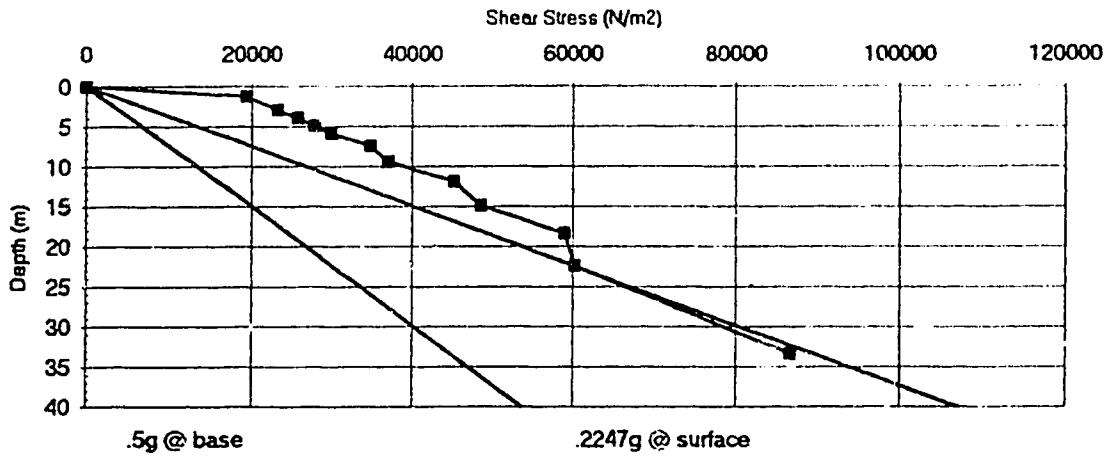
### 30 degree Infinite Slope Dynamic and Static Shear Stresses



### 30 degree Infinite Slope Dynamic and Static Shear Stresses

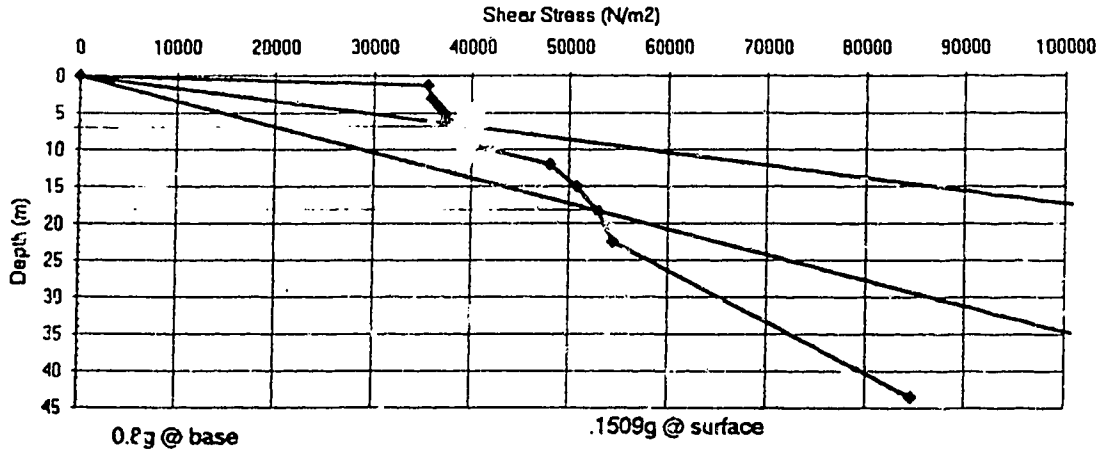


15 degrees Infinite Slope Dynamic and Static Shear Stresses





### 30 degree Infinite Slope Dynamic and Static Shear Stresses



## Appendix D - Description of the program QUAD4TB

Quad4TB is a program for evaluating the seismic response of plane soil structures using finite element analyses. Following a brief description of the numerical procedure used by Quad4TB is presented.

- Basic equations that governs the dynamic response of a soil structure:

In earthquake related problems, the following sets of equations (in matrix form) are required to be solved:

$$[M]\{\ddot{u}\} + [C]\{\dot{u}\} + [K]\{u\} = \{R(t)\} \quad (D.1)$$

where

- [M] = the mass matrix for the soil structure
- [C] = the damping matrix for the soil structure
- {u} = nodal displacement vector (dots represent time differentiation)
- {R(t)} = earthquake load vector which is a function of time

Equations D.1 are solved, by the program, using the direct step-by-step integration method. The basic approach is to replace the time derivatives appearing in Equations D.1 by differences of the displacement, {u}, at various instants of time. An important aspect of this method is the selection of an adequate time-stepping procedure. Quad4TB the *trapezoidal rule*, also known as Crank-Nicolson method. The selection of the time step in this method does not affect the numerical stability of the program, therefore is based on accuracy considerations alone. A detailed description of how to solve the Equations D.1 can be found in Cook et al. (1989).

- Main characteristic of the program:
  - Equivalent linear method
  - strain compatible rayleigh damping
  - strain compatible shear modulus

The advantage of Quad4TB is that it incorporates in the integration process the strain dependency of the shear modulus and the damping, which is a main characteristic of soils. This is done by solving the Equations D.1 for each integration step, with the strains computed, the soil properties are recalculated. A more detailed description can be found in Idriss et al., (1973).